Biogeographic and morphological variation in Late Pleistocene to Holocene globorotalid foraminifera

Inauguraldissertation

zur
Erlangung der Würde eines Doktors der Philosophie
vorgelegt der
Philosophisch-Naturwissenschaftlichen Fakultät
der Universität Basel

von

Kevin Richard Brown
aus
Untited Kingdom

Basel, 2007

Genehmigt von der Philosophisch-Naturwissenschaftlichen Fakultät

auf Antrag von:

Prof Andreas Wetzel

PD Dr Michael Knappertsbusch   Natural History Musem Basel

PD Dr Silvia Spezzaferri   Department of Earth Sciences
                                  University of Fribourg

(Mitglieder des Dissertationskomitees)
Basel, den 24 Mai 2007
(Datum der Fakultätssitzung)

                              H.-P. Hauri
                              Dekan
                              (Name des/der amtierenden
                              Dekanin/Dekans einsetzen)

I declare that I wrote this thesis:

"Biogeographic and morphological variation in Late Pleistocene to Holocene
globorotalid foraminifera."

with the help indicated and only handed it in to the faculty of science of the
University of Basel and to no other faculty and no other "university"

Date

Signature

K. R. Brown

Biogeographic and morphological variation in late Pleistocene to Holocene globorotalid foraminifera

Kevin Richard Brown

Natural History Museum Basel /
University of Basel

Abstract

Planktonic foraminifera are marine, calcite secreting protists. They have a long history of study in both industry and academia. Individual species show distinct biogeographical distributions and ecological tolerances. Traditionally species concepts are based on the gross morphology of the foraminiferal test. The closer the morphology of two species, the closer they are related. This has resulted in a single species being named by several authors from differing global locations and also, in long lived species, differing time intervals. This work investigates morphological variation of Late Pleistocene – Holocene menardiform globorotalids, and links this morphological variation to different ecological and environmental conditions. To achieve this 70 global sample sites are investigated covering a range of differing environmental conditions, but within constrained time limits. Where possible samples dated as Holocene have been used, where absolute dating was unavailable samples from about the *Emiliani huxleyi* acme zone, giving an upper age is given of 65 – 70 thousand years.

Analysis of morphological variation allowed identification of 2 intergrading morphoclines and a total of six distinct morphotypes (e.g. the menardi-form morphotypes α, β, χ and η and the two tumid form morphotypes ε and ϕ). The morphotypes are shown to have distinct though overlapping biogeographic distributions.
In the bivariate morphospace of spiral height versus axial diameter the equation $y = 2.07x - 15$ separates morphocline 1 (*G. menardii* morphologies) from morphocline 2 (*G. tumida* morphologies). Within morphocline 1 the line with equation $y = 3.2x - 160$ separates morphotypes α (G. menardii menardii) from morphotype β (*G. menardii cultrata*).

Morphotype β is interpreted as *G. menardii cultrata* and is seen to dominate environments with mean annual sea surface temperatures over 25°C. Morphotype α is interpreted as *G. menardii* menardii and becomes more dominant as sea surface temperatures become cooler. In areas where both morphologies are present in a sample we interpreted the situations a vicariant trophic depth adoption. *G. menardii cultrata* lives at shallow depths, while *G. menardii menardii* occurs deeper

within the water column. This interpretation is supported by stable isotope studies carried out on samples from the Gulf of Mexico and Caribbean region where the two morphologies show significantly different isotopic signals. *G. menardii cultrata* morphologically has a flattened smooth test with little secondary encrusting, while isotopically it has a shallow depth habitat and possible symbiotic relationship. *G. menardii menardii* morphometrically shows greater inflation and encrusting of the test and isotopically it shows a deeper and colder depth habitat. The presence of all ontogenetic stages within the two recognized morphological groups with distinct isotopic signatures, suggests that *G. menardii* may have two distinct subpopulations living at different depths within the Caribbean.

Ultrastructural studies on adult forms of morphotypes α and β from the same size fractions taken from a single sample, show that differences are present even in juvenile growth stages. Prolocular size and rate of growth suggest that morphotype α has a r-selected (rapid growth, opportunistic) mode of life. While morphotype β is k-selected (longer living, symbiont bearing, specialist) mode of life.

Morphotype η is interpreted as *G. menardii gibberula* this is the highest spired morphotype within the *G. menardii* group and is found only at the southerly extent of the sample set. Specimens have been identified in sample sites from the Western Pacific, which extends its known biogeographic range. It also has the highest spire of all the menardii forms and shows a correlation to the coldest sea surface temperatures.

Morphotype χ is only found in the northern part of the Indian Ocean and is interpreted as G. menardii neoflexuosa. It has a distinct flexure of the final chamber, but with removal of the final "flexed" chamber, the morphotype falls within morphotype β morphospace, to which is shows similar textural structure. The cause of the flexing is not clear, but as it is found in increased numbers during the summer monsoon, it has been suggested that it is a response to lowered salinity and an increase in turbidity of the surface waters.

Within morphocline 2 morphotype ε (*G. tumida)* is seen to intergrade the morphologically similar

but texturally different morphotype ϕ (*G. ungulata*). The diminutive size and delicate structure of *G. ungulata* is suggestive of it being the shallow dwelling juvenile form with being *G. tumida* the deeper dwelling more robust adult form. However, isotopic studies show differing depth habitats for the two morphotypes, with the heavier encrusted *G. tumida* showing a constantly deeper signal than the smoother more delicate form of *G. ungulata*, when comparing size equivalent specimens from the same sample sites. The first occurrence of *G. ungulata* is unclear but is believed to occur during the late Pleistocene. Because of this the results are interpreted as indicating ecophenotypic variation within a species, rather than just ontogenetic variation, with morphotype ϕ representing the shallow dwelling morphology, and morphotype ε the deeper dwelling morphology. Secondary encrusting of all specimens used in this present study indicates that encrusting is a function of which the foraminifera lived and not an indication of its stage of ontogeny or gametogenesis.

Contents

Ontogenetic growth in Recent menardiform globorotalids   115

List of Tables

List of Figures

List of Plates

Acknowledgements

Producing a thesis is not done in isolation, and requires a great deal of help, and encouragement, this is where I get to say some thank you's.

I am very greatful to my supervisor, Dr. Michael Knappertsbusch, for writing the proposal that made this project possible, and for the time and energy in discussions and correction of written manuscripts. I am indebted to Dr Silvia Spezzaferri for agreeing to stand as my co-referee.

Because of the nature of this project samples came from a number of sources over a number of years as the project grew. I would like to acknowleage the following people and sources: Curators of the DSDP and ODP core repositories, Rusty Lotti Bond and staff at the Lamont Doherty Core Repository. Dr. Barbara Donner, Bremen Core Repository. Dr. Richard Norris and Warren Smith at the Scripps Institute of Oceanography. Dr. Warner Brückmann, IFM-Geomar.

I would like to thank Dr. Brian Huber (US Museum of Natural History) for making available type specimens held with in their foraminiferal type collecion. Dr. Andy Henderson, (Natural History Museum London), for assistance in imaging of material held within their foraminiferal collections. I would like to acknowledge the help Dr. Barbara Seth of the University of Basel in carrying out the stable isotope analyses.

I would like to thank my collegues and friends at the Natural History Museum Basel for support and assistance: Roland, Angelo, Walter, André, Gerhard, Basil,

Daniela, Arne, Antoinette, Susanne, Daniel, Edi, Urs, Raffael, Markus, Antoine, and not forgetting our director, Christian Meyer. Thank you all for making my stay in Switzerland an unforgetable experience, the past four years have really flown by. To Denise and Thomas, who suffered too much curry an excess of Pink floyd, and Islay Malt, thank you both.

Thanks also go to Dr. Katarina Oblak, for her encouragement and correspondence, that has kept a smile on my face through the last two years, may we drink many more Slovenian bears.

Finally I would like to express my gratitude and love to my parents and family back in the UK. They may not have always understood what I was talking about or doing but they have always been there to support me, thank you both,.

Layout of thesis

Chapter 1   Introduction

Chapter 2   Digital imaging

This chapter is a brief introduction to digital imaging and its operation throughout this thesis. It highlights some of the problems that had to be overcome while carrying out this study.

Chapter 3   Global morphological variability in Late Pleistocene to Holocene menardiform globorotalia.

Chapter 3 describes the morphological variation found within the *Globorotalia menardii* and *G. tumida*. It shows the biogeographic distribution and the limits of morphological variation.

Chapter 4   Depth induced morphological variation in Recent Caribbean globorotalid foraminifera: evidence from combined morphological and isotopic studies.

A detailed study comparing the stable isotope signals with morphological variation within a distinct geographic region.

Chapter 5   Ontogenetic growth in Recent menardiform globrotalids

Investigation of the growth of *Globorotalia menardii* and *G. tumida*. Identification of ontogenetic stages and investigation of the rates of growth within the morphotypes.

Chapter 6   Synopsis.

Introduction

Planktonic foraminifera are calcite shell secreting marine protists. They have a long history of study; their morphological variation has formed the basis of biostratigraphic correlation used in academia and industry. Traditionally, information about evolutionary patterns and phylogenetic relationships of planktonic foraminifera has been derived from qualitative and quantitative descriptions of their fossil shells. However, recent work involving molecular study of extant planktonic foraminifera (Darling et al., 2000 & 2004; de Vargas et al., 2001) have challenged accepted views of the origin and speciation rates in planktonic foraminifera. Identification of cryptic speciation within planktonic foraminifera (Darling et al., 2000 and 2004, Huber et al., 1997) has challenged our acceptance of the large morphological variation often seen within a single species.

Most phylogenies of planktonic foraminifera e.g. those of Stainforth et al. (1975), Blow (1979), Kennett and Srinivasan (1983), Bolli and Saunders (1985), are based on the description of single specimens (holotype) and possibly a few additional specimens (paratype) designated by the author the same time as the selection of the holotype. Many of these species are described from a single locality, or time slice and no consideration of geographic variation in the global population or evolutionary trends through time were made. This has led rigid to species concepts, which has hampered recognition of the significance of fine scale variation along latitudinal and ecological gradients or transitional changes through time. Many taxa were thus introduced artificially without a sound appreciation of the biological and ecological meaning of size and shape of shells. Planktonic foraminifera can be described as being strongly polyphenotypic in that they show a great deal of morphological plasticity. This adds to the difficulty in describing a single species particularly, where two similar, possibly cryptic, species show a morphological overlap. To further complicate quantitative identification of a species, by the morphology of their hard parts, evidence is emerging that cryptic speciation is common within planktonic foraminifera (Huber et al. 1997, Darling et al., 1999 and de Vargas et al., 2001). Cryptic speciation is impossible to identify by morphological methods alone and requires independent evidence from isotopic, ontogenetic and

ultra-structural studies. A greater understanding of the morphological variation within a species and the relationship of this morphology to biogeographic distribution are needed to understand evolutionary patterns inferred from fossils deposited in the sedimentary archives.

1.1   Morphological variation through time

Evolutionary processes are influenced by ecological and environmental factors, among which temperature is especially influential (Stainforth et al 1975). This is seen in the greater variety of planktonic foraminifera observed in tropical and sub-tropical regions as compared to Polar Regions. Adaptation of a species to differing depth habitats can also lead to confusion and result in incorrect definition of new or subspecies. When a species is first described the author selects a specimen to represents the species, this is termed the holotype. At the time of naming the author can also select other specimens to represent morphological variation within the species; these are termed paratypes. So at anyone given time, a mean specimen and other specimens that vary away from this accepted mean value represent the concept of the species. The problem with this procedure is that new specimens are often described from a single locality or a few sites within a single regional area. In Figure 1.1 measured morphological characteristics of adult specimens show a concentration of specimens about a mean value. A scattering of individuals that deviate from the mean value represented by the oval line represents the maximum accepted morphological variation (morphospace) for the species concept.

Morphological characteristics tend to change gradually and progressively through time so that a purely objective definition of a species may be extremely difficult, particularly in a chronologically long-lived species (Stainforth et al 1975). The mean morphological value (connected by the line), and the maximum morphological variation (oval) are represented at successive time intervals. It can be seen that in successive time slices gradual change (evolution) results in only slight morphological variation. However early time slices are completely different form latter forms (Stainforth et al 1975).
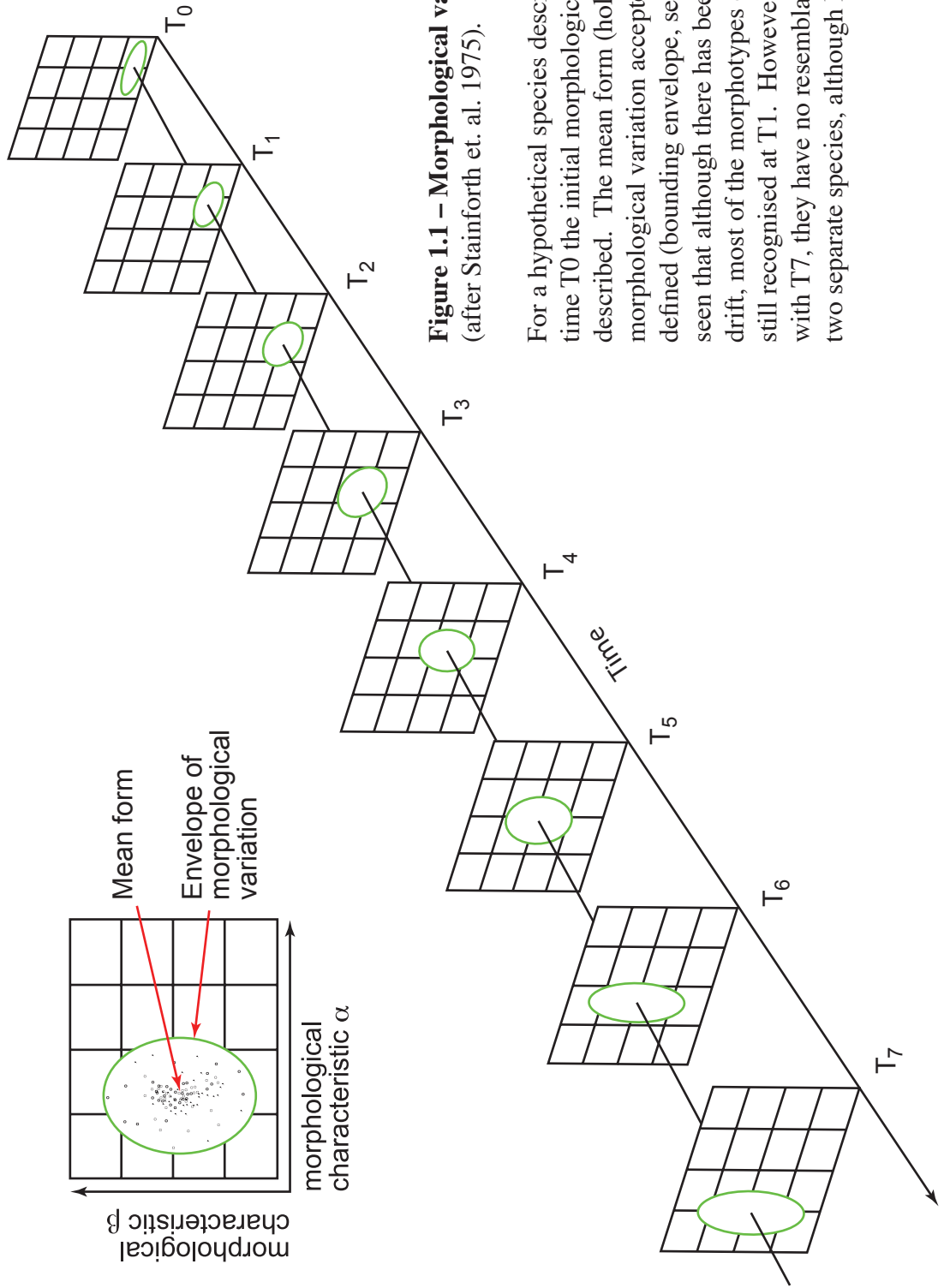
Figure 1.1 – Morphological variation through time (after Stainforth et. al. 1975).

For a hypothetical species described from rocks at time T0 the initial morphological characteristics are described. The mean form (holotype) and the extent of morphological variation accepted for the species can be defined (bounding envelope, see inset). At T1 it can be seen that although there has been some morphological drift, most of the morphotypes observed at time T0 are still recognised at T1. However when comparing T0 with T7, they have no resemblance, and would represent two separate species, although linked through evolution

To investigate the rates of morphological variation and the effect of differing environments on the morphology of a species time slices need to be taken over wide geographic areas and the morphological variation mapped out. To achieve sufficient sampling density is difficult, and is beyond the financial scope of any single project. This is where the DSDP, ODP and IODP cores can be exploited. They provide potential core site in all the worlds' oceans, some cores have already been processed and their residues are available for study in the Micropalaeontological references centers scattered around the globe.

1.1.1 Palaeontological interpretation of species concepts

In palaeontological studies morphological similarity between the remains of two organisms has been use to imply species relationships. The closer the morphological similarities of the skeletal remains then the closer two organisms were related. However because we are dealing with their fossilised remains, it is impossible to say if the two morphologically similar organisms could reproduce. This method of defining a species is known as the morphological species concept. In the micropalaeontological study of foraminifera, species associations are based on similarity in wall structure and overall test morphology. The morphological definition of a species has received much criticism because genetic studies have shown that there is often great morphological difference between genetically similar organisms. While recent studies on the genetics of planktonic foraminifera have revealed that morphologically indistinct organisms have differing genetic profiles (Darling et al., 2000 and 2004).

Ernst Mayr put forward the more commonly recognised biological or reproductive definition of a species in his 1942 book Systematics and the Origin of Species. Mayr wrote "a species is not a group of morphologically similar individuals, but a group that can breed only among themselves excluding all others." This definition is somewhat limited as it assumes that sexual reproduction occurs within the species, this leaves the term undefined for a large number of organisms, which reproduce asexually. To add further confusion, biologists frequently do not know whether two morphologically similar groups of organisms are potentially capable of interbreeding, as mate recognition plays a large part of mate selection. While hybridization between two species occurs

naturally and under experimental conditions, showing that in some species there is sufficient genetic overlap to produce viable young

A more recent modification of Mayr's definition of a species is used as " a reproductively isolated population that shares a common gene pool and a common niche. This definition defines a species reproductively, genetically, and ecologically (Gould 2002).

For more detailed discussion of the interpretation " species" and its implications to palaeontology refer to chapter 8 of Biostratigraphy: microfossils and geological time by Brian McGowan.

As this work studies the fossil remains of Late Pleistocene to Holocene planktonic foraminifera, a morphological view of species relationships has to be taken. It is however recognised that as the species studied in this work are still extent in the world's oceans, future genetic studies may force a reappraisal of species concepts within the planktonic foraminifera.

1.1.2 Evolution and its forcing mechanisms

Charles Darwin and Alfred Wallace independently proposed the theory of evolution of species through natural selection. Darwin recognised that the rate of growth of a population will always outpace the rate of growth of the resources in the environment, such as food supply. As a result, Darwin argued that not all the members of a population would be able to survive and reproduce. Those that did reproduce would be the ones that possessed variations however slight, that made them slightly better adapted to the environment. If the adaptations where heritable then the offspring of the survivors will also possess them. Over many generations, adaptive variations will accumulate in the population, eventually giving rise to a new species.

1.1.2.1 Phyletic gradualism

This is a theory of evolution, which hypothesises that evolution occurs at a continuous and uniform rate resulting in the gradual transformation of whole lineages. It is supposed that all species evolve at the same rate. This is the classic Darwinian theory of evolution.

1.1.2.2 Punctuated Equilibrium

In contrast to phyletic gradualism, punctuated equilibrium (Eldredge and Gould 1972) hypothesises that sexually reproducing species will show little or no evolutionary change throughout their history. When evolution does occur, it happens sporadically and occurs relatively rapidly. The hypothesis proposes that the large gene pool stabilises the population preventing any genetic variation becoming established any genetic variation that does occur being swamped but the large stable population. It is only at the periphery of the organism's geographic range, where genetic variation can become established due to restricted gene flow with the total population.

1.1.3 Speciation modes

Speciation is the evolutionary process by which new biological species arise. There are four hypotheses, which try to explain how the evolution of new species occurs in differing environments. Each hypothesis is based on the extent to which speciating populations are geographically isolated from each other. Figure 1.2 summarises the different modes.

1.1.3.1 Allopatric

Also known as geographic speciation, reproductive isolation occurs when populations are physically isolated by the development of an extrinsic barrier between the two populations. Intrinsic (genetic) isolation such that if the barrier between the two populations breaks down the two populations can no longer interbreed.

1.1.3.2 Peripatric

Occurs in an isolated peripheral populations; its mechanism is similar to allopatric in that the populations are isolated and prevented from exchanging genes. However, in peripatric speciation one population is much smaller than the other.

1.1.3.3 Parapatric

Evolution of reproductive isolation occurs when a population enters a new niche or habitat within the range of the parent species. Generally this occurs when there has been a drastic change to the

Original parent population occupying the original niche

1a. Isolation of a portion of population

2a. Movement into a new niche along the periphery of the Ancestral range

3a. Genetic polymorphism within the population

1b. Genetic drift within one or both isolated population's results in reproductive isolation

2b. Reproductive isolation occurs without complete isolation in adjacent niches

2c. Reproductive isolation occurs in isolated niche

3b. reproductive isolation occurs without the presence of a barrier

Allopatric

Parapatric

Peripatric

Sympatric

Result in all cases: when the two niches are recombined there are two species occupying the original niche.

after Ilmari Karonen 2007 Public Domain source

Figure 1.2   Speciation modes: the four hypothetical processes through which speciation occur.

Original parent population occupying the original niche
1a. Isolation of a portion of population
2a. Movement into a new niche along the periphery of the Ancestral range
3a. Genetic polymorphism within the population
1b. Genetic drift within one or both isolated population's results in reproductive isolation

2b. Reproductive isolation occurs without complete isolation in adjacent niches
2c. Reproductive isolation occurs in isolated niche
3b. Reproductive isolation occurs without the presence of a barrier

Result in all cases: when the two niches are recombined there are two species occupying the original niche.
After Ilmari Karonen 2007 Public Domain

environment within the original species' habitat. In parapatric speciation there is no extrinsic barrier to gene flow. The population remains continuous, but the population does not mate randomly. Individuals are more likely to mate with geographic neighbours than with individuals in a different part of the population's range. In this mode divergence and genetic isolation result because of a reduced gene flow within the population and differing selection pressures across the population's range. One common model of parapatric speciation is the clinal model, where populations diverge along an environmental gradient. The populations at either end of the gradient can become locally adapted to their environments, and this leads to speciation.

1.1.3.4 Sympatric

Rreproductive isolation occurs due to genetic polymorphism within the population. Unlike allopatric speciation there are no geographical barrier isolating one population from the other, generally the speciating populations generally share the same range.

1.2   Approach

1.2.1   Morphology

Globorotalia menardii and G. tumida are two extent planktonic foraminifera that share a similar lenticular-keeled morphology. The two species are closely related and are often mistaken, either by the presence of differing species concepts, or by deliberately lumping them together (Ericson and Wollin 1968). Schmid (1934) considered G. menardii and G. tumida to a single species with G. menardii being the micorospheric form and G. tumida the macrospheric form. Since the mapping work of Bé (1966) their biogeographic ranges are well known. In comparison to other planktonic foraminifera they have large shells that are known to be resistant to dissolution (Berger 1972). The larger size makes them easy to collect and orientate making them an ideal choice for morphological studies.

To determine the extent of the morphological variation a large a geographic distribution of samples sites is required that includes ecological gradients and extreme habitats for the species under consideration. This allows a range of environments to be investigated, attempts can be made link observed morphological characters to distinct environments or geographic regions. The uses of a well-selected set of measured variables allows direct comparison of specimens, from different regions and thus allowing identification of small, otherwise, looked over characters that maybe useful for determining the species. The use of quantative measurements allows us to define end members within the morphological variation of a species or sub-species.

Measurement of a constant set of variates of standard orientated specimens from Late Pleistocene and Holocene samples provides a base line for understanding the extent of morphological variation present within the species under consideration. Such a set of morphological measurements can later be counter-tested by molecular methods to better arrive at valid differential diagnosis for species distinction

1.2.2   Depth variation and vertical migration or depth separation of habitats

Stable isotopes of oxygen and carbon vary considerably but systematical with depth and latitudes within the oceans. By exploitation of stable isotopes within foraminiferal shells provide important information about the (depth) habitats of these organisms. Most planktonic foraminifera secrete their shells, in equilibrium or close to equilibrium with the seawater within which they live (Helmleben et al., 1989; Schweitzer and Lohmann, 1991; Spero 1998). Stable isotope analysis by these and other authors has shown that G. menardii and G. tumida produce their shells in the upper 50-100m of the water column. To understand migration of foraminifera through the water column throughout ontogeny, isotopic analyses are needed at various size intervals. Such investigations have been done on modern planktonic foraminifera in the past (e.g. Berger 1969, Brummer et al., 1990) but still need more research in order to be extendable to the fossil record. The isotope analyses can be combined with morphometric data allowing identification of depth stratification, or selection of environments within different morphological groups. Identification of water mass stratification via stable isotopes and related morphometry throughout ontogeny of species will lead to greater accuracy in interpretation of the paleoenvironment, where the organisms lived.

1.2.3   Ontogenetic variation and growth rates

Foraminifera are believed to have a life span of approximately 30 day (Hemleben 1989, Schweitzer and Lohmann, 1991). Growth in foraminifera occurs by secretion and addition of discreet chambers to the preexisting shell (Schweitzer and Lohmann, 1991, Bijma et al., (1990). Shell porosity has been suggested as an index to water temperature Bé (1968), and so is a further measure able character for palaeoenvironmental reconstruction. Shell porosity eventually also links environmental changes to the physiological intakes of the individual (e.g. growth, maintenance, reproduction) because the pores are the sites of elemental flux between the ambient water and the cytoplasm. The chamber volume providing a space for the cytoplasm gives indications about shell growth until maturity of the organism. The pore size and density are related to metabolic exchange into and out of the cell. Therefore it seems reasonable to assume that changes in either the chamber size or number and size of pores are related to changed in the metabolic rate of an organism, whether it is related to growth, reproduction, or maintenance of life function. To

investigate these interdependencies serial dissection of selected specimens was carried out under light microscope, and the dissected specimens imaged using a scanning electron microscope. The resulting 2D images allow measurement of the cross-sectional chamber area, which is a direct measurement, related to the physiological of the organism.

References

Bé, A.W.H. 1968. Shell Porosity of Recent Planktonic Foraminifera as a Climatic Index. Science, 161:881-884

Bijma, J., Faber, W.W., and Hemleben, C., 1990. Temperature and Salinity Limits for Growth ans Survival of Some Planktonic Foraminifers in Laboratory Cultures. Journal of Foraminiferal Research, 20:95-116

Blow, W.H. 1979. The Cainozoic Globierinida. E.J. Brill, Leiden (3 vols.),1413pp

Bolli, H.M., and Saunders, J.B., 1985. Oligocene to Holocene low latitude planktic foraminifera. In: Bolli H.M., Saunders J.B. and Perch-Nielsen K., Editors Plankton Stratigraphy Cambridge University Press.

Darling, K.F., Wade, C.M., Stewart, I., Kroon, D., Dingle R., and Leigh Brown A.J., 2000. Molecular evidence for genetic mixing of Arctic and Antarctic subpolar populations of planktonic foraminifers. Nature, 405: 43- 47.

Darling, K.F., Kucera, M., Pudsey,C.J., Wade C.M., 2004. Molecular evidence links cryptic diversification in polar plankton to Quaternary climate dynamics Proceedings National Academy Science 101(20): 7657-7662.

Emiliani, C., 1969 A New Paleontology. Micropaleontology, vol. 15, no. 3. pp. 265-300, pls. 1-22, july 1969.

Ericson, D. B., & Wollin, G., 1968 Pleistocene climates and chronology in deep-sea sediments. Science, vol. 162, no. 3859, pp. 1227-1234, text-figs. 1-6.

Fairbanks, R.G., Wiebe, P.H. and Bé, A.W.H. Vertical Distribution and Isotopic composition of Living Planktonic Foarminifera in the Western North Atlantic. Science vol 207 pp.61-63

Hemleben, Ch., Spindler, M., and Anderson, O., 1989. Modern Planktonic Foraminifera. Springer Verlag, Berlin, Heidelburg.

Huber, B.T., 1994. Ontogenetic Morphometrices of Some Late Cretaceous Trochospiral Planktonic Foraminifera from the Austral Realm Smithsonian Contributions to Paleobiology number 77

Kennett, J. P. and Srinivasan, M. S., 1983 Neogene planktonic foraminifera, a phylogenetic atlas. Hutchinson Ross, Stroudburg, Pennsylvania.

Mayr, E., 1942. Systematics and the Origin of Species

McGowan, B., 2008. Biostratigraphy: Microfossils and Geological Time
Cambridge University press, 479 pages.

Norris, R.D., 1998 Recognition and Macroevolutionary significance of Photosymbiosis in molluscs, corals, and foraminifera. Isotope Paleobiology and Paleoecology. The Paleontological society papers Vol 4. pp. 68-100.

Stainforth, R.M., Lamb, J.L., Luterbacher, H., Beard, H.J., and Jeffords, R.M., 1975
Cenozoic Planktonic Foraminiferal Zonation and characteristics of index forms. Article 62 The University of Kansas Paleontology Institute.

Schmid, K., 1934 Biometrische Untersuchungen an Foraminiferen [Globorotalia menardii (d'Orb.) – Globorotalia tumida (Brady) und Truncatulina margaritiera

Digital imaging.

The use of digital imaging in palaeontology for morphometric analysis is quite advanced nowadays. Higher resolution digital cameras and powerful computer software make it easy to produce high quality images easily. Images displayed on a computer screen are composed of smaller picture elements called pixels.

The quality of a digital picture depends on the spatial resolution, the number of grey-levels in a grey-level image and the number of channels available (1 channel in grey-level images, 3 channels, e.g. red, green and blue in a colour picture, or several channels in multi-channel false colour images). Spatial resolution in a video-image depends on the number of lines per second. After digitization lines are synchronously sampled by the frame grabber and often digitized (subdivided) into a new number of horizontal lines, whereby each line is subdivided into a number of horizontal pixels. The spatial resolution of a digital image is a function of the number of horizotal and vertical pixels per mm^2 available on the CCD chip. The grey-level resolution in and image indicates how many gradations between black (no signal) and white (100%) signal can be offered. In many devices there are $2^8 = 256$ grey levels per channel, which represents 8 bits per pixel.

2.1 Digital image caputure.

For all morphometric work digital image acquisition was carried out using a single chip colour CCD camera from KAPPA (model CF 11/2) mounted on a Leica MZ6 binocular microscope with Leica Ax stand and connected to a Macintosh computer. This camera was able to process a NTSC TV Signal to 640 x 480 pixel images or a PAL signal to 752 x 582 pixel images. The microscope is fitted with a Planopo 1x lens and has a 0.63x to 4x zoom body allowing images to be taken at a number of magnifications. Correct orientation of specimens was achieved by use of a hemispherical stage. The correct orientation of the specimens was taken when the spiral height (δX) was seen to be at a minimum and the overall length of the specimen (δY) at maximum value the system has been calibrated, so that pixel values can be directly converted to micrometers. Image capture was carried out using the public domain NIH Image program (developed at the U.S.

National Institutes of Health and available on the Internet at http://rsb.info.nih.gov/nih-image/). The captured images are composed of an average of 16 frames and have a size of 640 x 480 pixels at 256 grey-levels, and were saved in Tagged Image File format (Tiff). The size of each Tiff image is 308Kb.

2.2   Errors

Imaging the same object several times always introduces variation in the image, even when all parameters are held constant.

These variations include:

1. Positioning errors, that occur from the variation in manual positioning of the forams into the same orientation.

2. Illumination errors, because of variation in ambient light, different settings of the diphragm of the microscope or due to the use of filters.

3. Gery – level variation due to processing and converting the original gery-level image into a thresholded binarry black and white image in Raw format. The Raw format is required for input into the " Trace35_batch.out" program which extracts the outline coordinates for the object, see Knappertsbusch (2004)..

The ambient light in which the image is taken will vary through-out the day, or year unless the images are taken in a darkroom. Experimentation has shown that reflexion of light from either the background or the object can induce variation. Reflexion is very important in our perception of three dimensional shapes, because it introduces a slight variation of light intensities seen by the left and the righe eye under different angles of view and so enables us to see in three dimensions.

2.2.1   Orientation of specimens.

A study that involves the repeated measurement of a set of variates requires good confidence that each specimen is positioned accurately and imaging is done under constant orientation.

To investigate the accuracy in orientation of specimens, a single specimen was orientated 40

times repeatedly and each orientation was imaged. All foraminiferal specimens are positioned on a faunal slide in keel view with the apperture orientated to the right. Specimens are fixed in as near vertical position as possible but a small amount of variation cannot be avoided. To facilitate correct orientation under the microscope a hemispherical stage was used. All specimens were rotated and tilted so that they show the longest δX value and narrowest δY value. Between each image the specimen was completely removed from under the microsope, so as to requrie repositioning of the specimen prior to taking the next image.

Processing of all Tiff images was carried out by macro to produce the RAW files required for input into the "Trace35_batch.out". Measued variables were determined in the normal way using "Sprep53.out" and "KeelWidth100.out".

The results of the extracted outline data are shown in Table 2.1. Figure 2.1a contains a single image of a processed specimen showing the out line represented by 250 points outputted from "Sprep53.out" Figure 2.1b illustrates the outlines from all 40 specimens superimposed on top of each other.

The results show that only two specimens have values outside of the 95% confidence limits (images 1 and 2). This result demonstrate that a trained operator can achieve persistently accurate positioning of individual specimens into the same orientation. This experiment gives a high degree of confidence in the values measured from specimens studied in this thesis.

2.2.2 Illumination.

Variation in llumination is caused by either too much illumination or too little, and is often introduced by chosing an incorrect diphragm or setting an unfavorable light intensity. Too bright illumination causes overexposure and which results in the incorrect outline being traced. Another disturbing problem is reflective light, which appears on the saved Tiff file as white speckles within the background or on the object. These can lead to interference with the object giving incorrect readings of the outline coordinats or causing the "Trace35_batch.out" outline extraction program
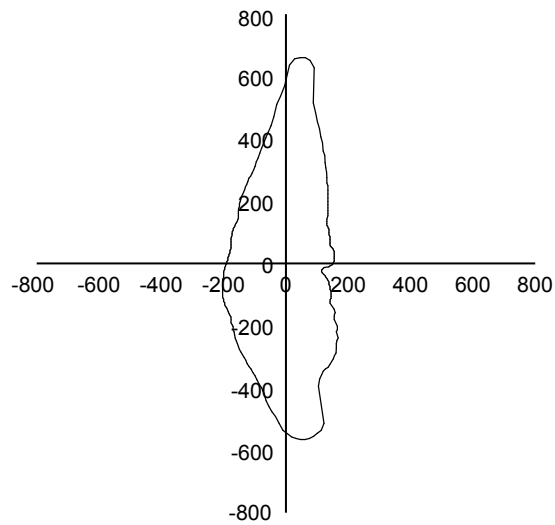
Figure 2.1a Single outline from the output of "S-prep53.out
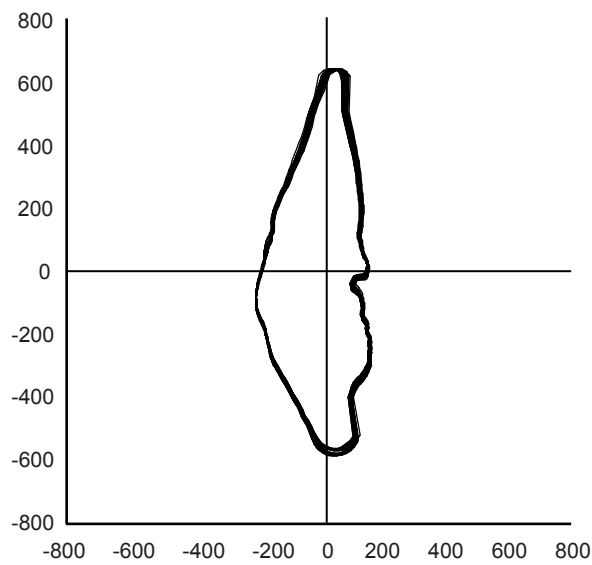
Figure 2.1b Superimposition of all 40 outlines

Superimposition of all 40 outlines of the specimen from the Output of "S-prep53.out showing how closely they correlate

Table 2.1   Results from the orientation experiment

Image number	∂X (μm)	∂Y (μm)	Ar (mm²)	D10 %	D90 %	Phi1°	Phi2°	Phi3°
image 1	371.8	1223.7	0.281	0.25	0.48	48.02	26.048	133.583
image 2	371.8	1227.1	0.284	0.26	0.48	46.353	26.816	133.42
image 3	368.4	1223.7	0.277	0.26	0.48	46.031	26.522	133.271
image 4	365	1220.3	0.274	0.25	0.48	45.79	26.38	133.46
image 5	365	1220.3	0.273	0.25	0.48	45.515	26.437	133.622
image 6	365	1216.9	0.273	0.26	0.47	44.172	26.944	133.469
image 7	361.6	1220.3	0.273	0.26	0.47	44.162	26.813	133.727
image 8	368.4	1223.7	0.277	0.28	0.47	46.814	26.239	132.903
image 9	361.6	1220.3	0.273	0.27	0.47	44.576	26.685	133.438
image 10	365	1220.3	0.274	0.27	0.47	45.551	26.358	132.866
image 11	361.6	1220.3	0.274	0.27	0.47	46.28	25.993	132.907
image 12	365	1216.9	0.273	0.26	0.47	44.491	26.699	133.49
image 13	361.6	1220.3	0.273	0.26	0.47	45.641	26.165	132.864
image 14	365	1220.3	0.273	0.25	0.47	44.655	26.768	133.316
image 15	365	1227.1	0.277	0.25	0.47	45.39	26.477	134.114
image 16	361.6	1216.9	0.270	0.25	0.46	44.585	26.553	133.588
image 17	361.6	1220.3	0.272	0.26	0.47	45.834	26.401	134.245
image 18	365	1220.3	0.272	0.25	0.47	44.952	26.532	133.614
image 19	361.6	1216.9	0.273	0.25	0.48	47.9	25.219	132.777
image 20	361.6	1216.9	0.272	0.26	0.48	44.592	26.529	134.12
image 21	365	1216.9	0.273	0.26	0.47	45.112	26.57	133.335
image 22	365	1220.3	0.273	0.25	0.47	45.212	26.506	132.982
image 23	361.6	1220.3	0.274	0.26	0.48	44.585	26.441	133.675
image 24	365	1220.3	0.272	0.26	0.47	44.2	26.875	133.624
image 25	368.4	1223.7	0.276	0.27	0.47	46.814	26.229	133.02
image 26	361.6	1220.3	0.272	0.25	0.47	45.078	26.335	134.035
image 27	365	1216.9	0.272	0.25	0.47	46.82	25.852	133.053
image 28	368.4	1220.3	0.276	0.26	0.48	46.253	26.633	133.495
image 29	365	1227.1	0.277	0.25	0.48	45.116	26.481	133.92
image 30	361.6	1220.3	0.273	0.26	0.47	45.395	26.375	133.863
image 31	361.6	1220.3	0.274	0.27	0.47	46.188	26.014	132.79
image 32	361.6	1220.3	0.274	0.27	0.47	45.347	26.326	133.401
image 33	361.6	1220.3	0.273	0.26	0.47	44.477	26.685	133.283
image 34	365	1223.7	0.277	0.28	0.47	43.939	27.134	134.291
image 35	361.6	1220.3	0.273	0.26	0.47	46.587	25.546	132.459
image 36	365	1216.9	0.273	0.26	0.47	45.953	26.243	132.928
image 37	365	1220.3	0.273	0.25	0.48	45.515	26.437	133.622
image 38	365	1220.3	0.274	0.25	0.48	44.85	26.532	133.46
image 39	365	1223.7	0.277	0.24	0.47	45.034	26.396	133.816
image 40	361.6	1220.3	0.272	0.25	0.47	45.167	26.321	134.035
min	361.6	1216.9	0.270	0.24	0.46	43.939	25.219	132.459
max	371.8	1227.1	0.284	0.28	0.48	48.02	27.134	134.291
mean	364.320	1220.64	0.274	0.258	0.473	45.474	26.413	133.447
Stdev	2.797	2.755	0.003	0.009	0.005	0.974	0.358	0.447
95% conf	5.483	5.399	0.005	0.018	0.010	1.909	0.702	0.877

to hang. Too little illumination results in a dull image leading to a poor separation of the object from the background, again resulting in an incorrectly traced outline. The use of crosspolarized filters strongly reduces glare and speckling and so overcomes this problem, however at the cost of lower light intensity on the object.

To investigate the effect of changes in the light two experiments were carried out. The first varied the size of the diaphragm of the binoclular, but kept the light source at a constant value. In the second experiment the of light source is varied and the diaphram opening is kept constant. Both experiments were repeated with and without the use of polarizing filters. The magnification was constantly set at 2x and a single specimen was positioned under the microscope and brought into optimum focus to give a good outline. The light source used was an Intralux 4000-1 from Volpi with 2 fiber-glass swan necks allowing lateral illumination

2.2.2.1 First experiment: diaphragma opening – without cross-polarized light.

The illumination was set at a fixed value of one. Processing of the image was carried out using a self-written macro in Nih-image called "automation" as it believed that method provides the most consistancy. The listing of macro automation is in appendix 1. Images were taken at diphragma values 1, 2, 3, 4 and 5 readfrom the body of the microscope. A 0 means a completely closed diaphragma and insufficient light is passed to allow imaging of the specimen. This procedure was repeated with with the illumination increased to a value of two. The resultant Tiff and processed Raw files are shown in Figure 2.2.

2.2.2.2 First experiment: diaphragma opening – with cross-polarized light

The above procedure was repeated but polarizing filters were placed on the tips of the fiber glass swan necks and between the microsope objective lense and the camera. All other parameters were unchanged as for the non-polarized series. With the illumination set at mark one, there was too little light for specimens to be traced to outline coordinates. The resultant Tiff and processed Raw images are shown in Figure 2.3.

Illumination set at 1

Illumination set at 2

Tiff-image Raw-image

Tiff-image Raw-image
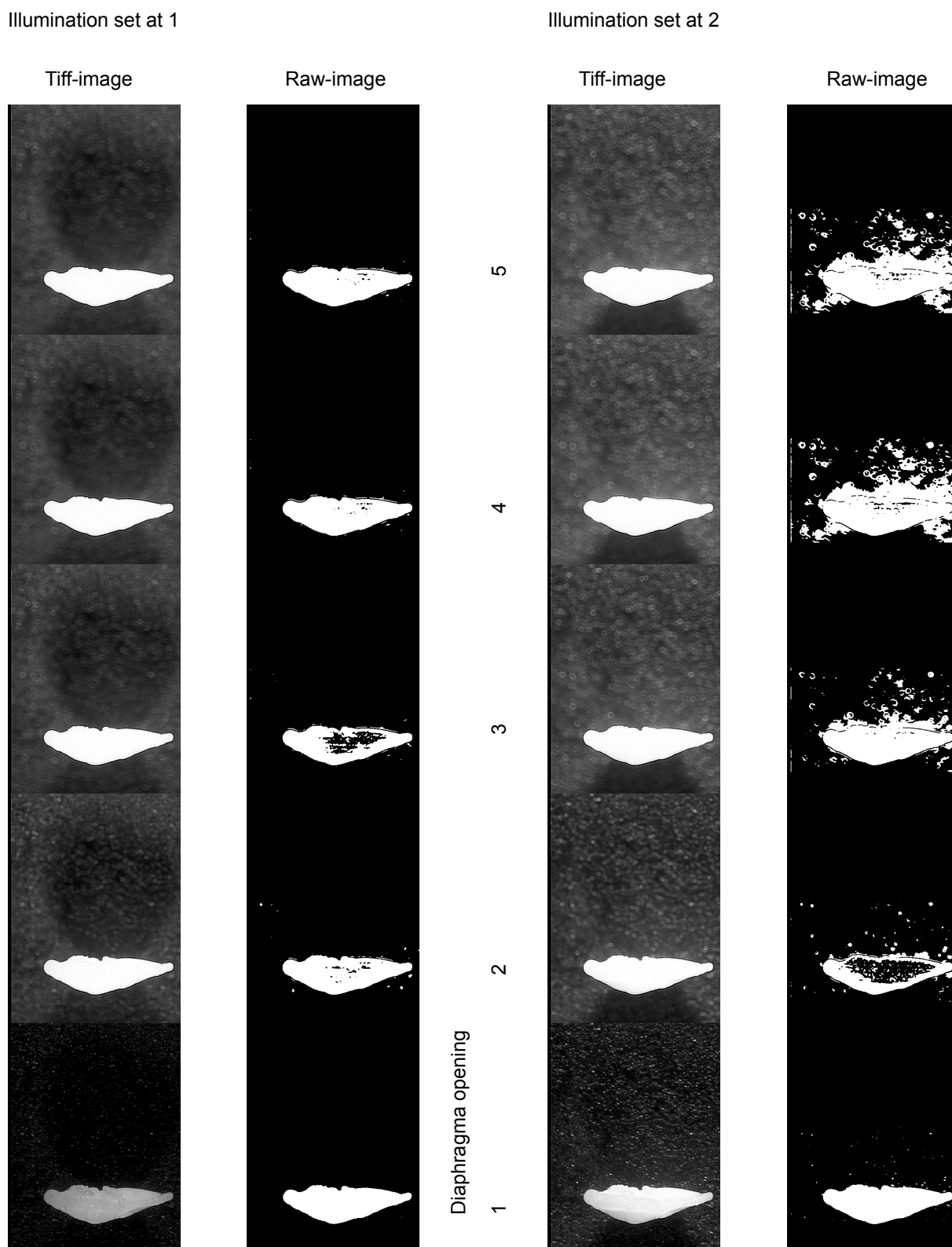
Figure 2.2   Experiment 1: changing diaphragma

Left column 256 grey scale Tiff images obtained during imaging
Right column processed binary Raw files.

Illumination set at 2
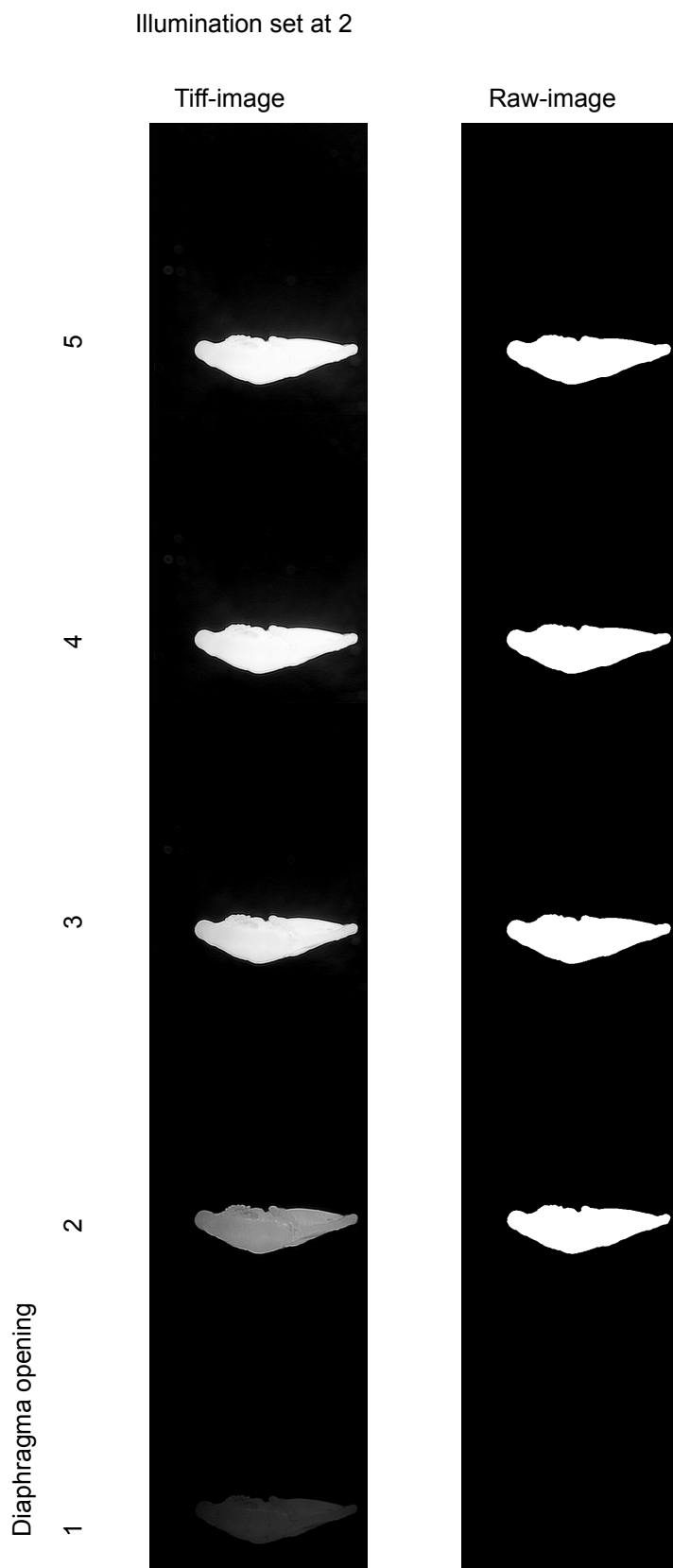
Figure 2.3   Experiment 1: changing diaphragma

Left column 256 grey scale Tiff images obtained during imaging
Right column processed binary Raw files.
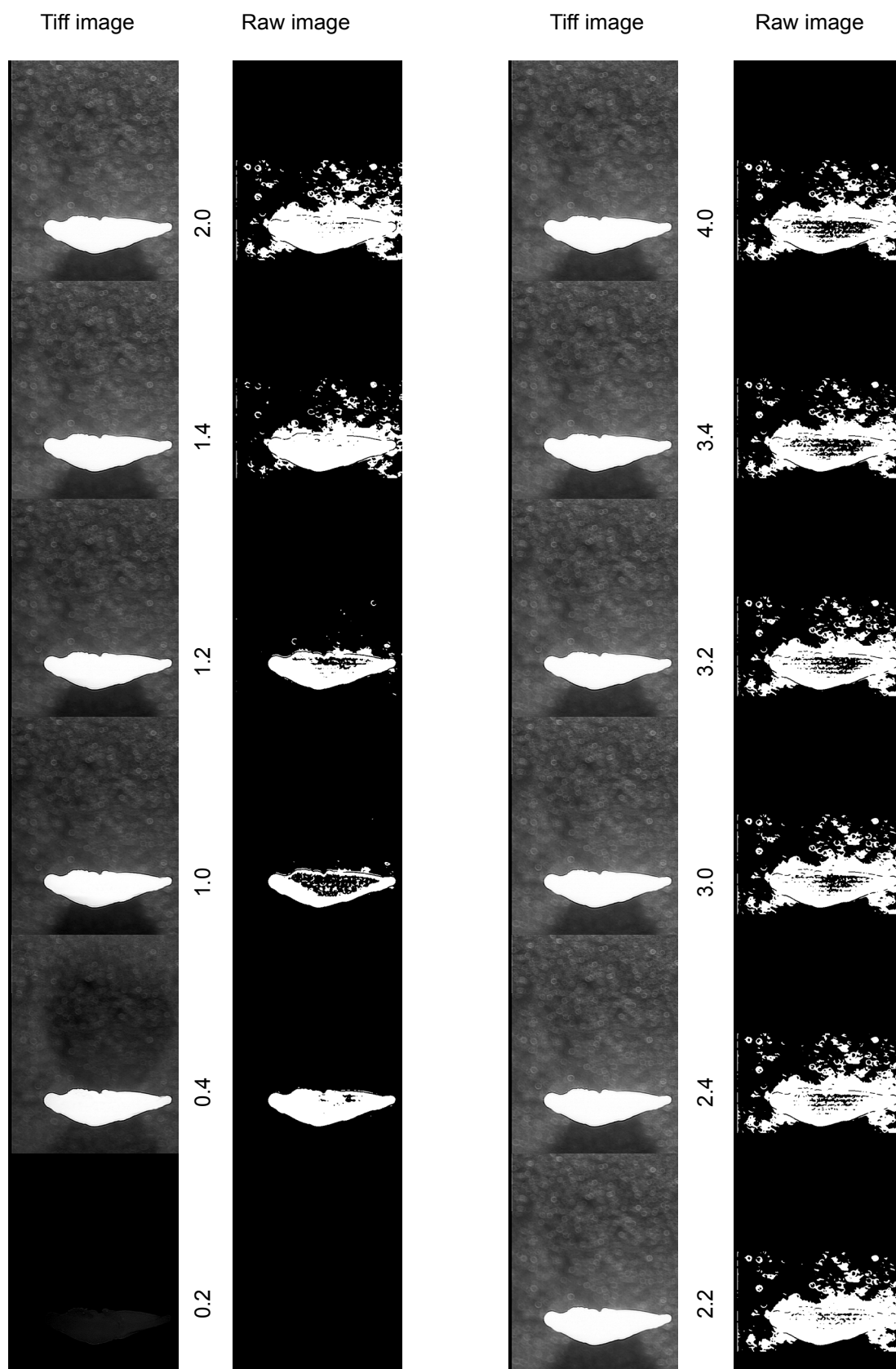
Figure 2.4   Experiment 2: Changing Illumination
Diaphragma opening set to 5 (Maximum opening)
Left column 256 grey scale Tiff images obtained during imaging
Right column processed binary Raw files.
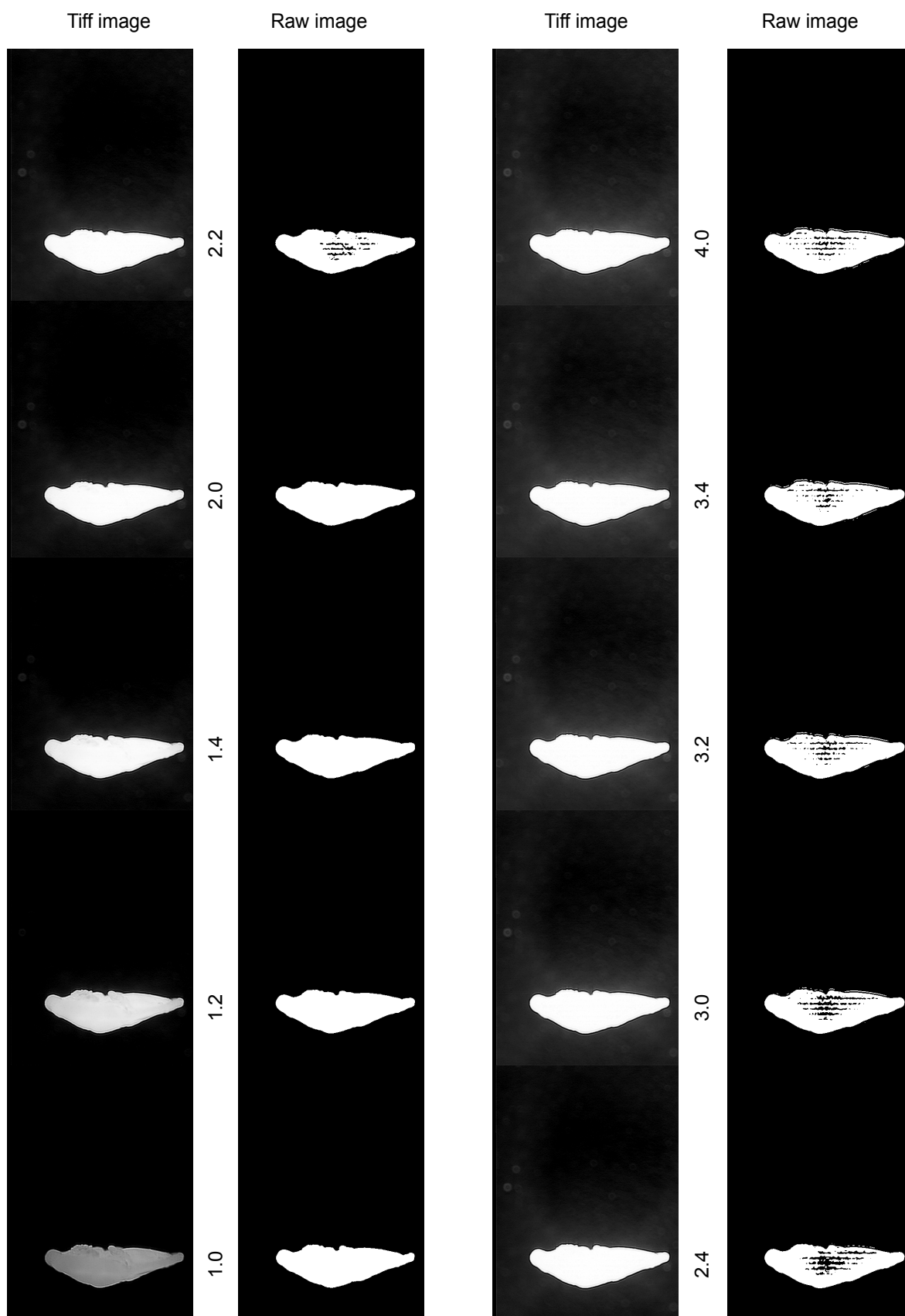
Figure 2.5 Experiment 2: Changing Illumination

Diaphragma opening set to 5 (Maximum opening)
Left column 256 grey scale Tiff images obtained during imaging
Right column processed binary Raw files.

2.2.2.3 Second experiment: Variation in strength of illumination.

With the diaphragma opening set to position 5 (= fully open) the illumination was varied from mark 0.2 to 4.0 using the scale on the Volpi light box. Images were taken and processed again using the Nih-Image macro "automation". The resultant pairs of images are shown in Figure 2.4 (non-polarized light) and Figure 2.5 polarized light.

2.2.2.4 Discussion

Figure 2.1 shows the pairs of Tiff and Raw images obtained after processing for non-polarised light. The left column of images pairs are with the illumination set at 1. The right column of image pairs show the situation with the illumination set at 2. The diaphragma opening is indicated between each column pair. With the illumination set at 1 and diaphragma opening at 1 the Tiff image shows low contrast, but the resultant Raw file produced with the macro "automation" has good definition and the field is clean of speckling. As the diaphragma is opened an increse in speckling is observed. This speckling would require removing by hand, using Adobe Photoshop, before the Raw file could be used for outline extraction. The level of speckling in each processed image is observed to increase with every subsequent increase in diaphragma opening. With the illumination set at 2 even with the diaphragma opening set at 1 there is a great deal of scattering in the background. The Raw files from a value of two and higher are considered unusable for morphometric analysis. In the repeated experiment using the polarizing filters, there was too little light for imaging with the illumination set at 1. Figure 2.2 shows the results for variation in the diaphragma opening with the illumination set at 2. Although the Tiff images show low contrast in comparison to those in Figure 1, all the Raw files except image 1 produced reasonable thresholded images.

Figure 2.3 illustrates the situation with the diaphragma opening set to maximum (5) and the light source varied between 0.2 and 4.0. All Tiff images from an illumination of 0.4 or higher produced good contrast. However, with these settings only illumination at 0.4 produced a reasonable black and white imaged that can be traced for outlines.

Figure 2.4 shows the same experiment 2, but with polarized filters used. With the illumination set below 1 it was not possible to obtain a usable Tiff image. With illumination values between 1 and

2.2 the Raw binary images are considered to be perfect for outline extraction. The Raw images from illumination between 2.4 and 3.0 are considered acceptable but would require manual post processing of the images to ensure that the correct outline is extracted, and to prevent program "Trace35_batch.out" hanging. With illuminations between 3.2 – 4.0 it would be possible to manually clean the images but the effort wold be greater.

2.2.3   Variation of image quality due to digital processing

All imaged specimens are processed to produce an optimal image for the "Trace35_batch.out" outline extraction program. For this program to read the image, it is necessary to have a black and white binary image without any header information (Raw format). Initially, all images were manually processed from the 256 level gray scale images to the binary Raw image using Adobe Photoshop, which was very time consuming. In order to increase efficiency the macro "automation" was written in Nih-Image. This macro allowed to semi-automate the grey-level image to black and white image conversion within seconds. In the following manual processing of images using Adobe Photoshop is compared with semi-automated processing using the macro "automation" are compared with each other. All other variables (illumination, magnification, diaphragma opening) were kept constant for this purpose.

2.2.3.1 Image caputure and processing

Basic collection of images wsing Nih-Image was perfomed in the folloing steps in Nih-image:

  Sharpen
  Smooth
  Sharpen
  Smooth
  Sharpen
  Smooth
  Multiply by 1.25 to increase Contrast.
  Save as Tiff file.

This sequence of processing steps was elaborated by experimentation and is implemented in the Nih-Image macro "Automation" (see appendix 2.1).

For continued manual processing in Adobe Photoshop, the Tiff file was converted into a black and

Table 2.2   **Comparison of the image processing methods**

Processing method - Hand

Specimen	26	27	28	29	30	31	32	33
δX (μm)	368.4	365	368.4	378.5	324.5	324.5	388.7	439.4
δY (μm)	1220.3	1196.5	1240.7	1159.1	1267.9	1210.1	1084.4	1352.9
Ar (mm^2)	0.2812	0.2739	0.283	0.2654	0.2554	0.2445	0.2634	0.3754
D10 %	0.28	0.29	0.27	0.23	0.34	0.26	0.28	0.22
D90 %	0.49	0.45	0.36	0.42	0.32	0.36	0.4	0.45
Phi1°	47.594	37.305	43.832	42.158	29.779	38.972	42.618	45.781
Phi2°	25.781	31.999	26.46	31.365	33.261	24.172	40.049	29.56
Phi3°	132.52	136.779	141.841	134.849	143.503	137.466	129.895	141.367

Processing method - Macro

Specimen	26	27	28	29	30	31	32	33
δX (μm)	368.4	368.4	371.8	378.5	324.5	324.5	381.9	439.4
δY (μm)	1220.3	1196.5	1244.1	1162.5	1267.9	1210.1	1081	1359.7
Ar (mm^2)	0.2827	0.278	0.2856	0.2663	0.2531	0.2441	0.2545	0.3787
D10 %	0.28	0.3	0.26	0.22	0.34	0.25	0.27	0.23
D90 %	0.49	0.44	0.36	0.42	0.32	0.36	0.4	0.47
Phi1°	44.685	37.698	44.215	42.17	29.701	39.029	43.06	46.74
Phi2°	27.188	32.204	26.583	31.234	33.463	24.16	39.602	28.947
Phi3°	133.844	136.614	141.786	135.394	143.789	137.346	130.426	141.222

Difference

Specimen	26	27	28	29	30	31	32	33
δX (μm)	0	3.4	3.4	0	0	0	-6.8	0
δY (μm)	0	0	3.4	3.4	0	0	-3.4	6.8
Ar (mm^2)	0.0015	0.0041	0.0026	0.0009	-0.0023	-0.0004	-0.0089	0.0033
D10 %	0	0.01	-0.01	-0.01	0	-0.01	-0.01	0.01
D90 %	0	-0.01	0	0	0	0	0	0.02
Phi1°	-2.909	0.393	0.383	0.012	-0.078	0.057	0.442	0.959
Phi2°	1.407	0.205	0.123	-0.131	0.202	-0.012	-0.447	-0.613
Phi3°	1.324	-0.165	-0.055	0.545	0.286	-0.12	0.531	-0.145

% difference

Specimen	26	27	28	29	30	31	32	33
δX (μm)	0.000	0.927	0.919	0.000	0.000	0.000	-1.765	0.000
δY (μm)	0.000	0.000	0.274	0.293	0.000	0.000	-0.314	0.501
Ar (mm^2)	0.532	1.486	0.915	0.339	-0.905	-0.164	-3.437	0.875
D10 %	0.000	3.390	-3.774	-4.444	0.000	-3.922	-3.636	4.444
D90 %	0.000	-2.247	0.000	0.000	0.000	0.000	0.000	4.348
Phi1°	-6.305	1.048	0.870	0.028	-0.262	0.146	1.032	2.073
Phi2°	5.313	0.639	0.464	-0.419	0.605	-0.050	-1.122	-2.095
Phi3°	0.994	-0.121	-0.039	0.403	0.199	-0.087	0.408	-0.103

white binary using the available tools under the menus Image/adjust. The image was edited from cleaning and then saved in Raw file format.

When using the macro "Automation" in Nih-Image a binary image was produced by using the built in density slice function, the optimum was value was determined by experimentation to be a value of 1.160. The binary functions "erode" and "dilate" are used iteratively to remove single white pixels from the edge of the thresholded and binarized image. Such single pixel wide embayments have been found to cause the "Trace35_batch.out" program to hang and must be removed prior to outline extraction. At the end the macro inverts the image and exports it in Raw format. After processing to Raw files outline data were generated using "Trace35_batch.out", "Sprep53.out" and "KeelWidth100.out" programs as described in Knappertsbusch, (1998, 2004, and 2007 (submitted to Carnets de Geologie).

2.2.3.2 Reults

The results outputted from "Sprep53.out" and "KeelWidth 100.out" are shown in table 2.2.

The differences were determined by subtracting the hand processed values from the macro values. If the values for the hand processed specimen are larger then the results will have a negative difference. If the macro processed values are larger then the difference will be positive. A zero indicated no difference. Percentage difference was determined by subtracting the hand processed result from the macro processed result and dividing by the mean of the hand and macro processed values then multiplying by 100.

2.2.3.3 Disscussion

From the table of the results neither method results in specimens having constantly larger or smaller values. Both methods give results that are very similar, the maximum variation observed for δX or δY measurements is 1.7%. The largest difference observed is for Phi1° angle being a 6% difference between the two methods. Maximum variation for the total area is 1.5%.

The results show, that there is no significant variation between the two methods. The main difference being the time saving using the macro to process the images.

2.3   Conclusions

Manual orientation of specimes into identical positions is possible at great accuracy.

1. Illumination, variation of diaphragma opening and the usage of polarizing filter have a great influence on the precise outcome of extracted outlines of the imaged object.

2. The use of polarzing filters significantly reduces specling of images.

3. When using polarizing filters good grey-level images are obtained at a greater range of diaphragma openings.

4. The use of polarizing filters strongly reduces the nesessary amount of post processing of the resulting Raw files, which is a significant increase in efficiency for the automatic collection of morphometric data from light microscopic images.

5. The application of macro "Automation" in Nih Image enhances speed, quality, repeatablity and precision of digital outline extraction of microfossils in reflected light.

Appendix 2.1

```
macro "Automation" [A]';
{Macro for processing foraminifers in reflected light,
using the Leica binocular, and with polarizers.
Written by Kevin Brown in 2004}
var
                counter,x,y: integer;
begin;
     AverageFrames('Average',16);
                for counter:=1 to 3 do begin
                          Sharpen;
                          Smooth;
                          end;
                          MultiplyByConstant(1.25);
end;

macro 'Saving as Tiffimage [T]';
begin;
     SetSaveAs('TIFF');
     SaveAs('name');
end;


macro 'Foram Processing For Single File [P]';
{for a single file}
var
    x,y:integer;

begin
    X:=GetNumber('Enter width of left black border (number of
pixels (55)):',x);
    y:=640;
        SetDensitySlice(1,160);
    MakeBinary;
    Invert;
                Erode;
                Dilate;
                Erode;
                Dilate;
    MakeROI(0,0,x,y);
    Fill;
    KillROI;
    MakeROI(350,0,480,640);
    Fill;
    KillROI;
```

```
        Invert;
   end;



macro 'Export as RAWfile [R]';
begin;
                  SetExport('RAW');
                  Export('name');
        StartCapturing;
end;



macro 'Rotate left [N]';
var
                  xscale,yscale,angle: integer
begin;
MakeROI(0,0,640,480);
                  xscale:=1;
                  yscale:=1;
                  angle:=-1;
                  ScaleAndRotate(xscale,yscale,angle);
end;



macro 'Rotate Right [M]';
var
                  xscale,yscale,angle: integer
begin;
MakeROI(0,0,640,480);
                  xscale:=1;
                  yscale:=1;
                  angle:=1;
                  ScaleAndRotate(xscale,yscale,angle);
end;
```

Global morphological variability in Late Pleistocene to Holocene menardiform globorotalia

Kevin Brown and Michael Knappertsbusch
Natural History Museum Basel
Augustinergasse – 2
Basel
CH 4001
Switzerland

Email: kevin-r.brown@unibas.ch

Tel: +00 41 61 2665 561

Fax   +00 41 61 2665 546

Abstract

Morphological analysis of over six thousand orientated specimens of "menardi-form" globorotalids from 70 Late Pleistocene – Holocene samples sites representing the range of this tropical group was carried out. Analysis of morphological variation allowed identification of 2 morphoclines and a total of six distinct morphotypes (e.g. the menardi-form morphotypes α, β, χ and η and the two tumid form morphotypes ε and ϕ,) which show association to distinct environmental conditions. In the bivariate morphospace of spiral height versus axial diameter the equation $y = 2.07x - 15$ separates morphocline 1 (*Gr. menardii* morphologies) from morphocline 2 (*Gr. tumida* morphologies). Within morphocline 1 the line with equation $y = 3.2x - 160$ separates morphotypes α (*Gr. menardii menardii*) from morphotype β (*Gr. menardii cultrata*).

Morphotype β is interpreted as *Gr. menardii cultrata* and is seen to dominate environments where the mean annual sea surface temperature is over 25°C. Morphotype α is interpreted as *Gr. menardii menardii* and becomes more dominant as sea surface temperatures become cooler. In areas where both morphologies are present in a sample we interpreted the situations a vicariant trophic depth adaption. *Gr. menardii* cultrata lives at shallow depths, while *Gr. menardii menardii* occurs deeper within the water column.

Gr. menardii gibberula represents another morphotype with the high spared forms of the *Gr. menardii* group and is found only at the southerly extent of the sample set. Specimens have been identified in sample sites from the Western Pacific which extends its known biogeographic range.

Within the morphocline 2 *Gr. tumida* and *Gr. ungulata* are very similar. The diminutive size and delicate structure of *Gr. ungulata* is suggestive of it being the shallow dwelling juvenile form with being *Gr. tumida* the deeper dwelling more robust adult form.

Key words

Foraminifera. Morphometrics. Morphotype analysis. Globorotalia.

3.1   Introduction

Foraminifera are marine calcite secreting protists, which have a wide geographical distribution and preservation of their calcitic shells in marine sediments is often excellent. These characteristics make them ideally suited for use in biostratigraphical correlation, climatic research and evolutionary studies. Phylogenetic relationships and lineages have been studied, and parent / daughter species relationships inferred using morphological characteristics and stratigraphic correlation (Kennett and Srinivasan 1983). Often foraminifera with intermediate morphology are present which show evolutionary trends e.g. Bolli's 1950 study of the *Globorotalia foci*, the *Globigerinodies orbulina* lineage (Blow 1956; Wade 1964, 1966) *Globorotalia* (*Turborotalia*) *centralis* to *Gr*. (*T*) *cerroazulensis* lineage (Blow and Banner, 1962) to name a few. However, recent advances in our understanding of extant foraminiferal species level diversity have occurred through the use of genetic techniques. Studies of ribosomal DNA (rDNA) has shown that what have been traditionally been considered to be a single species may represent several genetically distinct populations (Darling et. al., 1996, 1997, 2000, 2004, De Vargas and Pawlowski 1998, De Vargas et. al., 1999) a result with important implications to the application of traditional taxonomy, biostratigraphy and species concepts.

Basic questions about the morphological variation observed in extant species of planktonic foraminifera are:

1) Do accepted planktonic foraminiferal species represent single globally distributed species?

2) Are there identifiable populations with distinct morphological characteristics which have previously been grouped together?

3) Is the morphological variation observed ecophenotypic?

4) Are recognizable morphologies linked to distinct regional or large scale open marine habitats?

In this context the present work investigates:

1. The global morphological variation within the *Globorotalia menardii – Globorotalia*

tumida plexus, observed in Late Pleistocene – Holocene sediments.

2. The quantative criteria for subdivision of the modern *Gr. menardii* group, that are based on observed morphological variation.

3. The links between the identified morphologies and environmental factors.

Globorotalia menardii and *Globorotalia tumida* are recognized end members of a group of morphologically similar Neogene planktonic foraminifera. They share a distinctive trochospiral lenticular morphology which shows a range of variation. The earliest biometric studies of the *Gr. menardii – Gr. tumida* plexus was carried out in 1934 by Schmid. Studying material of Pliocene age from Ceram (Indonesia) Schmid concluded that *Gr. menardii – Gr. tumida* are single species with *Gr. menardii* representing a microspheric form and *Gr. tumida* the megalospheric morphologies of the species. Scott (1973) investigated morphological variation within the *Gr. menardii* group form sediments of the Western Pacific Ocean. His results showed that greatest morphological variation occurs in spiral height. The biogeographic range of both species is dominantly tropical, so much so that their presence or absence has been used to indicate warm / cold intervals within Atlantic and Caribbean cores (Emiliani 1964 and 1969, Ericson and Wollin 1968, Ruddiman 1971). In these studies, *Gr. menardii* and *Gr. tumida* are grouped together and referred to as the "*Globorotalia menardii*" complex. Also Todd (1964), in cores of Holocene age from Enwetok Atoll (Pacific Ocean) described „the menardii-tumida complex". Identifying end members but describing the majority of specimens as having "menardii-tumida intermediate transitional morphologies", no quantitative attempt to differentiation the morphologies was made until present. Stainforth et al. (1975) used the term "menardiform" to describe a subgeneric group of keeled globorotalids e.g. *Menardella* and *Globorotalia*.

3.1.1 Taxonomic concept

Genus: *Globorotalia* Cushman 1927.

Type species: *Pulvinulina menardii* var. *tumida* Brady ,1877

3.1.1.1 History of the genus name:

The genus Globorotalia represents a stratigraphically important group of Late Neogene planktonic foraminifera. They are recognized by a lenticular trochospiral test with extraumbilical-peripheral aperture, a non-spinose shell and a smooth wall texture. Blow (1969) subdivided the *Globorotalia* into two subgenera *Globorotalia (Globorotalia)* and *Globorotalia (Turborotalia)*, on the basis of presence or absence of a peripheral keel. These subgenera, however, ignore phylogenetic relationships and as such are artificial from a taxonomic view point (Kennett and Srinivasan 1984). Bandy (1972) erected several subgenera using the implied phylogenic relationships to further subdivide the Globorotalia. The two subgenera encountered during that study are *Globorotalia (Globorotalia)* and *Globorotalia (Menardella)*. Although these subgenera show similar taxonomic features they have distinct polygenetic lineages (Kennett & Srinivasan, 1983; Blow, 1979). Here in the *Gr. praescitula – acheomenardii – praemenardii - menardii* lineage was placed within the new subgenus *Globorotalia (menardella)*. While the *Gr. lenguaensis – paralenguaensis – merotumida – plesiotumia - tumida* lineage remained in the *Globorotalia (globorotalia)* subgenus.

3.1.1.2 History of species names:

The designation of a type specimen for *Gr. menardii* is historically controversial and complex, reference is made to Banner and Blow (1960, 1962), Todd (1962), Stainforth et. al. (1975, 1978). d'Orbigny first used the name *Rotalina menardii* in 1826 in a list of models of specimens found in beach sands collected near Rimini, Italy. The specimen was assumed to be Recent (Holocene) in age, however the specimen in now accepted as being reworked from nearby Miocene deposits. No illustration or description was given, at the time, only a model was made available to private subscribers and as such the name was not then made available. The specimens themselves and any topotypic material have been lost. The name was finally made available in 1865 when Parker, Jones and Brady applied the name *"Rotalina menardii"* d'Orbigny to specimens dredged

from the sea floor off the Isle of Man (Parker, Jones and Brady 1865: 20, pl. 3, fig. 81). In 1839 d'Orbigny described and illustrated *Rotalina cultrata* from beach sands collected in Cuba, Martinique, Guadeloupe, and Jamaica (Banner and Blow, 1960, Stainforth et. al. 1975). Much of the controversy has revolved around which of the two names has precedence as many authors regard *Gr. menardii* and *Gr. cultrata* to be synonymous. Banner and Blow 1960 erected a series of lectotypes to replace the lost d'Orbigny specimens, selecting material held within the Natural History Museum London. In 1982 the ICZN using plenary powers suppressed the lectotypes erected by Banner and Blow (1960), and accepted the specimen illustrated by Stainforth et. al.. (1978). The *Gr. menardii* ecotype selected is from the Upper Miocene (Tortonian) beds in the Senigallia section 70km southeast of Rimini, Italy and is believed to better represent d'Orbigny's *Gr. menardii menardii* (Stainforth et. al. 1978, Melville 1982).

In the present study the generic concept of Blow (1979) is followed, without however, applying subgeneric categories. On the species level identification of individual morphotypes was made by reference to illustrations and descriptions given in Stainforth et. al. (1975), Blow (1979), Kennett and Srinivarsan (1983), Bolli and Saunders (1985), and Cifelli and Scott (1986). Although there was an attempt not to have a bias to a particular concept, the most useful taxonomic schemes or our study were those of Blow (1979), Bolli and Saunders (1985), and Stainforth et. al. (1975). Wherever possible holotypes, lectotypes, neotypes and topotypes from the various publications above have been examined by the authors and compared to the specimens in the present study.

3.2   Materials and Methods

Sample site selection followed the distribution map of Bé (1977) the relative abundance of *Gr. menardii* in surface sediments. *Gr. menardii* has a tropical to subtropical distribution while *Gr. tumida* is known to have a primarily tropical distribution. Latitudinal limits of 30° north and 40° south of the equator were set with a total of 72 sample sites being identified covering a wide range of tropical to subtropical pelagic environments. On analysis 16 of the chosen sites contained no specimens of the *Gr. menardii - Gr. tumida* complex. Fig. 3.1 shows the global distribution of the sample sites. All samples sites were selected so that the material would be from above the local lysocline, with samples being selected from box-core surface samples, multi-corer samples, core tops and trigger weight samples (appendix 3.1). Where possible samples were selected from sites with well documented stratigraphies with Holocene age sediment being selected. If absolute dating was not available then sample sites that where known to be within the *Emiliani huxleyi* acme zone was chosen. Using these criteria the maximum age of the samples is limited to 85 – 90Kyrs before present (Thierstein et. al. 1977).

3.2.1   Sample processing

Bulk samples were dried for 24 hours at 50°C, the dry weight of the sample then being taken. Disaggregation of the sediment was carried out by gently heating the sample in water with a small amount of washing soda added. Samples were wet sieved at 63μm, the portion of the material <63μm being retained. The material ≥ 63μm was dried for 24 hours at 50°C. The washed residue ≥ 63μm fraction was then weighed again.

Washed samples were dry sieved at 125μm and divided into aliquots of varying fractions depending on the amount of material remaining following washing. In size fractions of <125μm globorotalid morphologies converge making identification of individual species and morphotype very difficult. For this reason the lower size limit of specimens was set at 125μm, no upper limits were set. All specimens are taken from the >125μm fraction, attempts where made to obtain a minimum of 75 specimens per sample. The decision only to sieve the sample at 125μm was taken to avoid
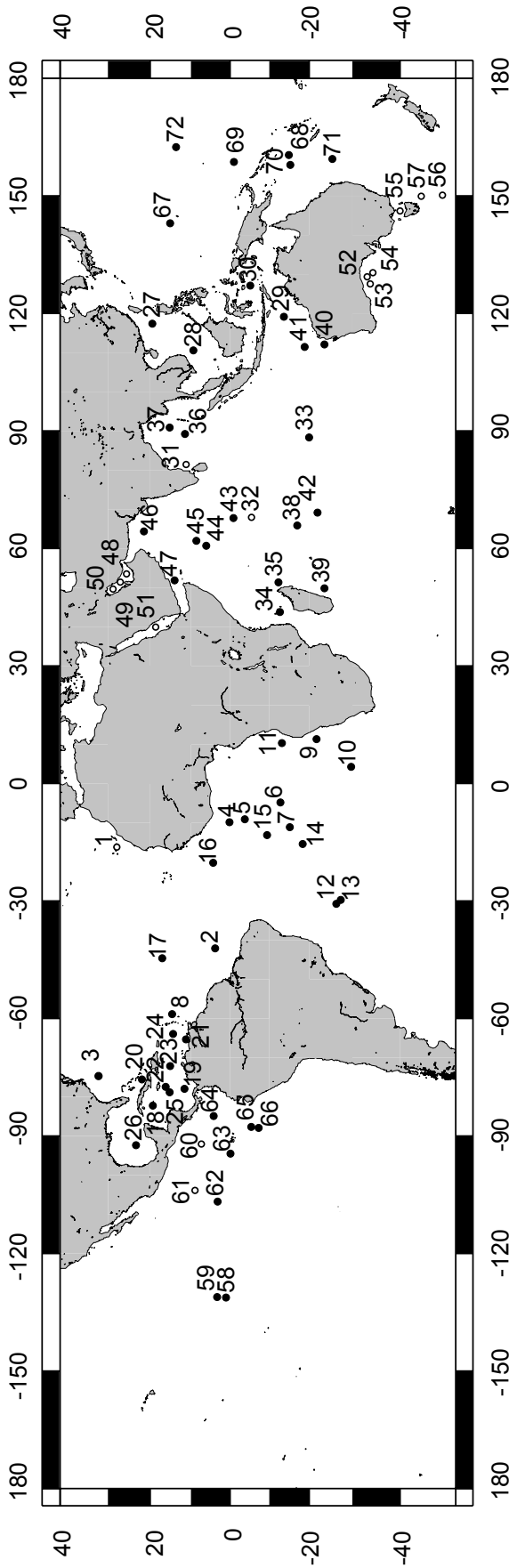
Figure 3.1   Global distribution of sample sites

Sample site distribution used within this study (for sample site locations see Appendix A).

Full circles indicate menardiform globorotalids present in sample.

Open circles indicate menardiform globrotalids absent in sample.

sampling bias within one size fraction and is believed to more accurately reflect the size distribution of the menardiform globorotalids within the sample. The only criteria imposed on selection of specimens were, that the tests were intact, with little or no signs of dissolution, or loss of the final chamber.

3.2.2 Imaging

For imaging all specimens were mounted in keel view on girdded faunal slides with the aperture uppermost positioned to the right. Any sinistral specimens in the samples were imaged as normal but the images were mirrored by using the tool in Adobe Photoshop software so that all specimens have their spiral side to the left side of the image. Digital image acquisition was carried out using a KAPPA CF 11/2 CCD camera mounted on a Leica MZ6 binocular microscope and connected to a Macintosh computer. The microscope is fitted with a Planopo 1x lens and has a 0.63x to 4x zoom body allowing images to be taken at a number of magnifications. Correct orientation of specimens was achieved by use of a hemispherical stage. The correct orientation of the specimens was taken when the spiral height (δX) was seen to be at a minimum and the overall length of the specimen (δY) at maximum value the system has been calibrated, so that pixel values can be directly converted to micrometers.

Image capture was carried out using the public domain NIH Image program (developed at the U.S. National Institutes of Health and available on the Internet at http://rsb.info.nih.gov/nih-image/). A suite of macros were written by ourselves to semi-automate and accelerate image capture and processing. Captured images have a size of 640 x 480 pixels at 256 grey-levels and were saved in TIFF format.

Figure 3.2a shows how the processing of the images reduces the grey-level image (Fig 3.2a-1) to a black and white image (Fig 3.2a-2), which is then saved to disk as a raw file. Cartesian coordinates (Fig 3.2a-3) were generated using the program 'Trace35batch.out', an outline detection program written by one of the authors, Knappertsbusch, (2004). By using the recorded magnification at which the image was captured, values of δX and δY in µm are generated.

Figure 3.2a Image processing steps

2a-1   Gray scale image of foramifera in TIFF format.

2a-2   Black and white raw format image for input to outline extraction programs.

2a-3   Representation of the outline data extracted from raw imagefile by Program Trace35batch.out.
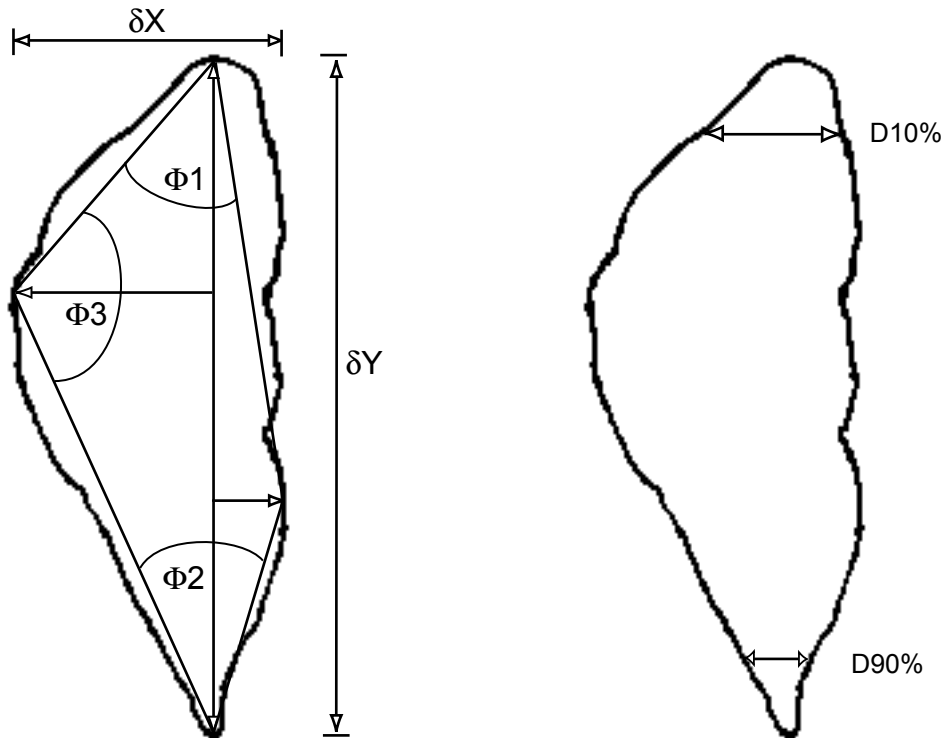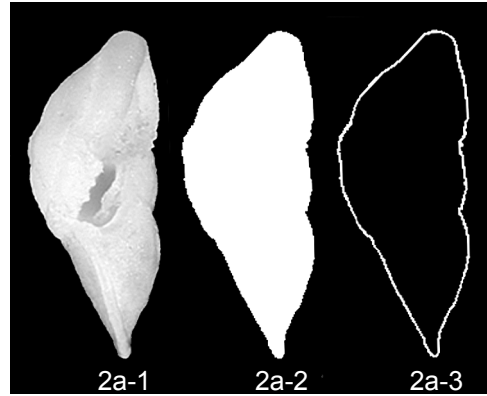
Figure 3.2b Illustration of the measured variates.

δX   spiral height in keel view.
δY   axial diameter in keel view.
φ1   upper keel angle.
φ2   lower keel angle.
φ3   spiral angle.
D10%   width of test 10% down δY.
D90%   width of test 90% down δY.

Analysis of the extracted outline was carried out using a suite of Fortran 77 programs written by one of the authors. The programs include Sprep52, and Keelwidth (Knappertsbusch 2004). Morphometric parameters that were determined are as follows (Figure 3.2b):

δX - spiral height in μm

δY - axial diameter in keel view, in μm

Ar - cross-sectional area in keel view, in mm^2

D10% - keelwith at 10% δy in μm

D90% - keelwith at 90% δy in μm

$\Phi 1$ - Keel angle (upper angle) in degrees

$\Phi 2$ - Keel angle (lower angle) in degrees

$\Phi 3$ - Spiral angle in degrees

The resultant text file is converted into an excel spreadsheet to allow ease of rearrangement, analysis and data plotting.

The results are presented as a series of scatter and contour plots. Scatter plots are used to show the range of morphological variation present, while contour plots are used to view the frequency of distribution and any trends within the sample population. Contouring of δX versus δY also allows for a more convenient analysis of morphotypes in the samples than in scatter plots, any modality within the distribution is clearly visible as peaks with in the contours, while trends can be seen as ridges. A matrix of scatter plots of all measured morphological characters showed that the best morphotype separation can be represented by three variates: δX, δY and the $\Phi 3$ angle. Contouring of the δX versus δY data was carried out using Surface III+ (available from the Kansas Geological Survey web site). The program was set to the intermediate smoothing option for the contours. It should be noted that the area between two contour lines represents a probability space representing a morphometric volume where it is likely to find a particular frequency of foraminifera. The δX versus δY data was first treated using Fortran77 program „Grid.out" from Knappertsbusch (2004), that produces a frequency distribution X Y Z matrix from the raw δX, δY data, with Z being the frequency of the specimens per grid-cell. The bin width was set at $\delta Y = 100$ and $\delta X = 50$ which

was determined as being the optimum setting for this data set, and giving a reasonable range for the Z-values. A decision was made not to use a mathematical transform on the results prior to plotting. This was done as the objective was to view the maximum extent of the variation present in the populations.

3.2.3   Error, Precision and Repeatability

One of the major difficulties to overcome was ensuring that all specimens are correctly orientated. An experiment involving the repeated orientation of a single specimen 40 times has shown that variation of the total area of the specimen is 2%; variations about the mean value of δX and δY varied by 1.8% and 0.8% respectively.

All specimens and CD ROMS containing specimen images in both Tiff and Raw format are deposited at the Natural History Museum Basel.

3.3   Results

A total of 6702 specimens of all morphotypes were imaged and analyzed.

The measured values of δX and δY variates for all specimens are plotted in figure 3.3, in the form of scatter and contour diagrams. These plots show that there are two divergent morphoclines within δX vs. δY data set, the upper arm being designated morphocline1 and the lower arm morphocline 2. A visual separation using a line with equation of y = 2.07x -15 was developed to aid the distinction of the two morphoclines, which is shown in figure 3.4.

The variation within the two identified morphoclines was further investigated with separations based on taxonomic differences, such as thickness of the keel, amount of encrusting, and the Φ3 angle. Biogeographic variation of the morphology was investigated by separating the samples into distinct geographic areas. Morphotype variability and regional abundance is represented in Figures 3.5 and 3.6 for the morphocline 1 (*Gr. menardii* group), and Figure 3.7a and 3.7b for the morphocline 2 (*Gr. tumida* group).

Specimens of morphocline 1 all share a similar lenticular biconvex morphology. A visual inspection based on the measured parameters allowed separation into four morphotypes α, β, η and χ. The separation of morphotypes α and β was aided by a separation line with the equation y = 3.2x –160, which was developed by Knappertsbusch (2007 submitted) in his study in the Eastern Equatorial Pacific and the Caribbean Sea samples following closure of the Panama isthmus. Morphotype α have increased δX values, they show a granular texture and a much heavier keel that is rope like in appearance. Sutures between chambers are much more are often limbate in appearance than in morphotype β. Morphotype β has thin keels, a smooth textural appearance and the most compressed morphology, which is generally more equally biconvex than morphotype α. Extreme forms, towards the larger end of the frequency distributions have a translucent hyaline appearance. It has been suggested (Kate Darling, oral communication 2006) that these hyaline forms may represent non-reproductive specimens. Morphotype η shows the highest spiral height (δX variate). They share the same heavy keel and granular texture as seen in morphotype α although final
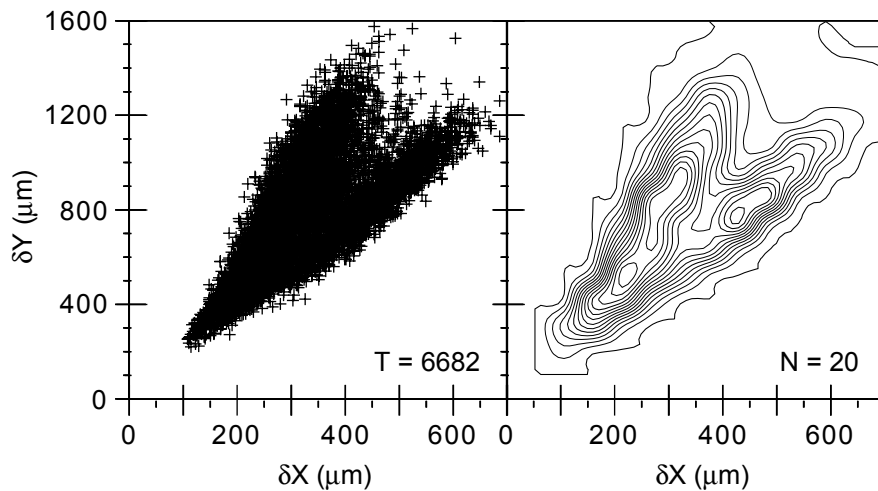
Figure 3.3   Global morphometric variation of Gr. menardii and Gr. tumida in the space of δX versus δY.

chambers can be quite smooth in appearance. The aperture is highly arched and an apertural lip is common. Pustules are common about the aperture. Specimens of morphotype η are differentiated from representatives of Morphocline 2 (morphotype ε) by the shape of the final chamber which is lobate. In morphotype η the spiral side shows greater inflation than the umbilical side. In morphotype ε the final chamber is often radially elongated, and it shows a more bilaterally equal biconvex outline in equatorial view. Morphotype χ is only present in the Indian Ocean, and is considered to be an aberrant form of α and β morphologies. It has a distinctive final chamber that is flexed between 60 – 90°.

Morphocline 2 was separated by taxonomic characters into two morphotypes ε and φ. Morphotype ε showed has a distinctive tumid shape, with the penultimate chamber and final chambers being radially elongated. Very often the final chamber may be aberrant, being diminutive in size. They have an equally biconvex test with heavy calcitic encrusting; the keel is very heavy and may be indistinct due to pustular overgrowth particularly around the aperture. Morphotype φ has a smooth texture, with very small keel and a hyaline appearance. The test is biconvex but there is an offset of the spiral apex against the point of maximum width on the umbilical side. The final chamber has a distinct arched appearance, with a carinate band along the outer edge. Good separation is seen when comparing D 90% against the φ2 angle.

Figure 3.4 Global morphometric variation in morphoclines 1 &2

Figure 3.4a
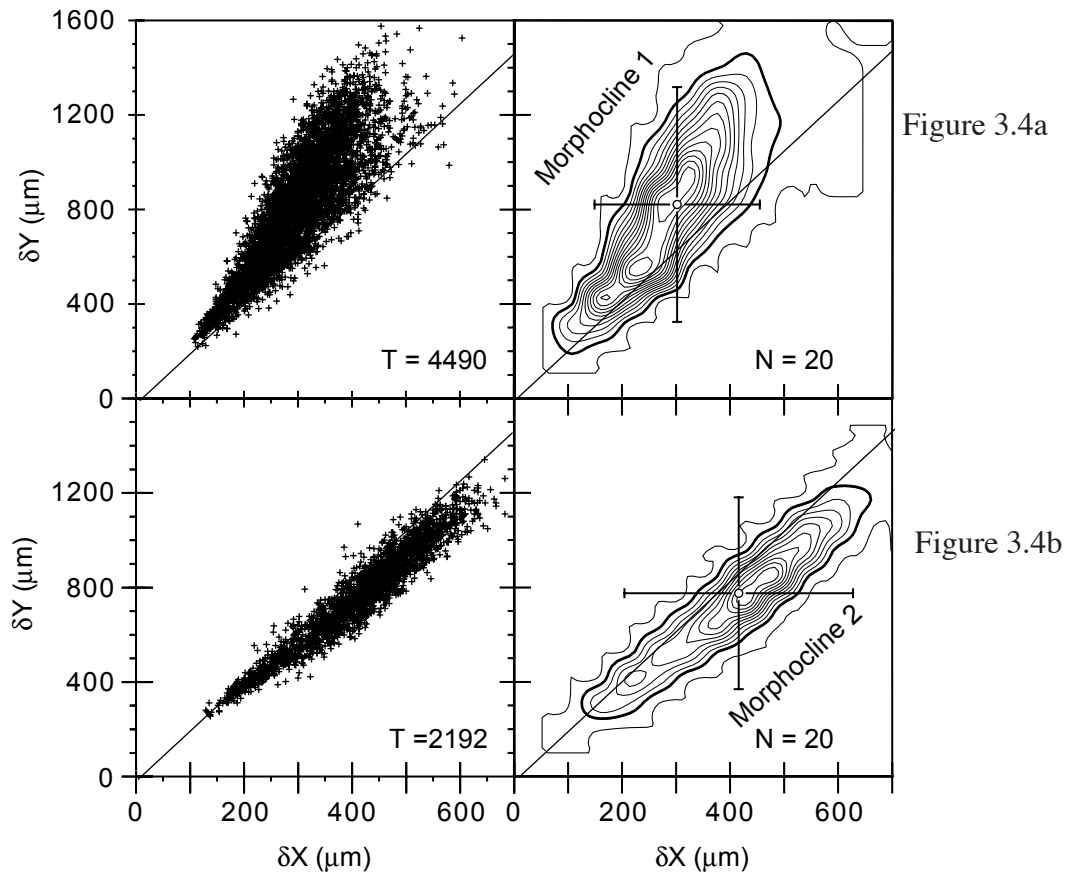
Figure 3.4b

Figure 3.4a   Global morphological variation in the *Gr. menardii* group (morphocline 1).

Figure 3.4b   Global morphological variation in the *Gr. tumida* group (morphocline 2).

T = Total number of imaged specimens in each group

N = Contour interval, number of specimens per gird-cell.

Open circle on the contour plots represents the global mean values for δX and δY for morphocline 1 and morphocline 2. The error bars show the 95% confidence intervals for the global data set for each morphocline.

The diagonal line (equation y = 2.07x -15) separates the two morphocline 1 from morphocline 2. The highlighted contour lines represent the area of frequencies of ≥ 20 specimens per grid-cell and are used as a reference line in Figures 11 and 12.

3.3.1 Histograms of the δX / δY ratios

A histogram is constructed by counting up the number of specimens that are found in individual classes (or intervals). Determining the optimum class interval or bin width has long been a topic of discussion among statisticians. If the bin width is too small the histogram will have to much detail, (under smoothing), multimodality can be introduced where none is present. While too wide a bin width the histogram will have too little detail (over smoothing). In this case multimodality within the sample can be masked. Another important consideration is the starting point of the first class interval. This will vary according to the specimens within individual samples. Only if two samples have specimens with exactly the same measurements will they share the starting points for the class intervals. This problem makes comparing two different histograms difficult.

To overcome these problems the following steps were taken:

1. The total global sample set for morphocline one was used to determine an optimum bin width which was then applied to each individual sample. For the global sample set of morphocline one the optimum bin width was determined to be $0.013\mu m^2$ (formula used given below).

2. The starting point of the first class or interval was set at zero for all histograms.

3.1.1.1 Bin width determination

The determination of optimum bin width follows the method outlined in Keating and Scott (1999), which is reproduced here.

The choice of bin width *(h)* is given by:

$$h = (3.49 * \sigma) \; / \; n^{1/3}$$

where: $\sigma = \min(S, IRQ/1.349)$, S is the sample standard deviation, n is the size of the sample, and IQR is the inter-quartile range of the data set.

Figure 3.9 illustrates the histograms for the Atlantic sample set. For brevity and clarity only
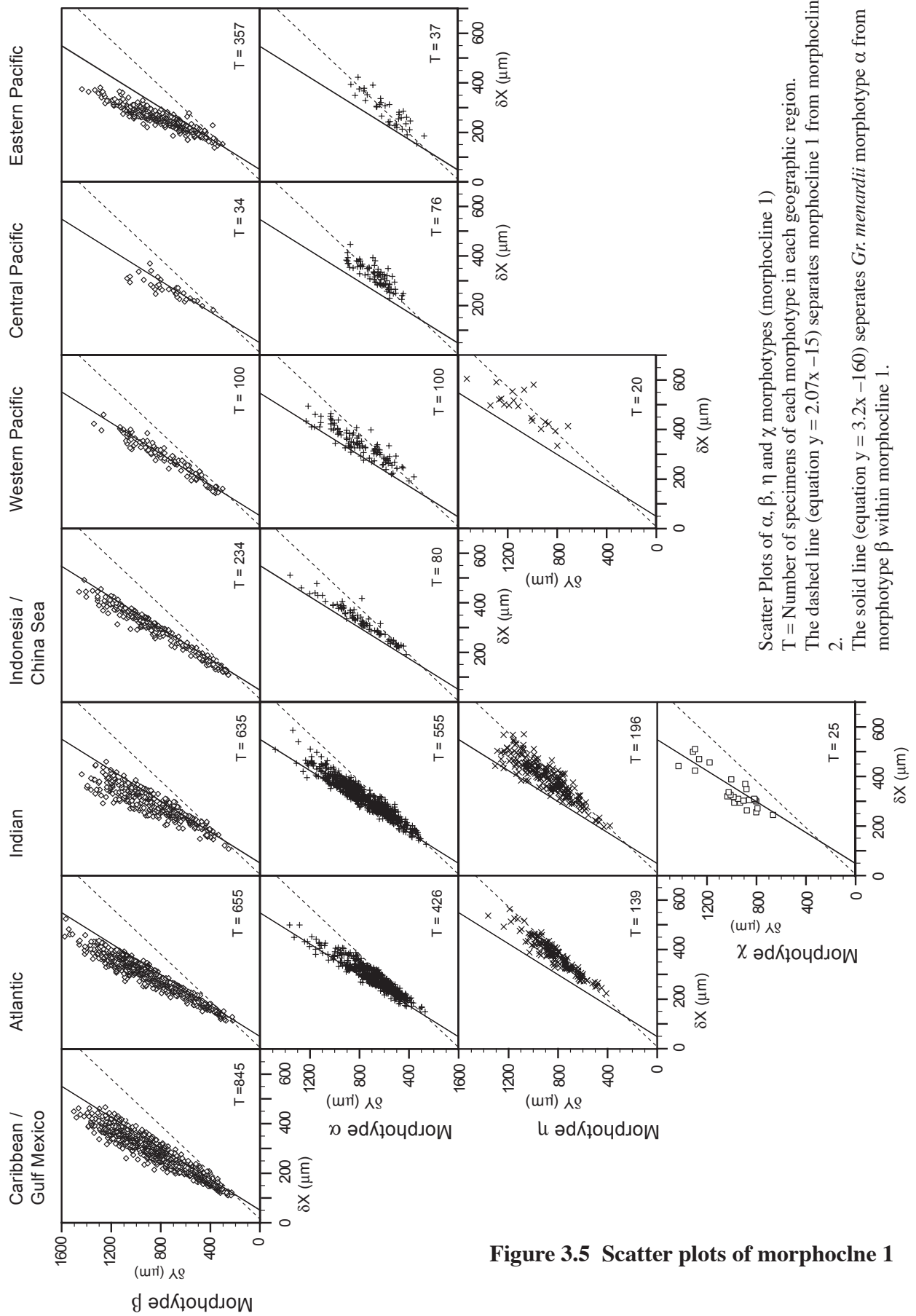
Figure 3.5 Scatter plots of morphoclne 1

Scatter Plots of α, β, η and χ morphotypes (morphocline 1)
T = Number of specimens of each morphotype in each geographic region.
The dashed line (equation y = 2.07x –15) separates morphocline 1 from morphocline 2.
The solid line (equation y = 3.2x –160) seperates *Gr. menardii* morphotype α from morphotype β within morphocline 1.

Figure 3.6 Contour plots of morphocline 1

Contour Plots of α, β, η and χ morphotypes (morphocline 1) as derived from the data shown in Figure 3.5 N = contour intervals in specimens per grid-cell
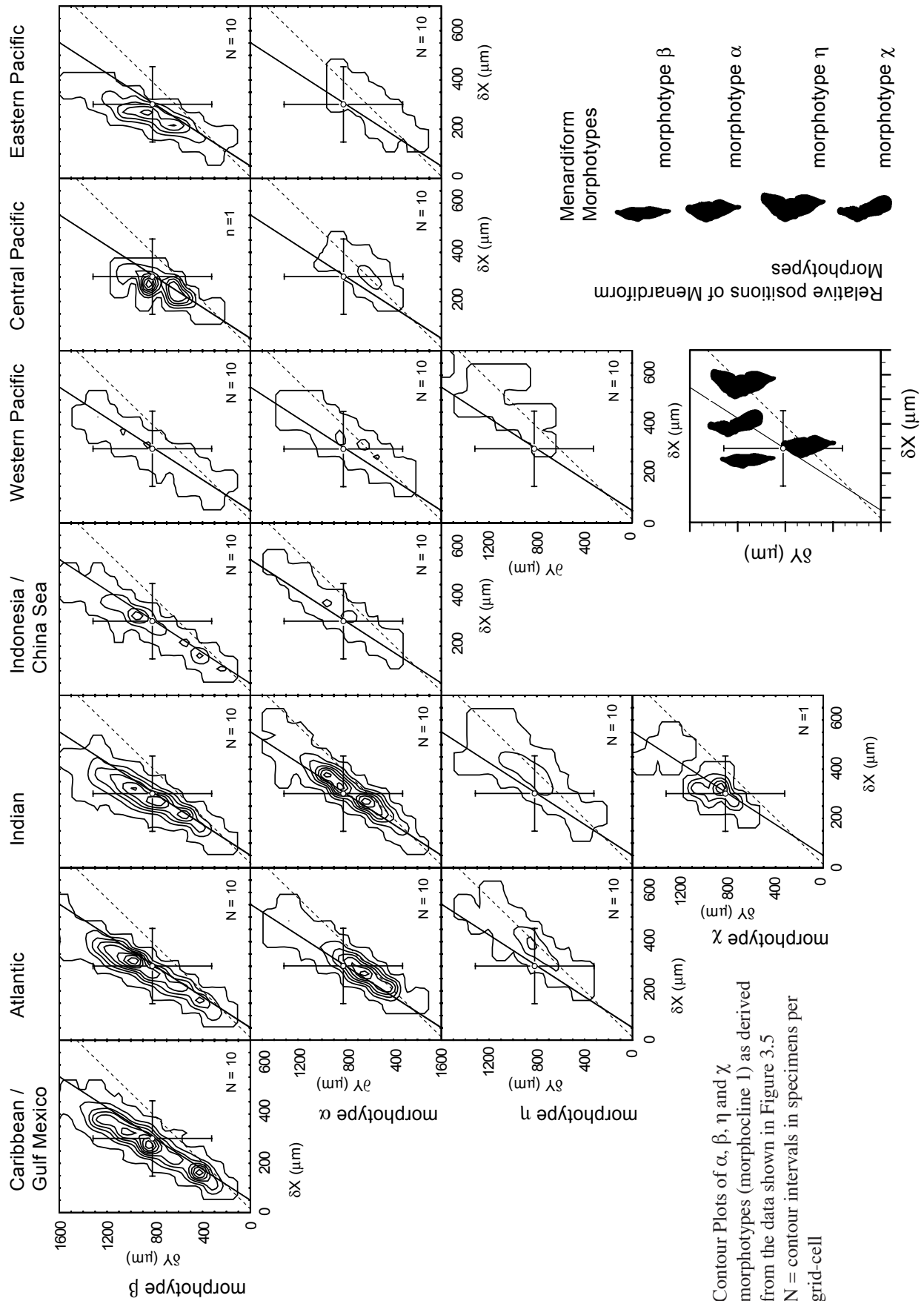
Figure 3.7 Scatter and contour plots of mophocline 2

Scatter plots (Fig. 3.7a) and contour plots (Fig 3.7b) of morphotypes ε and φ (morphocline 2)

T = Number of specimens included in each diagram.
N = Countour interval in specimens per gird-cell.
Open circles shown on figure 7b represents the global mean values for δX and δY as shown in

Figure 4 and are illustrated for comparison.

samples with over forty specimens of morphocline 1 are used. All histograms are arranged in latitudinal order left to right across the page and then down the page.

The histograms show a dominant unimodal distribution, although there is bimodality seen within a few. Two dominant modal points are observed one centered on δX/δY ratio of 0.33 and the other with δX/δY ratio of 0.45. The shift between the two dominant modal values is observed with latitude. Samples with the warmest temperatures show modal values with the lowest δX/δY ratios. The modal value moves toward the right of the histogram as sea surface temperature decreases (see figure 3.8). The majority of the histograms show a dominance of a single mode, with a skew towards the larger end of the distribution. This suggests the presence of a second subordinate masked population.

3.3.2 Factor analysis – Eigen space analysis

The previous morphotype characterization was done by contour analysis of the variates and by visual inspection of the multivariate data set at varying angles of view using the program rotator (Craig Kloeden, http://casr.adelaide.edu.au/rotater/). The program allows rotation of an XYZ data set in real time allowing visual inspection of the data. To further confirm the existence of distinct morphotypes a factor analysis of the measured variates was carried out. Most of the morphological variation can be described by three of the variates, e.g. δX, δY and Φ3. Figure 10 shows the stages in the course of analysis. Figure 3.10a shows the three dimensional data space defined by δX, δY and Φ3 axes. Figure 3.10b shows the same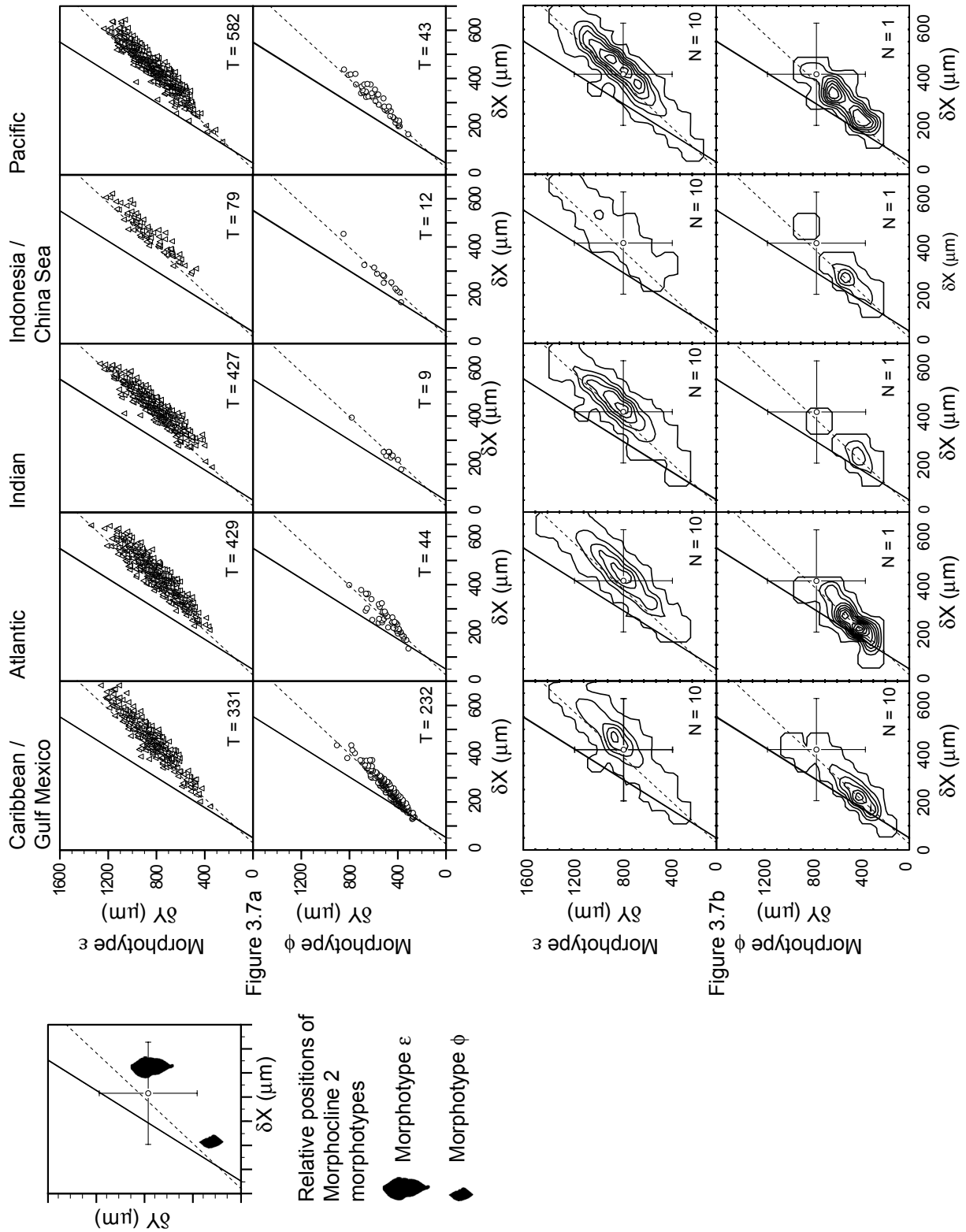 data but rotated by 45_ horizontally about δy the axis and slightly dipped about the Φ3 axis to best show morphological separation between the identified morphotypes.

3.3.2.1 Standardization of data

Standardization of the data was carried prior to factor analysis of the data. The method used is as follows: $U_{standard} = (U_{sample} - U_{mean})/U_{standard}$ deviation, where U stands for δX, δX or Φ3 (Davis 1986). The standardized data have a mean value of zero, the units of all are converted to standard deviations, which allows variates on differing ordinate scales to be directly compared to each
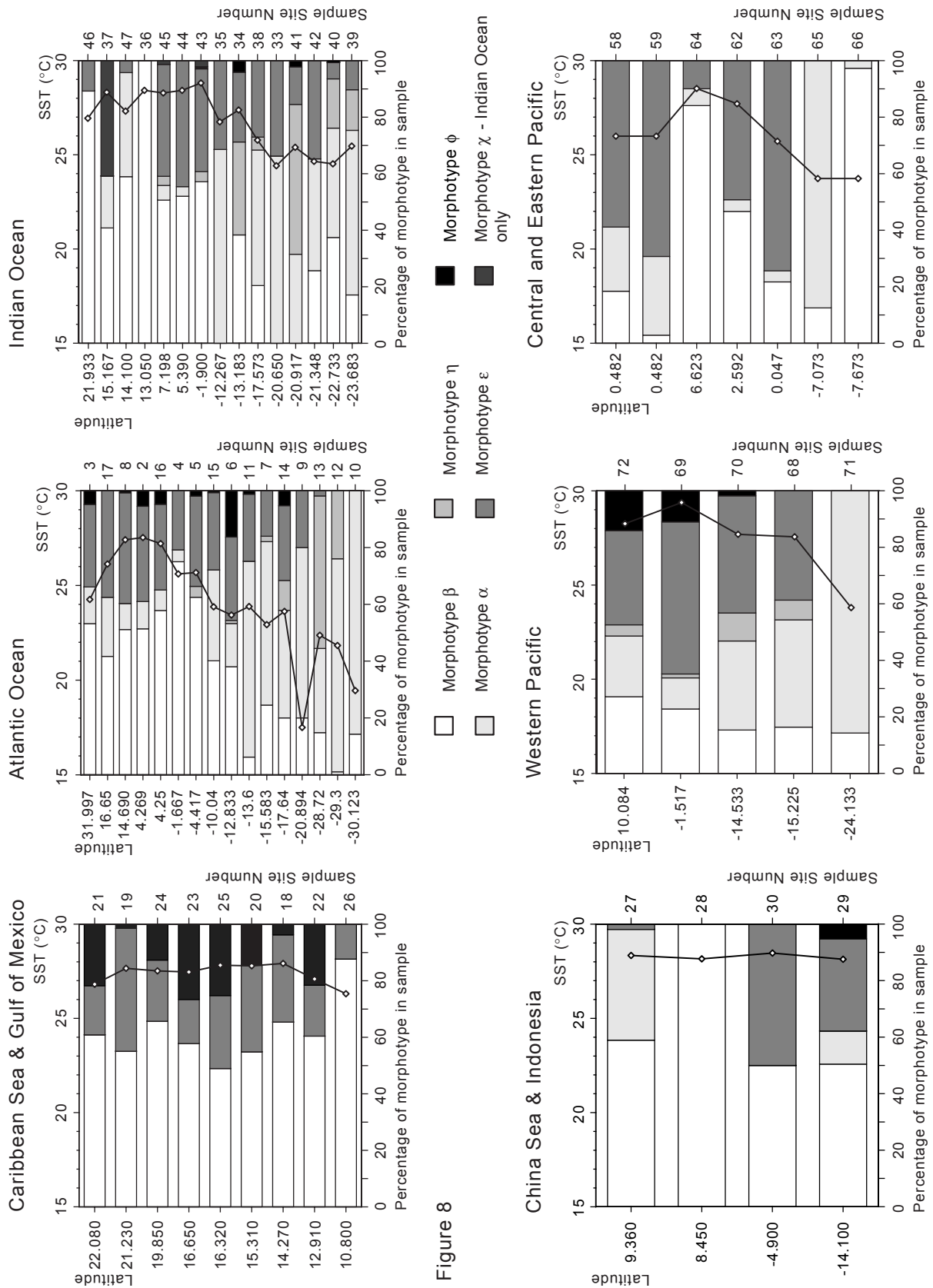
Figure 3.8 Morphotype abundance (in percent) per sample site.
Sample sites organised latitudinally. The mean annual sea surface
temperature (SST) at each sample site are overlain, (solid line).

Figure 3.9 Histograms of the δX/δY ratio for selected Atlantic samples.

Histograms of the δX/δY ratio for selected Atlantic samples.

Mode one is shown as the dashed line.

Mode two is shown as the dotted line.

All samples are arranged latitudinally (left to right, then down the page).
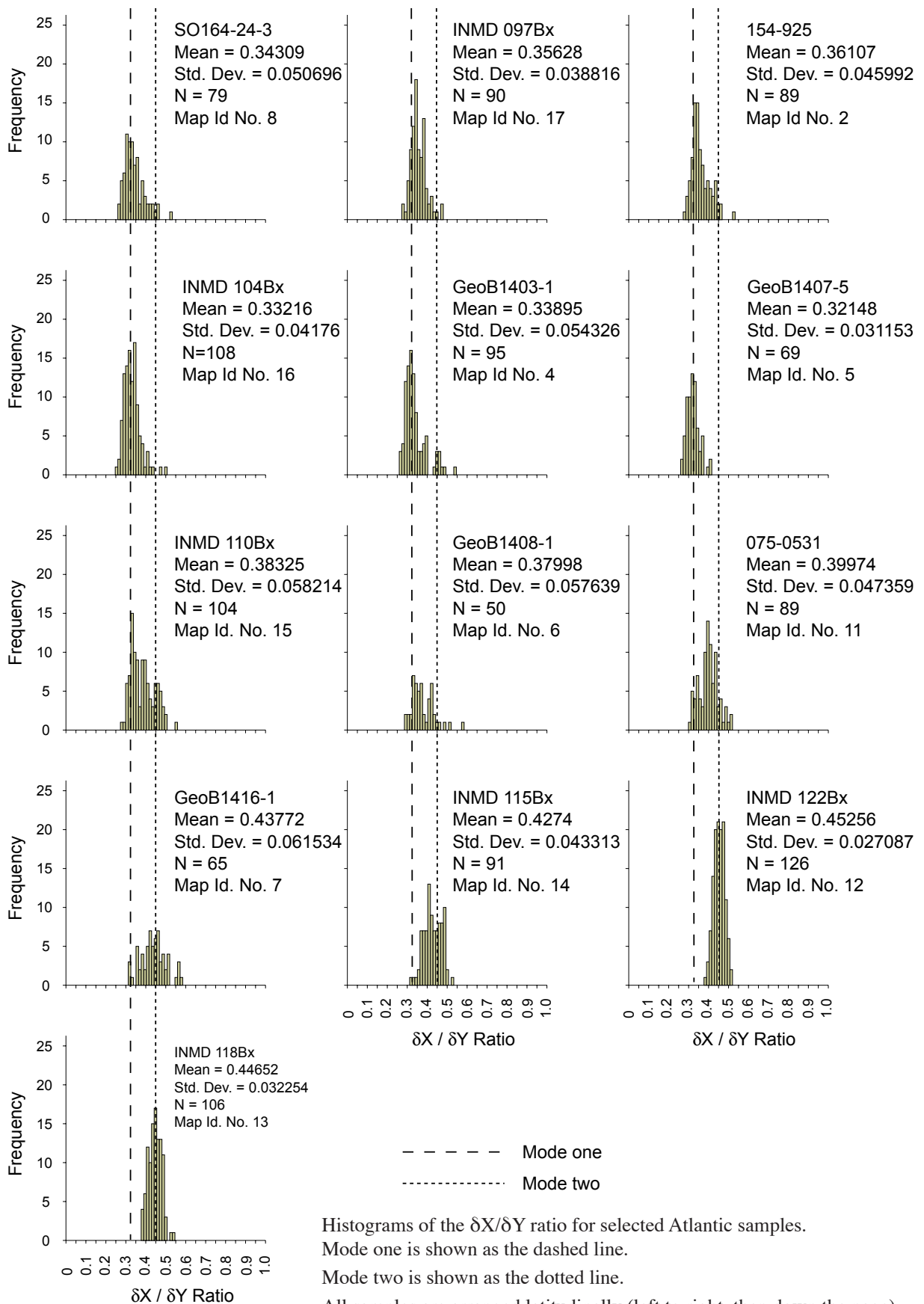
other. (See Figure 3.10c).

3.3.2.2 Factor analysis

Multivariate data analysis techniques that are grouped under the term „Factor analysis" are based on the eigenvalues and eigenvectors extracted from a covariance or correlation matrix. In the present study eigenvalues and eigenvectors for each species were calculated from the variance/ covariance matrix of the three variables δX versus δY, and $\phi 3$ using Fortran subroutine „EigenJ" from Davis (1973), which was modified to run as a stand alone program. The eigenvalues represent the magnitude of the principle component axes, while the eigenvectors represent their directional component. The space spanned by eigenvectors show the maximum variation of the data set, and so maximizes differences among different populations within the data. By simple operation it is possible to derive the corner points of rombohedral shapes (eigen space) that represents each morphotype at one standard deviation of the sampled population. (See figures 3.10d and 3.10e). Once the coordinates of the corners of the eigenspace romboheadrals were calculated, their co-ordinates were back transformed into the Cartesian coordinate system (Figure 3.10f). The rombohedrals produced represent the space occupied by approximately 68% (e.g. 1 standard deviation) of the sample population. The use of one standard deviation removes the extreme members from the data set all the morphotypes shown and so improves morphotype separation. The rombohedrals when viewed in δX, δY coordinates alone show some separation, however it is in Figure 3.10g, that the full separation of the morphotypes becomes evident. This analysis confirms our previous morphotype concept based on contour diagram analysis.

3.3.3   Biogeographic variability

To investigate the biogeographic distribution of the identified morphotypes, oceanographic data for each sample site was extracted from the World Ocean data base (Conkright et. al. 2001). Correlation with the following environmental parameters was attempted: Salinity, Temperature (annual mean and seasonal), depth of thermocline (annual and seasonal) and primary productivity. The best correlation found was that with sea surface temperature (annual mean) (SST). Figure 3.8 shows the percentage of each morphotype present in individual samples arranged latitudinally

for each geographic region, with the annual mean SST at each sample site overlaid. The results show that morphotype β dominates in warmer waters close to the equator and is the dominate morphotype in the Caribbean region. Morphotype α becomes more prominent as moving into higher latitudes and cooler SST's, while morphotype η is only present in the highest latitudes. Morphotypes ε and φ are restricted to the warmer low latitude regions. Morphotype χ is found only in the Indian Ocean. In general appearance, morphotype χ closely resembles morphotype β of which it is believed to be an aberrant form, the difference being the highly flexed final chamber.

3.4   Discussion

By investigation of the measured parameters shown here (δX/δY ratio, contour analysis, eigen analysis), and by visual comparison of the morphotypes with illustrated specimens and holotypes, we equate morphotypes to the following morphospecies:

Morphocline 1: (see also plate 3-1)

Morphotype α is equivalent to *Globorotalia menardii menardii*

Morphotype β is equivalent to *Globorotalia menardii cultrata*

Morphotype β+ with marginal spines is equivalent to *Globorotalia fimbriata*

Morphotype η is equivalent to *Globorotalia menardii gibberula*

Morphotype χ is equivalent to *Globorotalia neoflexuosa*

Morphocline 2: (see also plate 3-2)

Morphotype ε is equivalent to *Globorotalia tumida*

Morphotype φ is equivalent to *Globorotalia ungulata*

The assemblages studied show discrete groupings that represent distinct morphospecies clusters intergrading into each other along the respective morphocline. Morphocline 1, the *Gr. menardii*
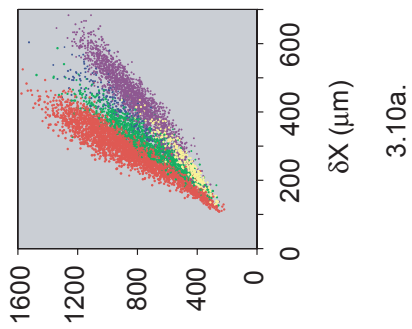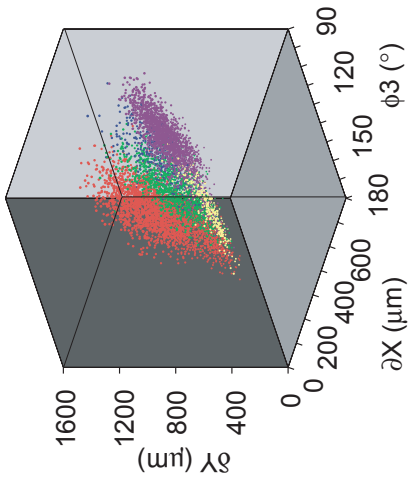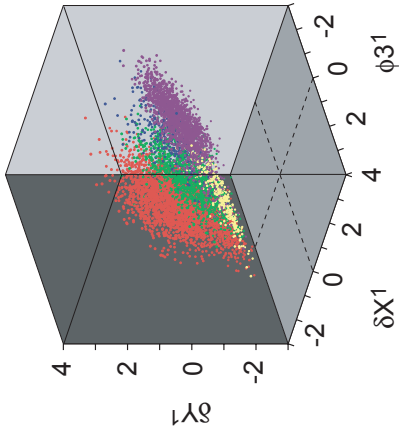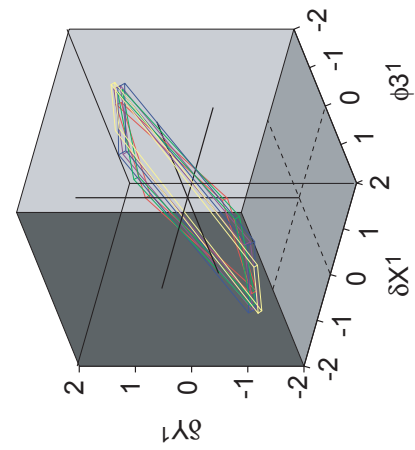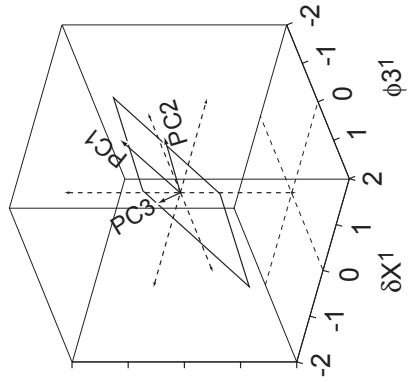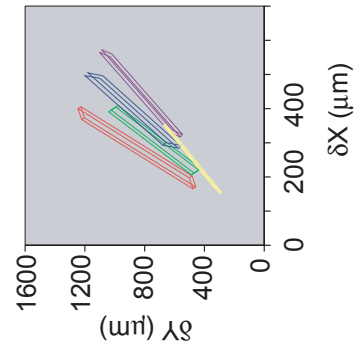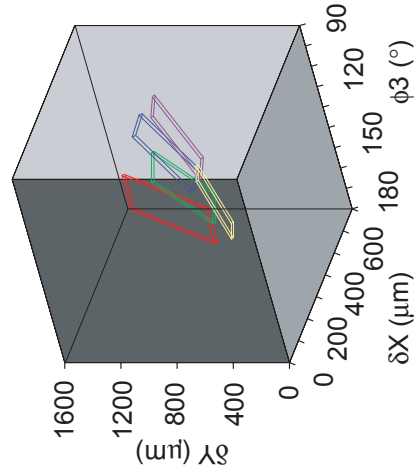
Figure 3.10   Eigen space plots

Figures 10 a-g represent the steps taken in carrying out the factor analysis of the data set. For more detailed explanation refer to section 3.4.1.2

cultrata – Gr. menardii menardii – Gr. menardii gibberula, morphocline appear to represent an ecophenotypic morphoseries controlled mostly by water temperature (Figure 3.7). Its geographic range shows significant overlap. However this can equally well be explained by vertical temperature gradients present in the oceans. In waters with a mean annual SST above 25°C, *G. menardii cultrata* is dominant. The *Gr. menardii menardii* morphology becomes more dominant as surface waters become cooler. The high spired *Gr. menardii gibberula* is present in the coolest waters. Globorotalia *fimbriata* (morphotype β+), is distinguished from *G. menardii cultrata* by having small radially arranged spines on the keel (Bolli and Saunder 1985). Other than the spines, morphometrically it coincides with *Gr. menardii cultrata* (morphotype β) of which it is assumed to be a variant.

The dominance of the *Gr. menardii cultrata* in the Caribbean and western tropical North Atlantic is believed to be a result of the development of the annual Western Atlantic Warm Water Pool. This is a body of water where the SST reaches over 28.5°C annually and results in a deep stratification layer of warm water. It occurs in the Western North Atlantic, Caribbean and Gulf of Mexico. This hypothesis is supported by Knappertsbusch (200t submitted) who found that the *Gr. menardii cultrata* is dominant at Caribbean DSDP site 502 in samples younger than 0.22Ma. Hemleben et. al. (1989) noted *"Gr. menardii* seems to be found deeper in warmer waters and shallower in colder waters"*, suggesting that the depth of habitat is related to water temperature. Scott (1973) hypothesized that the spiral height (δX) may be an adaptation to buoyancy in the water column. The viscosity of water is inversely related to temperature, in that viscosity of the water decreases as temperature increases. Scott suggested that populations in warm water masses would have the most compressed (flattened) tests, while those in colder waters would show greater inflation of the test. This idea was discarded when observations made on Caribbean cores by Emiliani (1969) did not show a close correlation between water temperature and inflation of the test. However looking at the plates from Emiliani (1969) it became clear that this author grouped together *Gr. menardii*, *Gr. tumida* and *Gr. menardii flexuosa* which certainly has led a to mixed isotopic signature. The data presented here supports the hypothesis of Scott (1973).

Morphocline 2 shows surprisingly less variation than is present in Morphocline 1, all regions showing a similar range of morphological variation. *Gr. tumida* and *Gr. ungulata* have a similar shape and the two taxa intergrade, with the difference being that *Gr. ungulata* has a smooth, thinner more delicate, finely perforate test, with a carinate band over the arch of the aperture. Both morphospecies, however, are restricted to tropical waters. Kroon (1988) assumed that *Gr. ungulata* was synonymous with *Gr. menardii* found in the Northern Indian Ocean, while Pearson (1995) noted that *Gr. ungulata* is possibly an ecological variant of *Gr. tumida*. From the morphological data presented here, the smaller size, and low levels of encrusting it is suggested that Gr. *ungulata* is a shallow dwelling juvenile of *Gr. tumida* and the *Gr. tumida* being the deeper dwelling adult form of the same species. This hypothesis is supported by the morphometric data presented here and was also proposed by Lamb and Beard (1972, p.57). The ratio of δX/δY places them on the same morphocline, and they share a diagnostic tumid morphology. However *Gr. tumida* has a geological record stretching back over 5 Ma, while *Gr. ungulata* is only known from the Late Pleistocene with any certainty. One possible explanation is that *Gr. ungulata* represents a more recent adaptive expansion into shallow waters, resulting in the observed morphological differences. An alternate explanation is that *Gr. ungulata* and *Gr. tumida* are different but related species, living separately in different depth environments. To test this would require high resolution investigation of cores at different locations, where both species have been identified, to allow identify of transitional morphologies between the two morphotypes. Stable isotope studies could be conducted to reveal depths of calcification and depth habitat of each morphotype through various size ranges (this is the subject of a further study).

3.4.1   Morphological variation and holotypes

The morphology of an organism is the phenotypic expression of its genetic make up. Therefore it is not unreasonable to assume that differing morphologies are an indication of differing genotypes. However, all species of planktonic foraminifera can be described as polyphenotypic, in that they show a range of morphological variations and adaptations. The difficulty is determining how much morphological variation is due to ecophenotypic and how much variation is due to genetic make up before it is considered to be a separate species. This is one of the problems when viewing

morphological variation through geological time particular when morphotypes intergrade. From the morphological data alone presented here it is difficult to conclude if the morphological variations observed within morphocline 1 is representative of separate, though closely related species or whether they represent species showing wide ecophenotypic variation. Identification of species using traditional Linnaean taxonomy is made by reference to a holotype and possibly a series of a few paratypes that were named by the original author to represent morphological variation observed within a species. The holotype is supposed to represent an average specimen. However, practice has shown that a holotype has rarely been selected from a suffiecntly large regional or global sample set. Often a holotype was assigned when a new species was found in a particular region, and only later was it found that it had been previously described in another region.

In the case of *Globorotalia menardii* the authors believe much of the confusion and difficulty identifying specimens is caused by the original assumption that the specimens d'Orbigny identified as *Rotalia menardii* and the later *Rotalina cultrata* are synonymous. This is reflected in the designation of the ecotype proposed by Stainforth et. al. 1978, and accepted after a decision of the ICZN (Melville 1982) suppressing the lectotypes erected by Banner and Blow (1960). As *Gr. menardii* is not found in the Holocene of the Adriatic Sea, the selected specimen from Upper Miocene strata is believed to be more representative of model of No. 10 d'Orbigny (1826) illustrated by Brady, Jones and Parker (1865). *Rotalina cultrata* d'Orbigny (1839) is from Holocene beach deposits from Cuba, Martinique, Guadeloupe, and Jamaica (Banner and Blow 1960, Stainforth et. al. 1978) the often assumed synonymy between *Gr. menardii menardii* and *Gr. menardii cultrata* ignores 5 million years of evolution.

Figure 3.11 illustrates the morphological variation that is present when comparing our Holocene data set with specimens identified in literature. The bounding envelope is the >20 contour line from figure 3.4(a), which is used here as a reference for the total morphological variation within the Late Pleistocene – Holocene *Gr. menardii* morphocline (1). The current ecotype (circled cross) is not representative of the morphological variation of *G. menardii* observed in the Holocene sediments. However, it is representative of the morphological variation observed in Miocene assemblages

Figure 3.11 Specimens identified in the literature as *Globorotalia menardii* or *G. menardii cultrata*
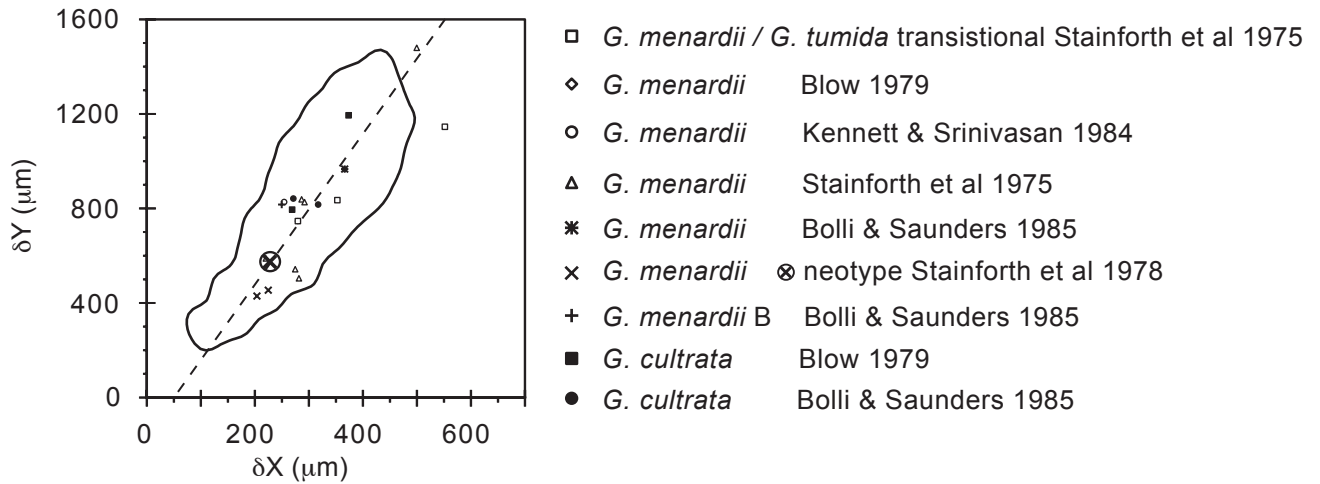
Specimens identified in the literature as *Globorotalia menardii* or *Gr. menardii cultrata*, plotted in the δX versus δY mophospace.

The closed line represents the N ≥ 20 contour line shown in figure 4a (second lowest line in Fig. 4a).

Figure 3.12 Specimens identified in the literature as *Gr. tumida* and *Gr. ungulata* and plotted in the δX versus δY morphospace
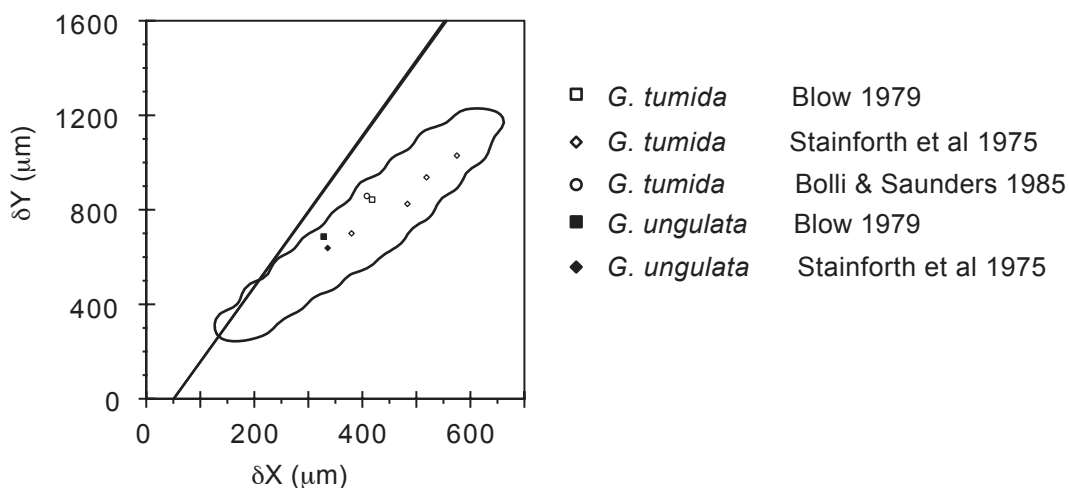
Specimens identified in the literature as *Gr. tumida* and *Gr. ungulata* and plotted in the δX versus δY morphospace..

The closed line represents the N ≥ 20 contour line shown in figure 4b (second lowest line in Fig. 4b).

from the Caribbean Sea as illustrated in Knappertsbusch (2007 submitted). Figure 3.12 shows the analogue measurements for the *Gr. tumida* and *Gr. ungulata* morphocline (2). Other than an overall increase in size the *Gr. tumida – Gr. ungulata* plexus shows little change in shape. This is possibly an indication of an adaption to a more stable environment, deeper in the water column than is the case in *Gr. menardii*.

3.5   Conclusions

1. Quantitative limits are developed as an aid to investigating morphological variation within two morphologically similar species. An empirical separation is proposed to distinguish menardii-forms from tumid forms, the line represented by the linear equation y = 2.07x -15 is shown to separate menardii from tumid morphologies. A second line represented by the equation y = 3.2x –160 is proposed to distinguish between *Gr. menardii cultrata* and *Gr. menardii menardii* morphotypes. A quick and easy rule to separate the menardii morphologies in specimens with $\delta X \geq 250\mu m$ is to use the $\delta X/\delta Y$ ratio. If this ratio is less than 0.37 the morphology follows that of *Gr. menardii cultrata*. If the $\delta X/\delta Y$ ratio is between 0.37 and 0.5 the morphology best represents *Gr. menardii menardii*. *Gr. menardii gibberula* overlaps the area of the *Gr. menardii menardii* morphology but generally is only identifiable in size fractions larger than $500\mu m$. The tumid morphologies seen in morphocline 2 generally have $\delta X/\delta Y$ ratios greater than 0.5. The above rules do not apply to size fractions of δX measurements $< 250\mu m$.

2. The six menardiform morphotypes α, β, η, χ, of morphocline 1; plus morphotypes ε and ϕ of morphocline 2, identified in this study and are recognizable in Holocene surface sediments around the world. Differentiation has been made on the basis of simple measurable variables of the shell in keel view position. These morphotypes are tentatively equated to the morphologies *Globorotalia menardii menardii*, *Globorotalia menardii cultrata*, *Globorotalia menardii gibberula*, *Globorotalia neoflexuosa*, *Globorotalia tumida* and *Globorotalia ungulata,* respectively. These species assignments, however,

Plate 3-1 Specimens from Morphocline 1

Top – *Gr. menardii cultrata*
Middle – *Gr. menardii menardii*
Bottom – *Gr. menardii gibberula*   Scale bar = 500μm
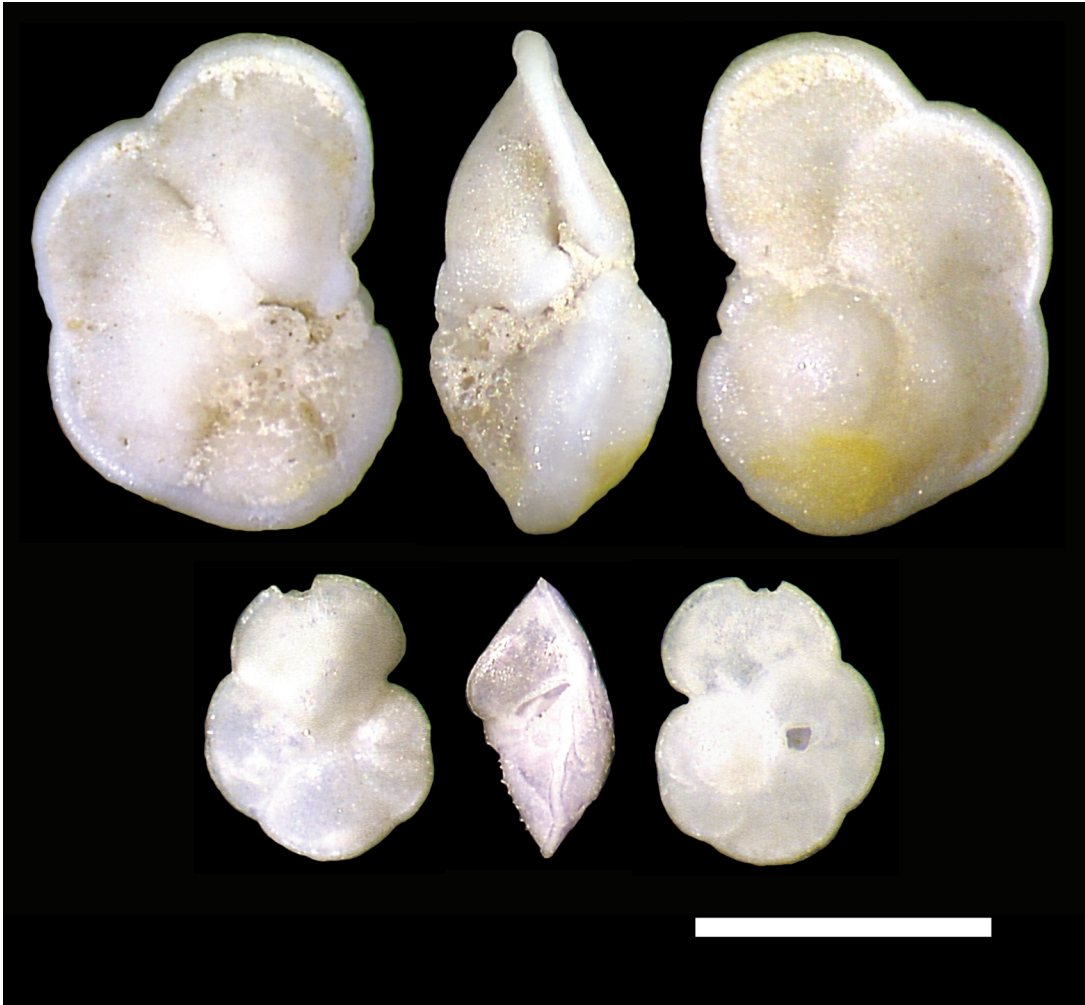
Plate 3-2 Specimens from Morphocline 2

Top – *Gr. tumida*
Bottom – *Gr. ungulata*
Scale bar = 500μm

need further confirmation on the basis of molecular taxonomy, culture experiments and biological observations. There is indication that the intra- and inter-morphotype variation observed is ecophenotypic, but this also requires further study, involving net sampling of live specimens from different environments.

3. For the identified extent morphotypes, genetic techniques need to be elaborated to answer the question of them being separate species. In combination with our morphometric results such information will serve as a model to reaccess the currently accepted phylogenies as it would give an indication of the extent of genetic variation and related maximum morphological variation.

4. The current practice of designation of a holotype and several paratypes, clearly is not sufficient to represent the morphological variation within planktonic foraminifera. A more objective way would be to have a representative series of specimens across the ontogenetic size spectrum and from various ecological niches. The authors accept the current ecotype for *Gr. menardii* as being representative of the Miocene *Gr. menardii*, but not being representative of the observed Holocene plexus of *Gr. menardii cultrata – Gr. menardii menardii – Gr. menardii gibberula*. The lectotypes erected by Banner and Blow (1960) do, however show a close resemblance to the Late Pleistocene – Holocene specimens encountered in this study. A possible solution would be to accept the ecotypes designated by Stainforth et. al. (1978) as the Miocene and Pliocene representatives of the plexus. The specimens selected by Banner and Blow (1960) could be used to represent the Late Pleistocene and Holocene end of the evolutionary plexus.

5. In summary the data presented here can be interpreted in three ways:

    a. Two populations living separately within the water column with different morphologies. This would produce a bimodal distribution within the frequency histogram. On the death of individuals, the shells from both populations would be mixed within the sediment. This distribution is seen in the Atlantic histograms in

sample sites 15, 6, 11 and 7.

b. Biogeographic separation of morphologies that have a strong regional overlap would be represented by a bimodal histogram with one modality being dominant, and possibly masking the second minor peak, (which may only be noticeable by a skew seen in the histogram). This case is dominant in the Atlantic.

c. Ecological forcing of the morphology of a single species that has sufficient genetic plasticity to produce the observed uni- to bimodal morphological variation (ecophenotpy).

Testing of the three hypotheses could be carried out using the methods outlined above. The use of a long term sediment trap would also allow the study of seasonal variation within the morphologies, which are not evident form sediment samples.

3.6 Acknowledgement

3.7   Reference

Bandy O.R., 1972. Origin and development of *Globorotlia (Turborotalia) pachyderma* (Ehrenberg) Micropaleontology, 18:294-318.

Banner, F.T., and Blow, W.H., 1960. Some primary typ of species belonging to the super-family *Globinerinaceae*. Contr. Cushman Found. Foram. Re*s.,* 11:1-41.

Banner, F.T., and Blow, W.H., 1962. The type specimens of *Globierina quadrilobata* d'Orbigny, *Globigerina sacculifera* Brady, *Rotalinia cultrata* d'Orbigny and *Rotalia menardii* Parker, Jones and Brady. Contr. Cushman Found. Foram. Res. 13:98-99.

Bé, A.W.H., 1977. An ecological, zoogeographic and taxonomic review of Recent planktonic Foraminifera. – In Ramsey, T.S., ed., Oceanic Micropaleontology 1: 1-100, Academic press, London.

Blow, W.H., 1956. Origin and evolution of the foraminiferal genus *Orbulina* d'Orbigny. Micropaleontology, 2;57-70.

Blow, W.H., 1969. Late Eocene to Recent Planktonic Foraminiferal Biostatigraphy In: *Proceedings of the first international conference on Planktonic microfossils Geneva, 1967* 1:199-422.

Blow, W.H., 1969. *The Cainozoic Globigerinida*. E.J. Brill, Leiden (3 vols.),1413pp.

Blow, W.H., and Banner, F.T., 1962. Part 2: the mid-tertiary (Upper Eocene to Aquitanian) Globigerinaceae. *In: Fundamentals of Mid-Tertiary Stratigraphical Correlation, ed. Eames, F.E., Banner, F.T., Blow, W.H. and Clarke, W.J.* 61-151. Cambridge University Press.

Bolli, H.M., 1950. The direction of coiling in the evolution of some Globorotaliidae. Contr. Cushman Found. Foram. Res., 1:82-9.

Bolli, H.M., and Saunders, J.B., 1985. Oligocene to Holocene low latitude planktic foraminifera. In: Bolli H.M., Saunders J.B. and Perch-Nielsen K., Editors Plankton Stratigraphy Cambridge University Press.

Conkright, M.E., J.I. Antonov, O. Baranova, T.P. Boyer, H.E. Garcia, R., Gelfeld, D. D. Johnson, R.A. Locarnini, P.P. Murphy, T.D. O'Brien, I. Smolyar, C. Stephens, 2002: World Ocean Database 2001, Volume 1: Introduction. Ed: S. Levitus, NOAA Atlas, NESDIS 42, U.S. Government Printing Office, Washington, D.C.

Cushman, J.A., 1927. An outline of a re-classification of the foraminifera. Contrib. Cushman Lab. Foram. Res., 3:1-107.

d'Orbigny, A., 1839. Historie Physique, Politique et Naturelle de L'ile de Cuba Arthus Bertrand, Libraire-Editeur, Libraire de la societe de gographie, Rue Hautefeuille, 21.

Davis, J.C., 1973. Statistics and data analysis in Geology. John Wiley and Son.

Davis, J.C., 1986. Statistics and data analysis in Geology. 2nd Edition John Wiley and Son.

De Vargas, C., and Pawlowski, J., 1998. Molecular versus taxonomic rates of evolution in planktonic foraminifera. Mol. Phyl. Evol., 9:463-469.

De Vargas, C., Norris R., Zaninetti, L., Gibb, S.W., and Pawlowski, J., 1999. Molecular evidence of cryptic speciation in planktonic foraminifers and their relation to oceanic provinces. Proc. Natl. Acad. Sci. USA, 96:2864-2868.

Darling, K.F., Kroon, D., Wade, C.M., and Leigh Brown, A.J., 1996 . Molecular evolution of planktic foraminifera. Journal of Foraminiferal Research, 26:324-330.

Darling, K.F., Wade, C.M., Kroon, D., and Leigh Brown, A.J., 1997. Planktic foraminiferal molecular evolution and their polyphyetic origins from benthic taxa. Marine Micropaleontology, 30:251-266.

Darling, K.F., Wade, C.M., Stewart, I., Kroon, D., Dingle R., and Leigh Brown A.J., 2000. Molecular evidence for genetic mixing of Arctic and Antarctic subpolar populations of planktonic foraminifers. Nature, 405:43- 47.

Darling, K.F., Kucera, M., Pudsey,C.J., Wade C.M., 2004. Molecular evidence links cryptic diversification in polar plankton to Quaternary climate dynamics Proceedings National Academy Science 101(20):7657-7662.

Emiliani, C., 1964. Paleotemperature Analysis of the Caribbean Cores A254-BR-C and CP-28. Geological Society of America Bulletin, 75:129-144.

Emiliani, C., 1969. A new paleontology. Micropalontology, vol. 15, no. 3: 265-300.

Ericson, D. B., and Wollin, G., 1968. Pleistocene Climates and Chronology in Deep-Sea Sediments. Science. 162:1227-1234.

Hemleben, Ch., Spindler, M., and Anderson, O., 1989. Modern Planktonic Foraminifera. Springer Verlag, Berlin, Heidelburg.

Kennett, J. P. and Srinivasan, M. S., 1983. Neogene planktonic foraminifera, a phylogenetic atlas. Hutchinson Ross, Stroudburg, Pennsylvania.

Keating J.P., and Scott D.W., 1999. Ask Dr. Stats: - A Primer on Density Estimation for the Great Home Run Race of '98.   - Stats # 25 spring 1999 16-22.

Knappertsbusch M., 2004. MorphCol - A collection of Fortran 77 programs for geometric morphometry. A technical report First edition, 14 September 2004 http://pages.unibas.ch/museum/microfossils/Research/MORPHCOL/Start.html.

Kroon, D., 1988. Distribution of extant plantic foraminiferal assemblages in the Red Sea and Northern Indian Ocean surface waters. *In Planktonic Foraminifers as Tracers of Ocean-Climate*

History. Geert-Jan A. Brummer and Dick Kroon Free University Press. Amsterdam.

Melville, R.V., 1982. Opinion 1234 *Rotalia menardii* Parker, Jones and Brady 1865 (Foraminiferida). Neotype designatied Bulletin of Zoological Nomenclature 39:253-254.

Pearson, P.N., 1995. Planktonic Foarminifer Biostatigraphy and the Development of Pelagic Caps on Guyots in the Marshall Islands Group. In: Haggety, J.A., Premoli Silva, I., Rack, F., and McNutt, M.K. (Eds.), Proceedings of the Ocean Drilling Program, Scientific Results, Vol. 144: 21-50.

Ruddiman, W.F., 1971. Pleistocen Sedimentation in the Equatorial Atlantic: Stratigraphy and Faunal Paleoclimatology. Geological Society of America Bulletin 82:283-302.

Schmid, K., 1934. Biometrische Untersuchungen an Foraminiferen. Ecologae geol. Helvetiae, 27(1):45-134.

Scott, G. H., 1973. Ontogeny and shape in *Globrotalia menardii* Journal of Foraminiferal Research 3(3):142-146.

Stainforth, R.M., Lamb, J.L., Luterbacher, H., Beard, H.J., and Jeffords, R.M., 1975. Cenozoic Planktoni oraminiferal zonation and characeristics of index forms. Article 62 The University of Kansas Paleontology Institute.

Stainforth, R.M., Lamb, J.L., and Jeffords, R.M., 1978. *Rotalina menardii* Parker, Jones and Brady, 1865 (Foraminiferida): Proposed suppression of lectotype and designation of Neotype Z.N.(S.) 2145 *Bull. Zool. Nomencl*. 34(Part 4):252-264.

Thierstein, H.R., Geitzenauer, K., Molfino, B., and Shackleton, N.J., 1977. Global synchroneity of late Quaternary coccolith datum levels: validation by oxygen isotopes. Geology, 5:400-404.

Todd, R., 1962. On Selection of Lectotypes and Neotypes. Contrib. Cushman Found. Foram. Res. 12(4):121-122.

Todd, R., 1964. Planktonic Foraminifera From Deep-Sea Cores of Eniwetok Atoll. Prof. Pap. U.S. geol. Surv, 260-CC, 1067-1111.

Wade, M., 1964. Application of lineage concept to biostratigraphic zoning based on planktic foraminifera. Micropalaeontology. 10:273-290.

Wade, M., 1966. Lineages of planktic foraminifera in Australia. In: *Committe on Mediteranean Stratigraphy, ed. Drooper, C.W., Reiss, Z., Rutsch, R.F., & Marks, P., pp. 30-39*.

Appendix 3.1

Map ID No.	Sample	Repository	latitude (deg)	longitude (deg)	water depth (m)	Core type	core sample depth	Region	notes	Dating
1	M24/13-2	Geomar	27.557	-16.197	3443	Piston core	core, top	Atlantic	Barren	
2	154-925B	ODP / DSDP	4.2689	-42.4197	3042.2	Rotary drill	1H 0-2cm	Atlantic		Holocene (Leg 154 Initial report)
3	164-997A	ODP / DSDP	31.9967	-74.5006	2770.1	Rotary drill	1H 0-2cm	Atlantic		Holocene (Leg 164 Initial report)
4	GeoB 1403-3	Bremmen	-1.6667	-10.1667	3692	gravity core	0-2cm	Atlantic		Late Pleistocene Pangea data
5	GeoB 1407-5	Bremmen	-4.4167	-9.6667	3516	gravity core	0-2cm	Atlantic		Late Pleistocene Pangea data
6	GeoB 1408-1	Bremmen	-12.8333	-5.5	1900	gravity core	0-2cm	Atlantic		Age model Meineke, Gerrit 1999 GeoB1408 Pangea, 54771
7	GeoB 1416-1	Bremmen	-15.5833	-12	3395	gravity core	0-2cm	Atlantic		Pangea data
8	SO164-25-3	Bremmen	14.6903	-58.2533	2720	multicore	0-2cm	Atlantic		Holocene (So164 - Rasta cruise report)
9	0175/1083A	ODP / DSDP	-20.894	11.218	2178	Rotary drill	1H 0-2 cm	Atlantic		(Leg 175 Initial report pg318) NN21b -E. huxleyiacme zone top 3 mbsf (0.090Ma)
10	0074-0526	ODP / DSDP	-30.123	3.138	1054	Rotary drill	1H 0-2 cm	Atlantic		NN21 (late Pleistocene Leg 75 initial report)
11	0075-0531	ODP / DSDP	-13.640	9.591	1267	Rotary drill	1H 0-2 cm	Atlantic		Pleistocene E. Huxleyi Acme 1H 83cm down core
12	122BX	Scripps inst.	-29.3	-33.008	3082	core, box	0-1cm	Atlantic		E. huxleyi acme zone
13	118BX	Scripps inst.	-28.717	-30.805	1693	core, box	0-1cm	Atlantic		E. huxleyi acme zone
14	115BX	Scripps inst.	-17.638	-16.212	3427	core, box	0-1cm	Atlantic		E. huxleyi acme zone
15	110BX	Scripps inst.	-10.038	-13.39	1959	core, box	0-1cm	Atlantic		E. huxleyi acme zone
16	104BX	Scripps inst.	4.245	-21.923	3279	core, box	0-1cm	Atlantic		E. huxleyi acme zone
17	097BX	Scripps inst.	16.653	-46.127	3619	core, box	0-1cm	Atlantic		E. huxleyi acme zone
18	0165-0998 A	ODP / DSDP	19.8551	-80.9706	3179.9	Rotary drill	1H 0-1cm	Caribbean		E. huxleyi acme zone (Leg 165 initial report) age depth model - Holocene
19	0165-0999 A	ODP / DSDP	12.9108	-77.1644	2827.9	Rotary drill	1H 0-1cm	Caribbean		E. huxleyi acme zone (Leg 165 initial report) age depth model - Holocene
20	0165-1000 A	ODP / DSDP	16.6517	-78.1211	915.9	Rotary drill	1H 0-1cm	Caribbean		E. huxleyi acme zone (Leg 165 initial report) age depth model - Holocene
21	0165-1002 C	ODP / DSDP	10.8017	-64.7872	892.6	Rotary drill	1H 0-1cm	Caribbean		Holocene (Leg 165 Initial report)

#										
22	SO164-18-1	Bremmen	21.2336	-74.35	1629	multicore		Caribbean		Holocene (So164 - Rasta cruise report)
23	SO164-02-3	Bremmen	15.3081	-72.785	2979.6	multicore		Caribbean		Holocene (So164 - Rasta cruise report)
24	SO164-24-3	Bremmen	14.2681	-63.4286	1545	multicore		Caribbean		Holocene (So164 - Rasta cruise report)
25	Vm 28 / 118	LDEO	16.317	-78.8	1348	Piston core	core, top	Caribbean		Pleistocene @ base of core length = 1023cm
26	RC 10 / 264	LDEO	22.083	-94.833	3464	Piston core	core, top	Caribbean		Pleistocene @ base of core length = 946cm
27	0184-1143 A	ODP	9.362	113.285	2771	Rotary drill	1H 0-15 cm	China Sea / Indonesia		NN21b (Leg 184 Initial report E.Huxlyi acme 2.88 mbsf)
28	Vm 19 / 134	LDEO	8.45	110	1031	Trigger weight core	core, top	China Sea / Indonesia		Pleistocene @ base of core length = 604cm
29	Vm 28 / 342	LDEO	-14.1	119.45	2730	Piston core	core, top	China Sea / Indonesia		Pleistocene @ base of core length = 762cm
30	Vm 28 / 335	LDEO	-4.9	126.883	3806	Piston core	core, top	China Sea / Indonesia		Pleistocene @ base of core length = 1112cm
31	Vm 29 / 20	LDEO	11.533	81.7	3557	Piston core	core, top	Indian	Barren	Pleistocene @ base of core length = 557cm
32	SO28-034	Sonne	-6.022	67.832	3994	Box core	core, top 0-3cm	Indian	Barren	
33	Vm 19 / 163	LDEO	-20.65	86.35	4169	Piston core	core, top	Indian		Pleistocene @ base of core length = 156cm
34	Vm 19 /205	LDEO	-13.183	44.15	3546	Piston core	core, top	Indian		Pleistocene @ base of core length = 850cm
35	Vm 34 / 69	LDEO	-12.267	51.467	4391	Piston core	core, top	Indian		Pleistocene @ base of core length = 893cm
36	RC 12 / 341tw	LDEO	13.05	89.583	2988	Trigger weight core		Indian		Pleistocene @ base of core length = 1099cm
37	RC 12 /343	LDEO	15.167	90.567	2666	Piston core	core, top	Indian		Pleistocene @ base of core length = 824cm
38	RC 14 / 19	LDEO	-17.573	63.547	3568	Piston core	core, top	Indian		Pleistocene @ base of core length = 1620cm
39	RC 14 / 18	LDEO	-23.683	49.85	3844	Piston core	core, top	Indian		Pleistocene @ base of core length = 292cm
40	Vm 33 / 65tw	LDEO	112.583	-22.733	1769	Trigger weight core		Indian		Pleistocene @ base of core length = 469cm
41	Vm 34 / 42	LDEO	-20.917	111.75	1750	Piston core	core, top	Indian		Pleistocene @ base of core length = 423cm
42	SO28-058	Geomar	-21.348	68.6	2459	Box core	core, top 0-3cm	Indian		
43	SO28-018	Geomar	-1.9	67.342	3035	Box core	core, top 0-3cm	Indian		

#	Sample	Source	Lat	Lon	Depth	Method	Interval	Ocean		Reference / Age
44	SO28-011	Geomar	5.39	60.252	3859	Box core	core, top 0-3cm	Indian		So28-005 (6.663, 61.133) C14 data 13.1K ± 0.09
45	SO28-003	Geomar	7.198	61.558	3585	Box core	core, top 0-3cm	Indian		Sirocko, Frank (2002): Radiocarbon (14C) SO28-05KL, PANGAEA
46	M1/9-11048-1	Geomar	21.933	64.167	2808	Box core	core, top 0-3cm	Indian		
47	VA01-247	Geomar	14.1	50.997	2344	Box core	core, top	Indian		
48	M 1/9-1190C	Geomar	26	53.5	70	Box core	core, top	Indian (Gulf)	Barren	
49	M 1/9-1174B	Geomar	27.5	51.367	45	Box core	core, top	Indian (Gulf)	Barren	
50	M 1/9-1156B	Geomar	29.027	50.122	42	Box core	core, top	Indian (Gulf)	Barren	
51	VA01-140K	Geomar	19.083	39.508		Box core	core, top	Indian (Red Sea)	Barren	
52	182-1126 B	ODP / DSDP	-33.509	128.067	785	Rotary drill	1H 0-15	Indian Ocean / Tasman sea	Barren	Holocene (Leg 182 Initial report)
53	182-1127 A	ODP / DSDP	-33.357	128.481	479	Rotary drill	1H 0-15	Indian Ocean / Tasman sea	Barren	Holocene (Leg 182 Initial report)
54	182-1129 C	ODP / DSDP	-33.297	128.481	203	Rotary drill	1H 0-15	Indian Ocean / Tasman sea	Barren	Holocene (Leg 182 Initial report)
55	189-1168 A	ODP / DSDP	-41.390	144.413	2463.3	Rotary drill	1H 0-15	Indian Ocean / Tasman sea	Barren	Holocene (Leg 189 Initial report)

#	Sample	Institution	Latitude	Longitude	Depth	Method	Interval	Ocean		Notes
56	189-1171 C	ODP / DSDP	-48.500	149.112	2147.8	Rotary drill	1H 0-15	Indian Ocean / Tasman sea	Barren	Holocene (Leg 189 Initial report)
57	189-1172 A	ODP / DSDP	-43.960	149.928	2621.7	Rotary drill	1H 0-15	Indian Ocean / Tasman sea	Barren	Holocene (Leg 189 Initial report)
58	009-0077 A	ODP / DSDP	0.482	-133.228	4291	Rotary drill	1H 0-1 cm	Pacific (C)		Late Pleistocene (Leg 009 Initial report) total cored 18.3m age correlated with 77B
59	009-0077 B	ODP / DSDP	0.482	-133.228	4291	Rotary drill	1H 4-5cm	Pacific (C)		Late Pleistocene (Leg 009 Initial report) 10 m/m.y. base of Pleistocene placed at 18m down core
60	026BX	Scripps inst.	6.552	-92.755	3567	core, box	0-1cm	Pacific (E)	Barren	
61	020BX	Scripps inst.	8.798	-104	3129	core, box	0-1cm	Pacific (E)	Barren	
62	009-0082 A	ODP / DSDP	2.592	-106.942	3767	Rotary drill	1H 0-2cm	Pacific (E)		Holocene / Late Pleistocene (Leg 009 Initial report) 24.3 m/m.y. base of Pleistocene placed at 31m down core
63	009-0083 A	ODP / DSDP	0.047	-95.738	3646	Rotary drill	1H 60-64cm	Pacific (E)		Holocene / Late Pleistocene (Leg 009 Initial report) 21.1 m/m.y. base of Pleistocene placed at 30m down core
64	016-158	ODP / DSDP	6.623	-85.237	2369	Rotary drill	1H 0-2cm	Pacific (E)		Cocos Ridge. Holocene/Late Pleistocene (Leg 016 Initial report) pg160 DSDP158 pg665
65	SO78-152-6	Geomar	-7.073	-88.458	4187	Box core	core, top	Pacific (E)		C14 dating Pangea SO78 data
66	SO78-152-7	Geomar	-7.673	-88.463	4187	Box core	core, top	Pacific (E)		C14 dating Pangea SO78 data
67	SO57-0061	Geomar	14.495	143.087	240	Box core	core, top	Pacific (W)	Barren	

68	Vm 33 / 119	LDEO	-15.225	161.35	4532	Piston core	core, top	Pacific (W)		Pleistocene @ base of core length = 381cm
69	Vm 35 / 17	LDEO	-1.517	159.667	2679	Piston core	core, top	Pacific (W)		Pleistocene @ base of core length = 1263cm
70	RC 10 / 131	LDEO	-14.533	157.967	2933	Piston core	core, top	Pacific (W)		Pleistocene @ base of core length = 501cm
71	RC 12 / 112	LDEO	-24.133	159.05	2566	Piston core	core, top	Pacific (W)		Pleistocene @ base of core length = 474cm
72	0144-872 A	ODP / DSDP	10.084	162.85	1082	Rotary drill	1H 2-3cm	Pacific (W)		Holocene (Leg 144 Initial report E.huxleyiacme zone)

Depth induced morphological variation in Recent Caribbean globorotalid foraminifera: evidence from combined morphological and isotopic studies.

Kevin Brown
Natural History Museum Basel
Augustinergasse – 2
Basel
CH 4001
Switzerland

Email: kevin-r.brown@unibas.ch

Tel: +00 41 61 2665 561
Fax   +00 41 61 2665 546

Abstract

Globorotalia menardii and *Globorotalia tumida* are two recent foraminiferal species that share similar morphological characters. However both species show a range of morphological variation. To investigate this variation combined morphological and geochemical studies were carried out at selected Caribbean and Gulf of Mexico sample sites.

Over 1800 orientated specimens were imaged and morphometric measurements taken. Specimens for isotopic analysis were selected to investigate the extremes of the observed morphological variation. Specimen selection was carried out at a range of differing size fractions to investigate changes in isotopic signal through ontogeny.

Morphometric results show that while *G. menardii* represents a range of morphological variation the two extremes correspond to Blow's (1969 and 1979) *G. menardii menardii* and *G. menardii cultrata*. Isotopically the two morphologies show significantly different isotopic signals. *G. menardii cultrata* morphologically has a flattened smooth test with little secondary encrusting, while isotopically it has a shallow depth habitat and possible symbiotic relationship. *G. menardii menardii* morphometrically shows greater inflation and encrusting of the test and isotopically it shows a deeper and colder depth habitat. The presence of all ontogenetic stages within the two recognized morphological groups, their distinct isotopic signatures, suggests that *G. menardii* may have two distinct subpopulations living at different depths within the Caribbean.

G. tumida intergrades with the morphologically similar but texturally different *G. ungulata*. Isotopic results show differing depth habitats for the two, and the results are interpreted as indicating ecophenotypic variation within a species.

Secondary encrusting of all specimens used in the present analysis indicates that encrusting is a function of which the foraminifera lived and not an indication of its stage of ontogeny or gametogenesis.

4.1   Introduction

Most foraminiferal taxa were originally erected for biostratagraphical purposes. Traditionally identification of species was made by reference to the gross morphology of the foraminiferal test. Names have been assigned to specimens that were assumed to be of different species, only later study was it shown that they frequently represented an ecophenotypic morphological continuum of which the identified species are extreme end members. Recognition of environmental variation within such a changing morphological plexus is important as it is the only key to understand the continuous influence of palaeoceanographical conditions on evolution of new species. Complications, which occur while interpreting foraminiferal species, include next to paleoenvironmental influence, the shell growth during ontogeny, and the more recent discovery of cryptic species which are indistinguishable from each other but are genetically different (Darling et al., 2000, 2004).

In order to decipher such difficulties in detail the closely related planktonic foraminiferal group *Globorotalia menardii* and *Globorotalia tumida* were inspected. Representatives of these forms are morphologically similar, sometimes with great morphological overlap Knappertsbusch 2007. The Caribbean region was selected for this study as *G. menardii* shows a range of morphologies. The region also shows very little seasonal variation in depth of the thermocline and temperature, when compared to other regions. Removing seasonal variation in temperature allows greater confidence in interpretation of the isotopic results being representative of the depth habitat of the organism rather than seasonal variations in water temperature.

4.1.1   Taxonomic history and concept

The origin and phylogeny of the menardiform has led to different taxonomic treatment globorotalids in the literature with conflicting implications. Schmid (1934) concluded on the basis of early biometric studies that *G. menardii* and *G. tumida* belong to a single species; with *G. menardii* being the microspheric and *G. tumida* the macrospheric forms. Ericson et al., (1961), Ericson and Wollin (1958 and 1968), Emilliani (1969) have combined *G. menardii* and *G. tumida* into

a poorly defined plexus, the presence or absence of which was used to define Late Pleistocene paleoclimatic variations. Parker (1964) described the "*Globorotalia menardii-tumida* complex", but recognized that while the end members are distinct and pose no problems in differentiating between *G. menardii* and *G. tumida* there is a tendency in early ontogenetic stages for them to show an intermediate morphology between the two. A similar observation is made about the Pacific menardiform globorotalids by Thompson (1982).

Bandy (1972) recognized *G. tumida* and *G. menardii* not only as separate species but unnecessarily grouped them to differing subgenera Globorotalia and Menardella, respectively. *G. menardii* fell in the Menardella lineage, *G. archeaomenardii – G. praemenardii – G. menardii*. *G. tumida* became the descendant of the Globorotalia subgeneric lineage: *G. lenguaensis – G. paralenguaensis - G. merotumida – G. plesiotumia -tumida*. Stainforth et al., (1975), Cifelli and Scott (1986), recognize that *G. menardii* as a highly polyphenotypic species. While Banner and Blow (1960) Blow (1969, 1979) Bolli (1970), Bolli and Saunders (1985), Knappertsbusch (2007) recognized two distinct subspecies of *G. menardii*: *G. menardii menardii* (morphotype α) and *G. menardii cultrata* (morphotype β), each having distinct geographic distribution and morphology.

The depth habitat of *G. menardii* and *G. tumida* has been previously studied by both 'plankton net collection and isotopic analysis. Depths cited have varied from author to author. Bé (1960) recognized *G. menardii* and *G. tumida* as being a "deep-water species living in the upper few hundred meters." But noted that, "thick shelled specimens, which show selective thickening of earlier chambers on the last whorl, are characteristic of specimens caught in plankton tows below 300m". This suggests that Bé (1960) recognized the morphological variation present within the species. Fairbanks et al., (1982) showed that *G. menardii* was found in water depths down to 500m with greatest concentration in the upper 200m. Schweitzer and Lohmann (1991) showed that isotopically the *G. menardii* and *G. tumida* grow within the upper 50m of the water column, and that secondary encrusting occurs between 50 and 100m. This places the depth habitat for the menardiform globorotalids within the upper part of the thermocline.

During this study identification of specimens was made by reference to figures and text in the following Atlases: Blow (1979), Stainforth et al., (1975), Kennett and Srinivasan (1983), and

Bolli and Saunders (1985). Morphotype designation follows Knappertsbusch (2007). Morphotype designations are used rather than subspecies designation, because at the present time the actual status is unclear and could only be resolved by possible future genetic work. By comparison with the various atlases already mentioned it was observed that *G. menardii* (morphotype α) closely resembles *G. menardii menardii*, while *G. menardii* (morphotype β) resembles what has been identified as *G. menardii cultrata*.

The goal of this study aims to solve the following questions:

1) Find evidence for vicariance and possible sympatry or a depth parapatry within the investigated species.
2) Reconstruct the habitat of different menardiform morphotypes in Caribbean Sea.
3) Clarify the significance of encrustation by isotope analysis.
4) Investigate the relationships between morphotypes, encrusting and depth habitat.

4.2   Materials and Methods

Figure 4.1 and Table 4.1 show the distribution of the sample sites in the Gulf of Mexico and Caribbean Sea. The Caribbean Sea was chosen because seasonal variation in sea surface temperature is only in the region of 1.5 to 3°C, resulting in little seasonal change in the depth of the mixed layer or the depth of the thermocline. Samples sites were chosen from above the local lysocline and have known stratigraphies, which allowed selection of Holocene material. Material was obtained from a number of sources and was selected from box core surface samples (to a depth of 1.5cm) or ODP core top material.

4.2.1   Sample processing

Bulk sample material was dried overnight at 40°C, prior to weighing. Disaggregating of the

sediment was carried out by gently heating the sediment in water, with a small amount of washing soda. All samples were wet sieved at 63µm before being dried overnight at 40°C, the <63µm fraction was retained and dried. A micro splitter was used to split the samples into two sub sets. One half was used for morphometric analysis, the other for geochemical analysis. The half used for morphometric analysis was dry sieved at 125µm, and split into varying aliquots dependent on the amount of material. No further size splitting was carried out, all specimens being picked from the >125µm fraction. Aliquots of each sample were picked until over 75 specimens were obtained. Picking from a single size split is believed to prevent a size bias in picking large numbers of specimens from a single size fraction, and better represents the size distribution observed within the samples. The only criteria imposed on selection of specimens were that they were whole, with no signs of dissolution or loss of the final chamber. Specimens that had aberrant chambers or showed signs of damage caused earlier in ontogeny were mounted and imaged but not used in either the morphological or geochemical analyses. Morphological analysis was carried out prior to selection of specimens for geochemical analysis. All samples and prepared slides are deposited at the Natural History Museum Basel.

4.2.2   Digital imaging

For imaging purposes specimens were mounted on girded faunal slides in keel view, with the aperture to the right. Correct orientation of specimens is achieved by use of a hemispherical stage, this being taken when the spiral height (δX) was seen to be at a minimum and the overall length of the specimen (δY) at maximum value. The system has been calibrated, so using the magnification at which the image was taken; pixel values can be directly converted to micrometers. Any dextral coiling specimens were imaged and mirrored using the tool in Adobe Photo Shop prior to extraction of morphometric data.

Digital image acquisition was carried out using a KAPPA CF 11/2 CCD camera mounted on a Leica MZ6 binocular microscope, connected to a Macintosh computer. The microscope is fitted
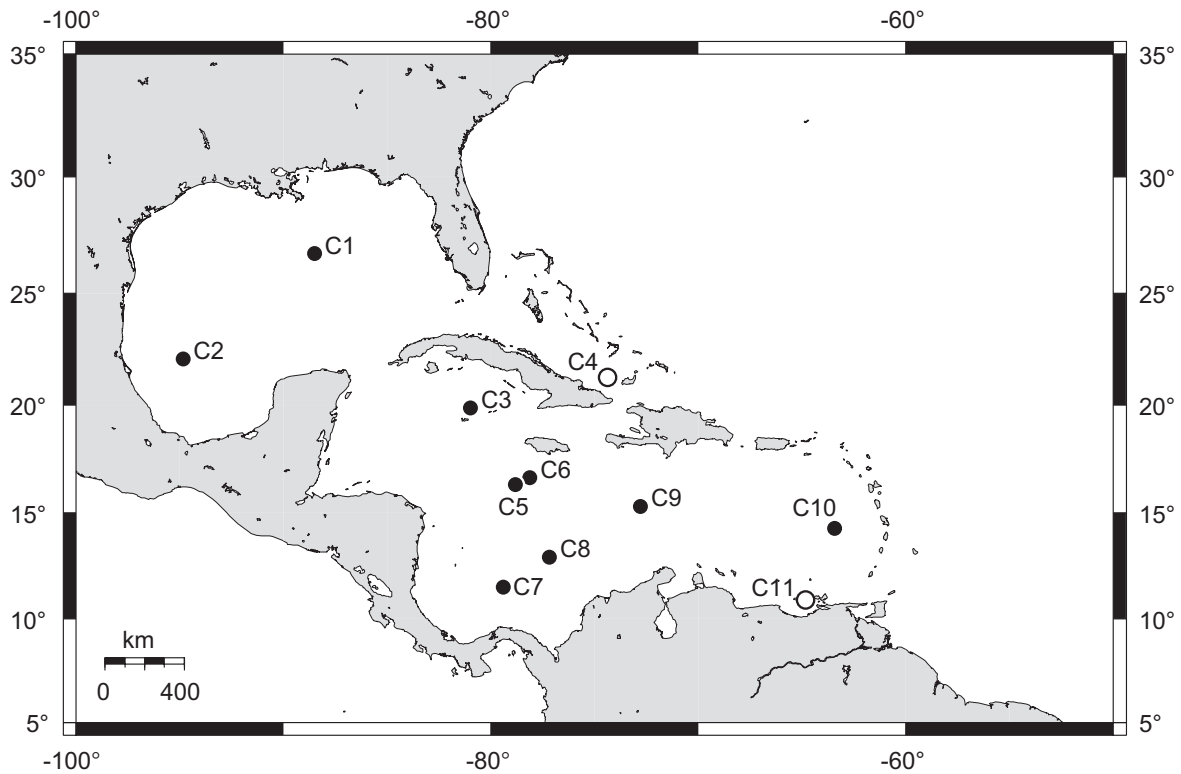
Figure 4.1   Map showing the position of sample sites within the Caribbean.

Map showing the position of sample sites within the Caribbean. Open circles denote sample sites where specimens were imaged but lacked insufficient material for isotopic analysis.

with an Achromat 1x lens and has 0.63x – 4.0x zoom body allowing images to be taken at a range of magnifications. Image capture was carried out using the public domain NIH Image program (developed at the U.S. National Institutes of Health and available on the Internet at http://rsb.info. nih.gov/nih-image/), a suite of specially written macros, was used to accelerate image capture and processing. Captured images have a size of 640 x 480 pixels in 256 Grey scales and are saved in Tiff format, and are deposited in the form of CD-ROMs at the Natural History Museum Basel. Each imaged specimen was given a unique identifier code that allows reference to both the sample site and its position on the faunal slide. Processing of the images reduces the image to a black and white negative, which is saved as in raw format. Cartesian co-ordinate data was generated using a suite of FORTRAN programs including "Trace33-bach.out" (Knappertsbusch,

1998). Morphometric measurements such as δX, δY, and Φ3, were generated using the FORTRAN programs "Sprep53.out" and "KeelWidth100.out" (Knappertsbusch 2004). Figure 4.2 shows an example of an extracted out line with the two main measured variates δX and δY used to distinguish morphotypes and to investigate the morphological variation within *G. menardii* and *G. tumida*.

4.2.3 Isotope analysis

The material used in the geochemical analysis was dry sieved using a sieve stack comprised of the following mesh sizes: 125μm, 250μm, 310μm, 500μm, 710μm, and 1000μm. Following sieving, individual specimens were hand picked under a binocular microscope from each size fraction and split whether they showed heavy or light surface encrusting. Specimens from each of the size fractions were imaged prior to geochemical analysis. When there was insufficient specimens for geochemical analysis, additional specimens were selected from the material that had been used for morphometric analysis were used.

All picked specimens were soaked in ethyl alcohol and cleaned in an ultrasonic bath to remove as much infilling material and surface contaminants as possible. Following ultrasonic treatment the excess alcohol was drained off and the specimens were left to air dry on filter paper. For geochemical analyses samples weighed between 100 and 150μg. This resulted in most samples being comprised of multiple specimens, the number varying in each size fraction, only in the larger size fractions (>710 μm) was it possible to carry out single specimen analysis.

Stable isotope analysis was carried out at the Central Analytical Laboratory for Earth and Geosciences Department of Geosciences University Basel. Samples were placed into 12 mL Exetainer vials (Labco Ltd., U.K.) and closed using gas tight screw caps with rubber septum. The vials are placed in the GasBench sample tray (heated to 72°C) and further processed using the phosphoric acid method following the procedure of Spötl and Vennemann (2003). Carbon isotope data are obtained at the Institute of Environmental Geosciences, University of Basel, using a continuous flow mass spectrometer (CF-IRMS, DELTA^{plus} XP, Thermo, Bremen, Germany) equipped with a Gas-Bench II. $^{18}O/^{16}O$ and $^{13}C/^{12}C$ isotope ratios are reported as δ^{18}O and δ^{13}C values [‰] relative to VPDB defined in terms of NBS19 = -2.2 ‰ and 1.95‰, respectively. The accuracy of the isotope ratios was monitored by analyses of two standards (NBS19 and an in house
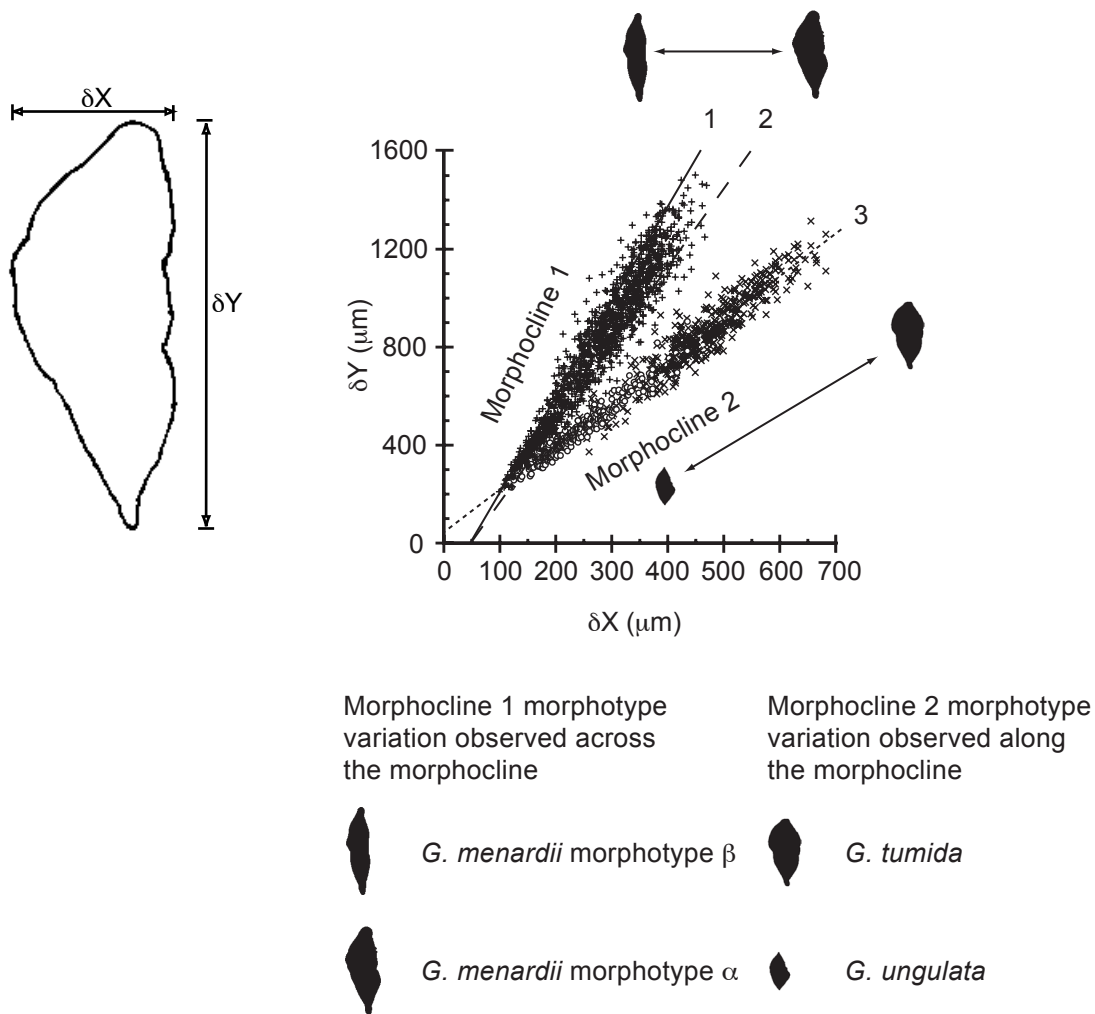
Figure 4.2   Diagram of an extracted outline

Diagram of an extracted outline showing the two measured variates used in the morphological analyses. δY represents the maximum diameter, and δX the spiral height of the test. The spiral side is directed to the left. These two variates are believed to give good separation between them menardiform and tumidform morphologies and show the range within both morphologies.

The scatter plot shows the combined plot of all sample sites.
The three lines labelled 1, 2 and 3 were used to select specimens for geochemical analysis. Lines 1 & 2 are used to investigate the stable isotope signal of the morphological variation observed across (δX variate) morphocline 1; and line 3 was used to investigate the isotopic variation in the differing morphologies along mophocline 2.

standard) giving respective $\delta^{18}O$ values of -2.20±0.01 (1SD, n=30) and -16.13±0.02 (1SD, n=30), and $\delta^{13}C$ values of 1.95±0.01 (1SD, n=30) and -35.27±0.01 (1SD, n=30), during the cause of this study. The long-term reproducibility for both $\delta^{18}O$ and $\delta^{13}C$ data is generally better than 0.1‰.

4.3 Results

4.3.1 Morphometric studies

4.3.1.1 δX versus δY measurements

The morphometric results are presented in Figure 4.3 arranged as a matrix of δX against δY for each sample. The scatter plots are latitudinally arranged from NW (Gulf of Mexico) to SE (off Venezuela). A composite for all Caribbean sample sites is shown in Figure 4.2.

The composite bivariate plot (Figure 4.2) shows two widely diverging branches of data. An upper branch (crosses) consists of *G. menardii*. It predominantly represents morphotype β (*G. menardii cultrata*), with a minor admixture of morphotype α (*G. menardii menardii*) of Knappertsbusch (2007). The lower branch consists of a continuum ranging from *Globorotalia ungulata* (circles, lower portion and *G. tumida* (oblique crossed, upper portion of the branch). The measurements show clearly that in the δX vs. δY morphospace *G. ungulata* intergrades into *G. tumida* within the same branch. Plates 1 and 2 illustrate how representatives of *G. menardii* can be distinguished from *G. tumida* and *G. ungulata* on the basis of axial aspects. In the size fractions below 200μm it becomes difficult to morphologically distinguish between juvenile *G. menardii* and *G. ungulata* or *G. tumida*.

Within the upper branch (*G. menardii*) it can be seen that for any given value of δY there is a range of specimens that vary in the δX values. Moving from line 1 towards line 2 specimens become progressively more inflated in the δX variate and show greater encrusting. Line 3 was placed through the center of morphocline 2 (*G. ungulata – G. tumida*) as the variation in morphology runs along the axis. Lines 1 and 3 are used as visual guides to aid selecting specimens for isotopic analysis and have no other significance in relation to the morphology of the species. Line 2 separates morphotypes α from morphotypes β within morphocline 1 as shown in Knappertsbusch 2007.

4.3.1.2 Encrusting

Microscopic inspection revealed that G. menardii and G. tumida frequently exhibit encrustation to varying degree (see plate 1 for G. menardii morphotypes and plate 2 for G. tumida). Encrustation e.g. the thickening of the shell due to secondary calcite deposition leads to changes in the δX vs. δY ratio and in some cases may identification of representatives of the G. menardii morphotypes from those of the G. tumida. Of the G. tumida forms, most shells showed heavy encrustation appearing as sugar-like coarse calcite in juvenile and adult forms. Only a few exceptions were found where G. tumida showed a low-crusted shell (Plate 2 figure 1a). In theses special cases specimens were distinguished from very similar looking G. ungulata by lacking the diagnostic carinate ridge over the aperture on the final chamber of the latter.

In morphocline 1 the degree of encrusting is reduced as shells decrease their δX vs. δY ratio. In morphocline 2 encrusting increases along the axis of the morphocline, with G. ungulata showing little or no encrusting to G. tumida that shows extreme encrusting.

4.3.2 Isotopic results

Figure 4.4 is similar to Figure 4.3 but explicitly shows the selection of specimens that are used for stable isotope analysis along morphoclines 1 and 2.

4.3.2.1 Size dependent isotopes in G. menardii

The isotopic analyses for the *G. menardii* (morphocline 1) are shown in Figure 4.5. The plot shows the results for both the $\delta^{18}O$ and $\delta^{13}C$. All results are shown as $^0/_{00}$ values relative to VPBD. Again, individual sample site plots are arranged latitudinally as in Figures 4.3 and 4.4. Overall mean values of $\delta^{18}O$ and $\delta^{13}C$ for all *G. menardii* are plotted against shell size in the upper right of the figure. For comparison purposes the same data are plotted from the shallow dwelling and symbiont bearing *Globigerinoides sacculifer* in the lower left side of the figure (open symbols = $\delta^{18}O$, filled symbols $\delta^{13}C$).

In all samples a positive correlation is seen between $\delta^{18}O$ values and increasing size. Encrusted
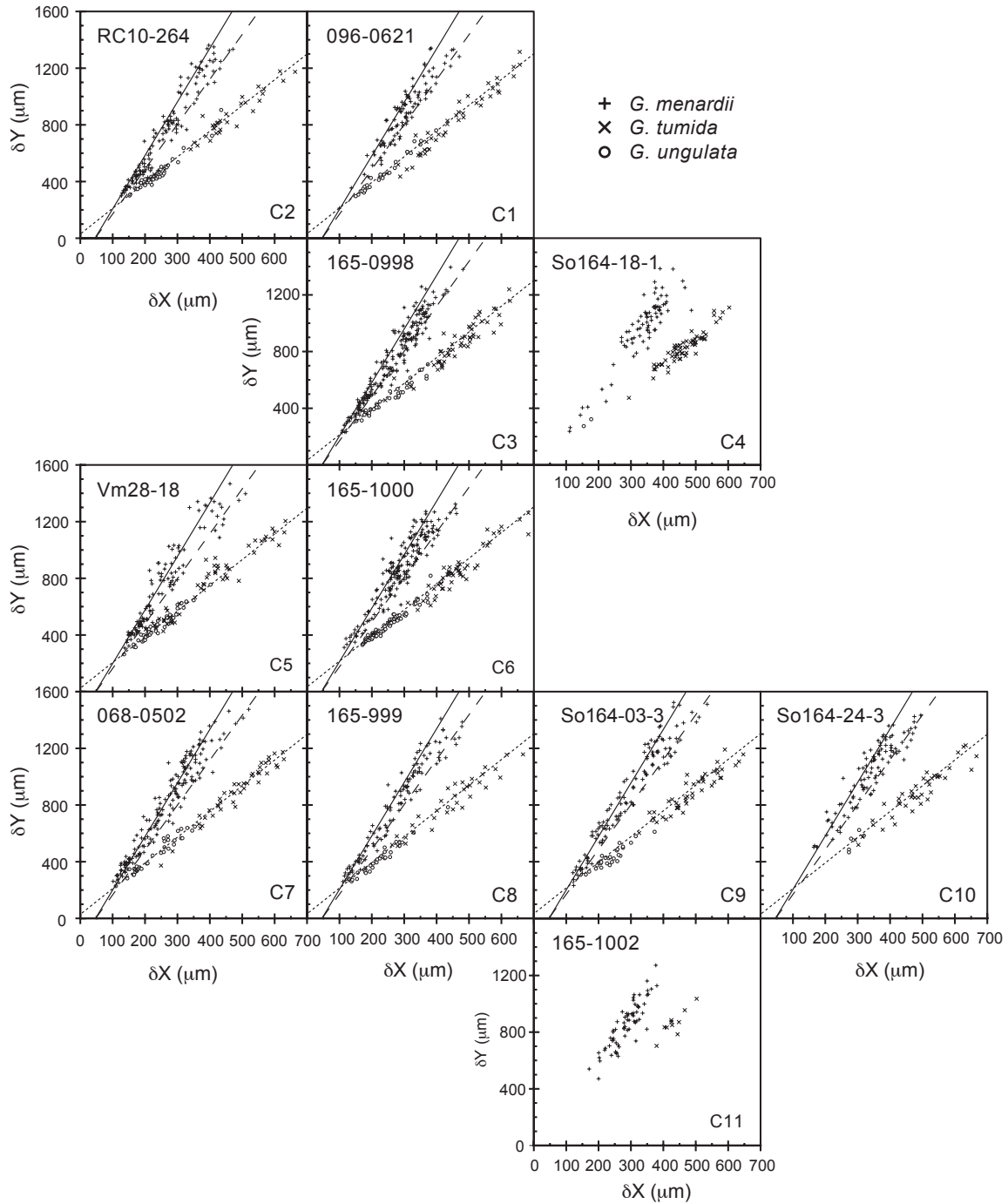
Figure 4.3   Morphometric data for the individual sample sites arranged latitudinally, (northwest to southeast).
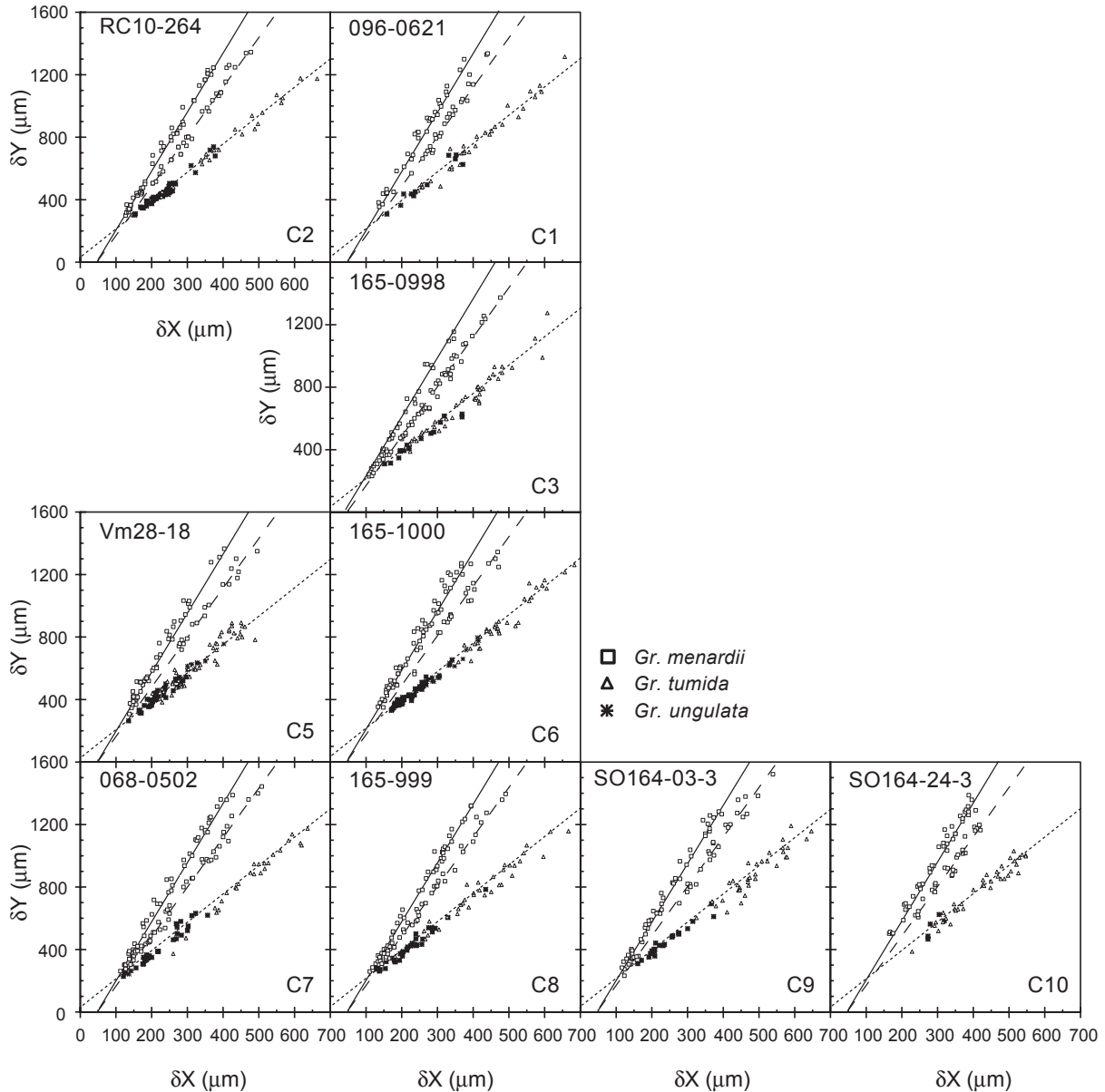
Figure 4.4   Same as figure 4.3 but shows only specimens that were selected for geochemical analysis only

Two distinct morphoclines are seen within the data. The insert is a combined plot of all sample sites. The C numbers in each grid correspond with the map codes. Three lines labelled 1, 2 and 3 were used to select specimens for geochemical analysis.

Lines 1 & 2 are used to investigate the stable isotope signal of the morphological variation observed across (δX variate) morphocline 1; and line 3 was used to investigate the isotopic variation in the differing morphologies along mophocline 2.

specimens are consistently more enriched in $\delta^{18}O$ (more positive values) than the low encrusted specimens of the same size fraction. The $\delta^{18}O$ increase with shell-size for both low and heavy encrusted specimens appear parallel to each other throughout all samples. This signature signal is well recognizable in the mean values.

A similar trend of increasing $\delta^{13}C$ values with increasing size is also seen. However in contrast to $\delta^{18}O$ values there is no clear differentiation seen between low and heavy encrusted *G. menardii* morphologies. In several samples the $\delta^{13}C$ increase with size is not monotonous but shows a steepening interval before the 315 – 500μm size fraction. A comparison of *G. menardii* isotope data with those of the shallow dwelling *G. sacculifer* from the same provenance illustrates similar trends of increasing $\delta^{18}O$ and $\delta^{13}C$ with size. In particular the $\delta^{18}O$ values are very close to those seen for the low-crusted *Globorotalia menardii* specimens that correspond to morphotype β. The $\delta^{13}C$ results show the same size-dependent increase until the 315-500μm size fraction, from where onwards it plateaus. The similar isotopic behavior between the low-crusted *G. menardii* and shallow dwelling *G. sacculifer* suggests that both species share a similar depth habitat. Replotting the data from Schweitzer and Lohmann (1991) (not shown) shows a similar trend of increase in $\delta^{18}O$ with size for both crusted and low crusted *G. menardii* types. However, their results show greater overall depletion in the $\delta^{18}O$ and $\delta^{13}C$ signals, this difference is thought to result from different sample areas.

4.3.2.2 Size dependent isotopes in *G. tumida* and *G. ungulata*

Figure 4.6 shows the isotopic results for the *G. tumida* – *G. ungulata* group (morphocline 2). All plots show both $\delta^{18}O$ and $\delta^{13}C$ against shell size. Again, an increase in $\delta^{18}O$ values with increasing size is observed. Greater separation is seen between *G. tumida* and *G. ungulata* than is seen between the two morphologies of *G. menardii*. The $\delta^{18}O$ values of *G. tumida* are more positive than those for the encrusted *G. menardii* of the corresponding size fractions and the slope of this increase is steeper. The $\delta^{18}O$ results for *G. ungulata* always show greatest depletion in $\delta^{18}O$, (most negative values) and are comparable to the low crusted *G. menardii*. Values of $\delta^{13}C$ increase in value with size increase to varying degree between samples. The slope of the size dependent $\delta^{18}O$ increase of *G. ungulata* is much flatter than that observed for Gr. tumida. This suggests that *G.*

ungulata remains at a similar shallow depth throughout ontogeny. In the plots for samples C6, C8 and C9 there are rare specimens, which were identified as low encrusted forms of *G. tumida* (see plate 4-2 - 1b i-iii). They show a tumid test with radially elongated final chambers similar to a typical *G. tumida*. These specimens have a thin walled, hyaline appearance typical of *G. ungulata* but lack the diagnostic carinate ridge observed over the aperture in *G. ungulata*. They are morphometrically similar to *G. tumida* but texturally similar to *G. ungulata*. It must be noted, that these low encrusted *G. tumida* fit with the isotopic signature of *G. ungulata*!

The tumid-form mean values are plotted in the upper right of the figure. When mean isotopic data is compared to the mean values of the menardiform globorotalids, a more pronounced isotopic separation between the *G. tumida* and *G. ungulata* is evident. *G. tumida* shows the greatest $\delta^{18}O$ values indicating the deepest depth habitat of all the observed specimens. Again the *G. sacculifer* data is included in the lower right for comparison. This isotopic data points to a generally deeper dwelling *G. tumida* and a shallow dwelling *G. ungulata*.

4.3.3 $\delta^{18}O$ versus $\delta^{13}C$ data

Figure 4.7 shows the means of $\delta^{18}O$ plotted against the means of $\delta^{13}C$ as a function of shell size for morphocline 1 (the menardiform globorotalids fig.4.7i.), morphocline 2 (the tumid-form globorotalids fig. 4.7ii.) and *G. sacculifer* (fig. 4.7iii.). The measurements from the individual samples are shown as a matrix of plots in appendices 4.1a. through 4.1c. The error bars on the plots indicate the range of values observed in each sample. The numbers beside the data points encode the size fractions. The mean $\delta^{18}O$ versus mean $\delta^{13}C$ demonstrates a clustering into low and heavy crusted specimens of *G. menardii*. Clusters for low and heavy encrusting show parallel from small specimens (e.g. more negative $\delta^{18}O$ and $\delta^{13}C$) to large specimens (more positive $\delta^{18}O$ and $\delta^{13}C$ signals). These observations point to a deeper habitat for crusted specimens than of the low-crusted specimens.

In Figure 4.7 ii. a distinct separation between *G. tumida* and *G. ungulata* occurs along the $\delta^{18}O$ axis. *G. ungulata* is depleted in $\delta^{18}O$ indicating a warmer (shallower) habitat, comparable to that of the low crusted *G. menardii*. Alng the $\delta^{13}C$ axis no distinct separation can be seen. This suggests that members of morphocline 2 dwelled in $\delta^{13}C$ enriched e.g. more eutrophic waters. For
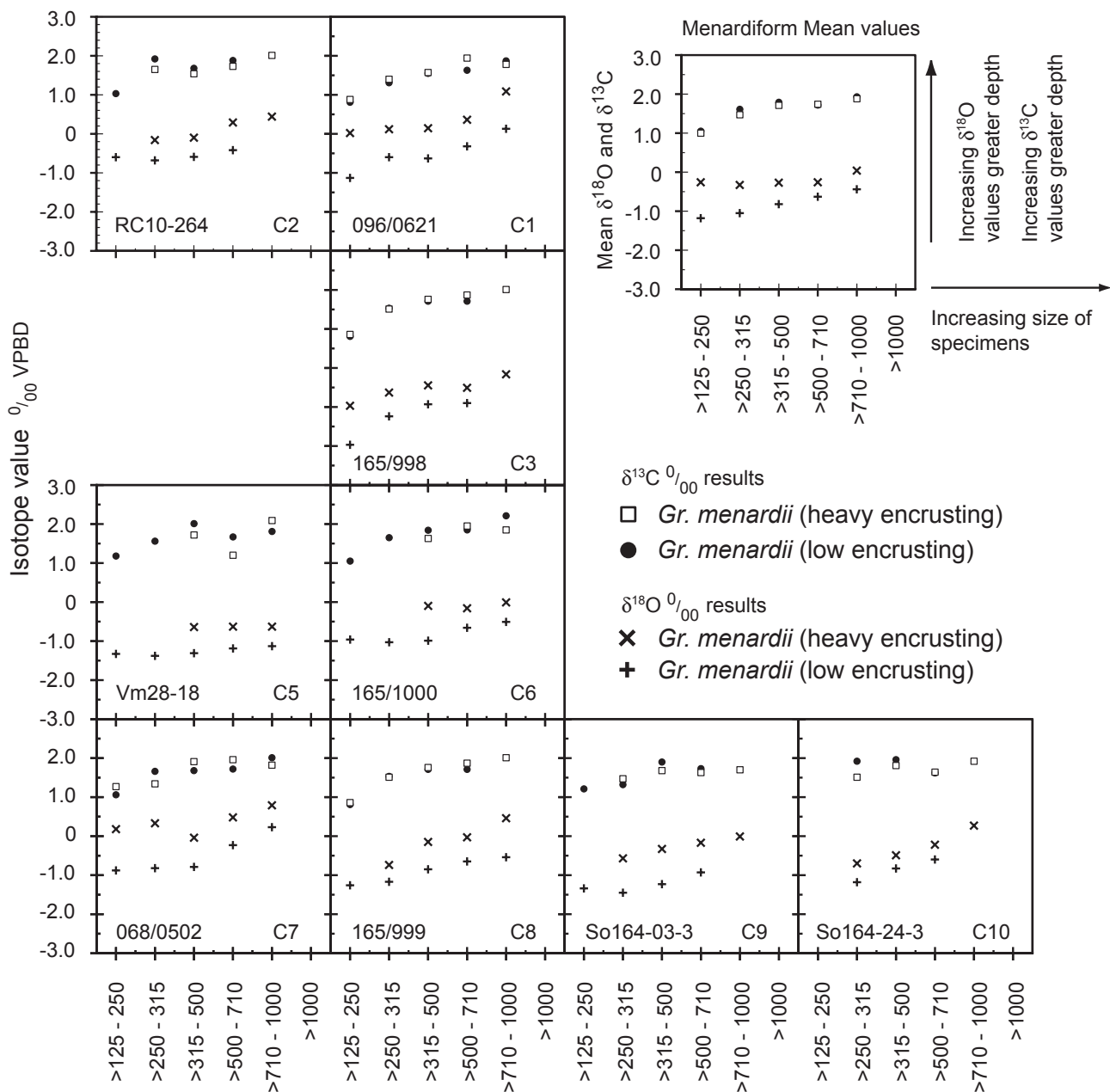
Figures 4.5   Size dependent variation of δ18O and δ13C in morphocline 1 (Gr. menardii).
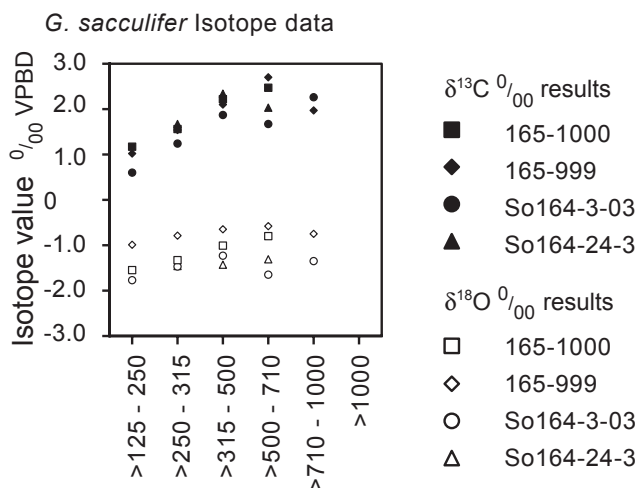
Isotope values are given in ⁰/₀₀ relative to VPBD. All plots are arranged latitudinally from northwest to south east. C numbers in the plots correspond to map sample sites. The mean value of all sample sites is included in the upper right of the plot. For comparison data from the shallow dwelling G. sacculifer is included at the bottom of the figure.

comparison the mean isotopic values for the contemporaneous *G. sacculifer* are shown in Figure 4.7 iii. In *G. sacculifer* a positive trend of δ^{18}O vs. δ^{13}C parallels a unidirectional ontogenetic size increase, vertical descent of maturing individuals.

4.4   Discussion

Figure 4.8 is a summary plot for the combined, δ^{18}O vs. δ^{13}C data for *G. menardii* (morphocline 1) and *G. tumida – G. ungulata* (morphocline 2). The isotope data of the shallow dwelling *G. sacculifer* are plotted as a reference. Groupings described in the previous section are highlighted.

4.4.1   Morphocline 1 – *G. menardii*

The low-encrusted group of *G. menardii* occupies a similar field as *G. sacculifer* suggesting a similar shallow depth habitat within the water column. As specimens become larger they show an increase in δ^{18}O value, indicating downward migration through the water column within the habitat. The δ^{13}C signal of the low crusted *G. menardii* shows a greater range than that observed within the crusted specimens. Such a signature is typically seen in symbiont bearing species (Norris 1998). Hemleben et al., (1989) describe *G. menardii* as having a facultative symbiotic relationship with chrysophyte algae. While Spero (1998) illustrates a symbiont bearing *G. menardii*; in his figure 1d the specimen resembles that of the low-crusted morphotype β identified in this study.

In morphocline 1, morphotypes α and β show corresponding size fractions from small juvenile forms to large adult forms. When this is combined with the isotopic signals it gives evidence for a separation of menardiform globorotalids into a shallow, symbiont bearing narrow keeled and a deeper living, non-symbiont, and heavier keeled populations. Both deep and shallow populations of *G. menardii* show a corresponding size-related trend in δ^{18}O, while only the low crusted forms show a distinctly wider -range of δ^{13}C values. These results suggest that encrusting of the test is a function of the environment within which the organism lived and disagrees with the idea of heavy encrusting representing gametogenic calcification as the major process for secondary calcite crust formation.
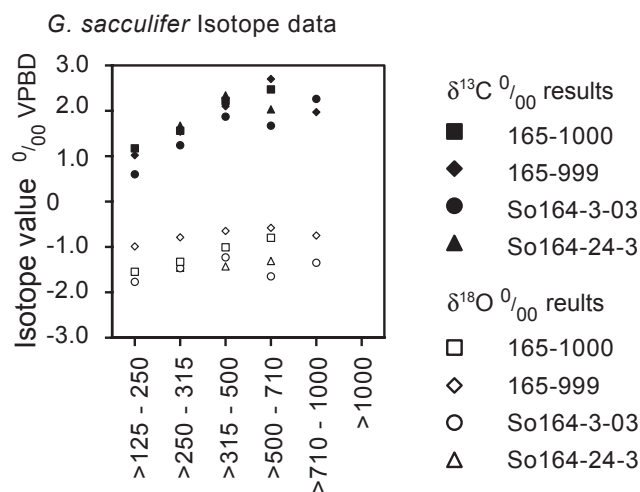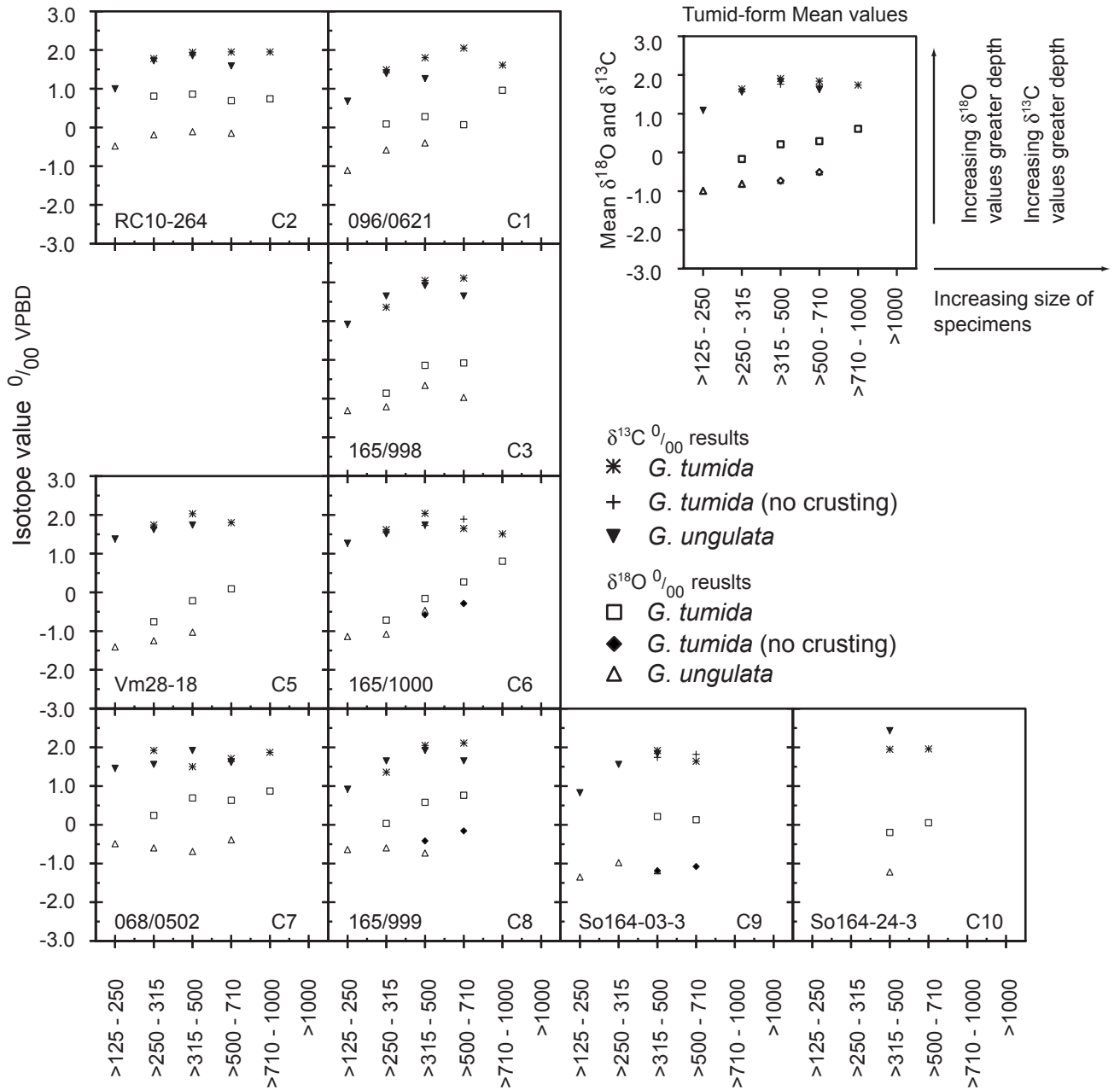
Figure 4.6   Size dependent variationof of δ¹⁸O and δ¹³C in morphocline 2
(Gr. tumida – Gr. ungulata).

Isotope values are given in ⁰/₀₀ relative to VPBD. All plots are arranged latitudinally from northwest to south east. C numbers in the plots correspond to map sample sites. The mean value of all sample sites is included in the upper right of the plot. For comparison data from the shallow dwelling *G. sacculifer* is included at the bottom of the figure.

Although the isotopic signals may vary between sample sites, the difference seen in the isotopic data between crusted and low-crusted *G. menardii* appears constant. A symbiotic relationship would require the *G. menardii* to remain higher in the photic zone, which is in agreement here with the depletion seen in the $\delta^{18}O$ signal of the low-crusted specimens. Norris (1996) argued that symbiotic relationships have played a major role in diversification of planktonic foraminifera, while Hemleben et al., (1981) suggested that symbiosis is an evolutionary adoption to more oligotrophic environmental conditions. The morphological trends and isotopic results of this work are similar to trends observed in extinct Globorotalids, which evolved rapidly in the Late Miocene and Pliocene. This rapid evolution has been linked to the emergence of the Central American Isthmus and the resultant changes in tropical ocean currents. The new species are believed to be endemic to the Atlantic (Chaisson 2003). Gasperi and Kennett (1993) showed that *G. limbata* has a constantly shallower depth habitat than its ancestral species *G. menardii*. For the extinct *G. pertenuis*, *G. exilis* and *G. miocenica*, Chaisson (2003) showed how the adaptation to shallower habitats resulted in flatter morphologies with smooth and finely perforated tests. These trends are similar to those seen for the low-crusted *G. menardii* of this study. It is interpreted that *G. menardii* is evolving to take advantage of a new niche, which is reflected in a modification of shell morphology.

4.4.2 Morphocline 2 – *G. tumida* – *G. ungulata*

The $\delta^{18}O$ signal from *G. tumida* and *G. ungulata* show differing depth habitats, with the *G. tumida* being significantly deeper than *G. ungulata*. Interestingly *G. tumida* also shows a greater rate of chamber size increase throughout ontogeny *G. ungulata*. This suggests faster maturation under more eutrophic conditions at greater depth in *G. tumida* than in *G. ungulata*. Both species show similarity in $\delta^{13}C$ values, which suggests neither morphology, has a symbiotic relationship. Morphometrically *G. ungulata* intergrades with *G. tumida*; the main variations being that of size and level of encrusting. Pearson (1995) suggested that *G. ungulata* may be an ecophenotypic variation of *G. tumida*. While Lamb and Beard (1972) suggest that they represent ontogenetic variants. The morphometric and isotopic data presented here suggest that they are ontogenetic morpho-variants, with *G. ungulata* representing the shallow dwelling juvenile and *G. tumida* the deeper dwelling adult.
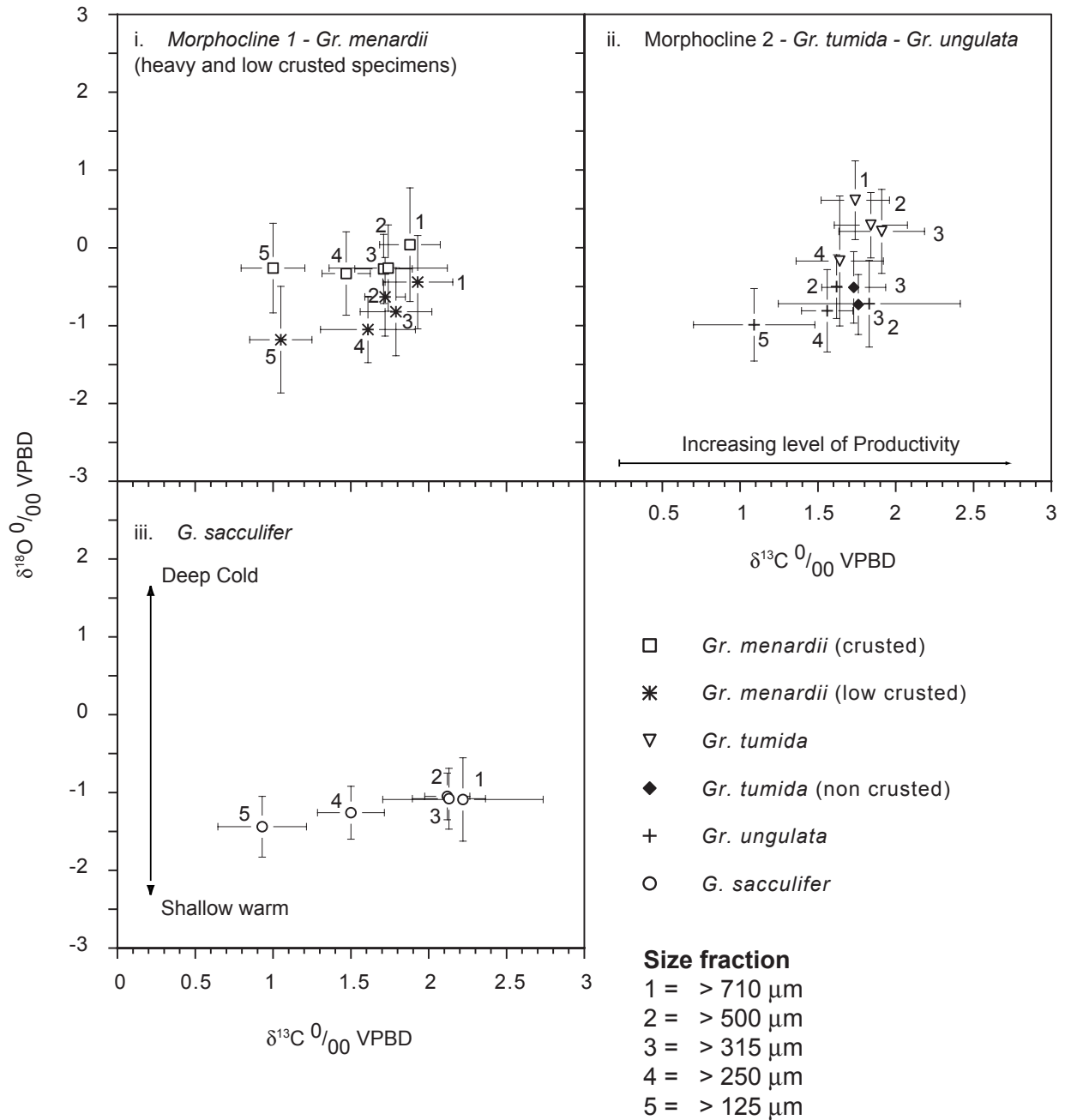
Figure 4.7   Plots of mean δ¹⁸O against mean δ¹³C for all isotopic measurements carried out

Results are shown in ⁰/₀₀ relative to VPBD. The error bars show the variation about the mean for any given size fraction.

The numbers next to the symbols indicate the size fraction, the greater the size fraction the smaller the number.

i.   Shows the results for morphocline 1
ii.   Shows the results for morphocline 2
iii.   Shows the results for the shallow dwelling symbiont bearing G. sacculifer

However, the first occurrence of *G. tumida* is placed at the base of Zone N18. The first occurrence of *G. ungulata* is not known with any certainty, ranging (depending on authors), from N19 (Blow 1969 – specimens not illustrated), late Pleistocene (Stainforth et al.,, 1975) to the base of the Holocene (Bolli and Saunders 1985). Even though the fossil record is biased towards larger adult forms, one may expect that the ontogenetic variants *G. tumida* and *G. ungulata* would have a similar biostratagraphical range. In reality they do not have a similar range, which supports the idea that *G. ungulata* represents a recent evolutionary adaptation, with *G. tumida* evolving to take advantage of a new shallower depth habitat.

Figure 4.9 is a summary diagram that illustrates the proposed "depth habitat hypothesis" for the *G. menardii – G. tumida plexus*. Two subpopulations are seen the shallow dwelling morphologies (*G. menardii* morphotype β and *G. ungulata*) and the deeper dwelling morphologies (*G. menardii* morphotype α and *G. tumida*).

The "depth habitat hypothesis" is seen as a dual pair of depth dependent population, e.g. morphocline 1 (shallow *G. menardii* morphotype β and deeper *G. menardii* morphotype α) and morphocline 2 (shallow *G. ungulata* and deeper *G. tumida*) respectively. In the present study morphocline 1 is interpreted as two vicariant, reproductively isolated populations. Morphocline 2 is interpreted as two trans-bathymetric ontogenetic series – in principle the same species: The *G. tumida* morphotype lives at depth, the *G. ungulata* morphotype lives at surface.

4.5   Conclusions

1. The globorotalid species *G. menardii* shows a range of intergrading morphologies. The end members of the series show distinct ecological signals. Morphological variation and isotopic signals appear linked, with the most positive $\delta^{18}O$ signals corresponding to the greatest inflation of the test. The presence of all corresponding size fractions within the two recognized morphologies suggests that there are two distinct subpopulations of menardiform globorotalids within the Caribbean region. The more compressed low
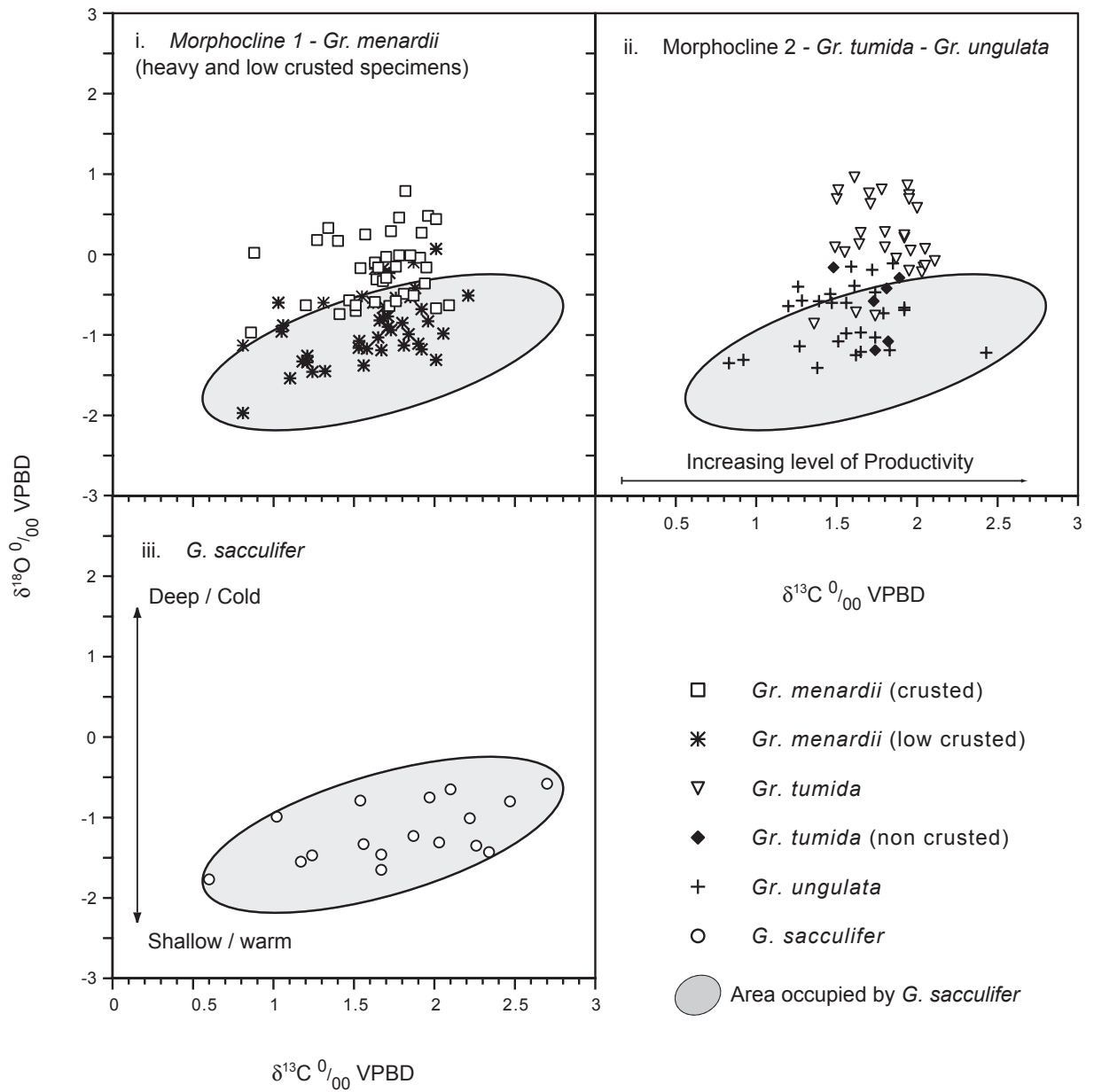
Figure 4.8   Summary plot of δ18O against δ13C, showing all individual measurements (in $^{0}/_{00}$ relative to VPBD).

The shaded area represents the area occupied from the shallow dwelling *G. sacculifer*.

i.   Shows all morphocline 1 results.
ii.   Shows all morphocline 2 results.
iii.   Shows the results from *G. sacculifer*.
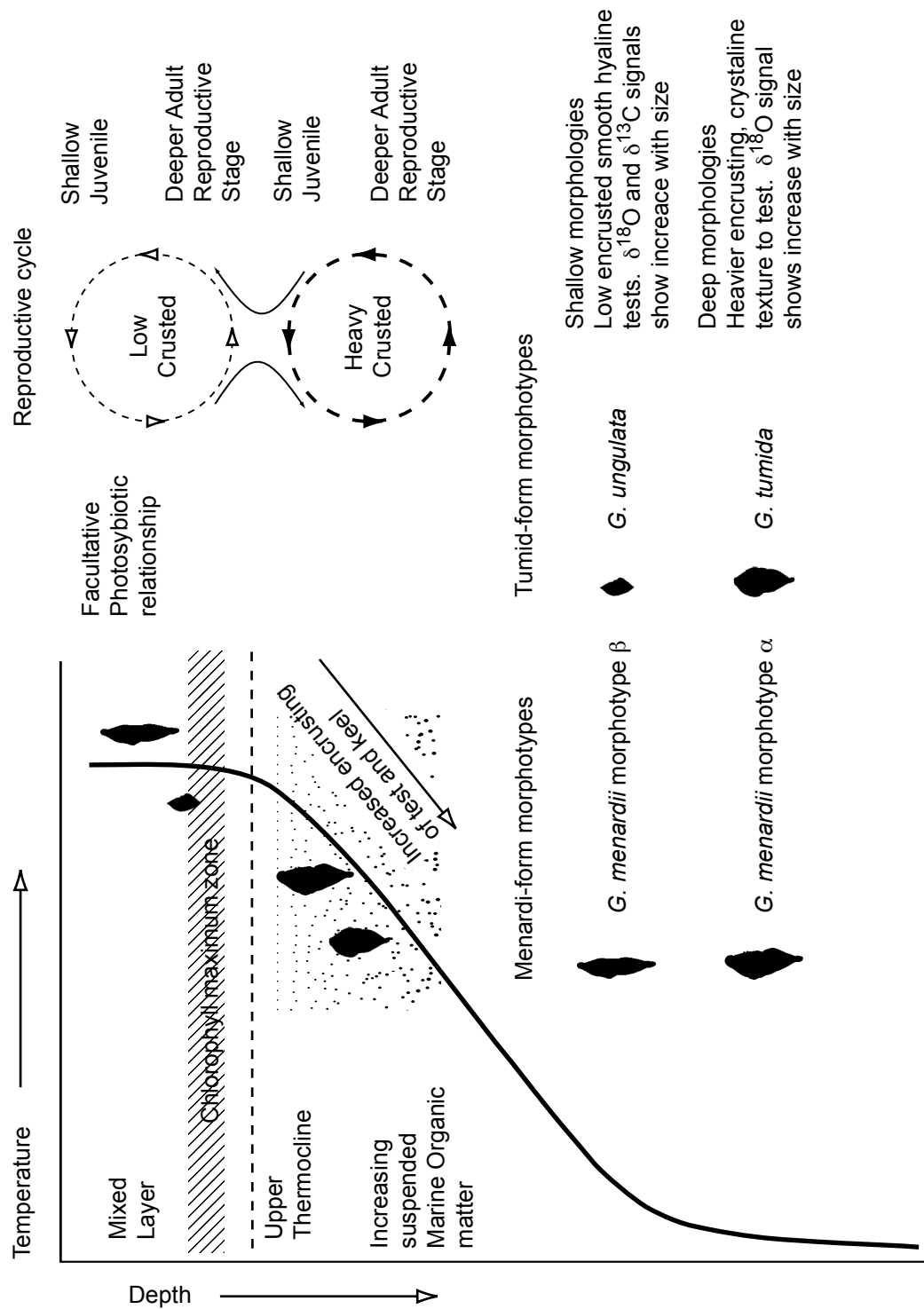
Figure 4.9   Summary diagram illustrating the hypothesized two subpopulations identified within this work.

The $\delta^{18}O$ signal of *Gr. tumida* places it in the deepest depth habitats. The variation in the $\delta^{18}O$ and $\delta^{13}C$ seen in the low crusted *Gr. menardii* suggests a symbiotic relationship. The lower d13C variation observed in the *Gr. ungulata* suggests that it is, although shallow dwelling, asymbiotic.

encrusted morphotype β possesses an isotopic signal that indicates a shallower depth habitat above the thermocline with a probable symbiotic relationship. Morphotype α has a more robust, encrusted form with greater inflation and an isotopic signal indicating an asymbiotic deeper depth habitat below the photic zone in the upper thermocline.

2. Morphometrically *G. tumida - G. ungulata* are a distinct group and should not be included in with *G. menardii* in census work. The isotopic variation seen in the *G. tumida* and *G. ungulata* shows two distinct depth habitats. The morphological variation is believed to represent an ecophenotypic response, with *G. ungulata* representing a more recent adaptation of *G. tumida* into a shallower habitat.

3. Care needs to be taken when selecting material for geochemical investigation: Mixing of morphotypes in a single sample could result in errors in the isotopic values as they could represent two individuals that lived in differing environmental conditions.

4. Inflation and encrusting of the test is related to the depth at which the foraminifera lived rather than an indication of the ontogenetic stage of the individual.

5. The possibility that the depth separation is resulting in a divergence within the *G. menardii* population in the Caribbean cannot be ruled out. This evolutionary trend towards a flatter more compressed shallow dwelling morphology has been seen before in the *G. menardii* plexus during the Late Miocene and Pliocene.

6. This study is limited to the Caribbean Sea region. This was done on purpose as seasonal variations in SST and Salinity within the Caribbean region are minimal. This setting reduces any seasonal variation in the isotopic signals present. It is believed that the isotopic signals observed are a result of perennial depth stratification on centennial to millennial or longer time scales within the *G. menardii* and *G. tumida – G. ungulata* and not seasonal variations.

'

4.6   Acknowledgement

Plate 4-1-key Menardiform Globorotalids (Morphocline 1)

Size fraction >710μm
Specimen 1 (1a-i., 1a-ii., and 1a-iii)   *Gr. menardii* morphotype α (*G.menardii menardii*)

Size fraction >500μm
Specimen 2a (2a-i., 2a-ii., and 2a-iii)   *Gr. menardii* morphotype α (*G.menardii menardii*)
Specimen 2b (2b-i., 2b-ii., and 2b-iii)   *G. menardii* morphotype β (*G. menardii cultrata*)

Size fraction >315μm
Specimen 3a (3a-i., 3a-ii., and 3a-iii)   *Gr. menardii* morphotype α (*G.menardii menardii*)
Specimen 3b (3b-i., 3b-ii., and 3b-iii)   *G. menardii* morphotype β (*G. menardii cultrata*)

Size fraction >250μm
Specimen 4a (4a-i., 4a-ii., and 4a-iii)   *Gr. menardii* morphotype α (*G.menardii menardii*)
Specimen 4b (4b-i., 4b-ii., and 4b-iii)   *G. menardii* morphotype β (*G. menardii cultrata*)
                                                – hyaline appearance of test is evident.

Size fraction >125μm
Specimen 5a (5a-i., 5a-ii., and 5a-iii)   *Gr. menardii* morphotype α (*G.menardii menardii*)
Specimen 5b (5b-i., 5b-ii., and 5b-iii)   *G. menardii* morphotype β (*G. menardii cultrata*)
                                                – hyaline appearance of test is evident.

All illustrated specimens are taken from Sample site SO164-2-03. Specimens are arranged with
dividing bars separating size fractions.
Images were taken using a JC KY-F75U colour video camera mounted on a Leica MZ6 microscope
filled with a 1.0x planapochrometric lens. Images comprise stacks of 50 individual images montaged
using the Auto-Montage Pro Version 5.01 software package from Syncroscopy

>710 μm

1a-i   1a-ii   1a-iii   500 um

>500 μm

2a-i   2a-ii   2a-iii   500 um   2b-i   2b-ii   2b-iii

>315 μm

3a-i   3a-ii   3a-iii   100 um   3b-i   3b-ii   3b-iii

>250 μm

4a-i   4a-ii   4a-iii   100 um   4b-i   4b-ii   4b-iii

>125 μm

5a-i   5a-ii   5a-iii   100 um   5b-i   5b-ii   5b-iii
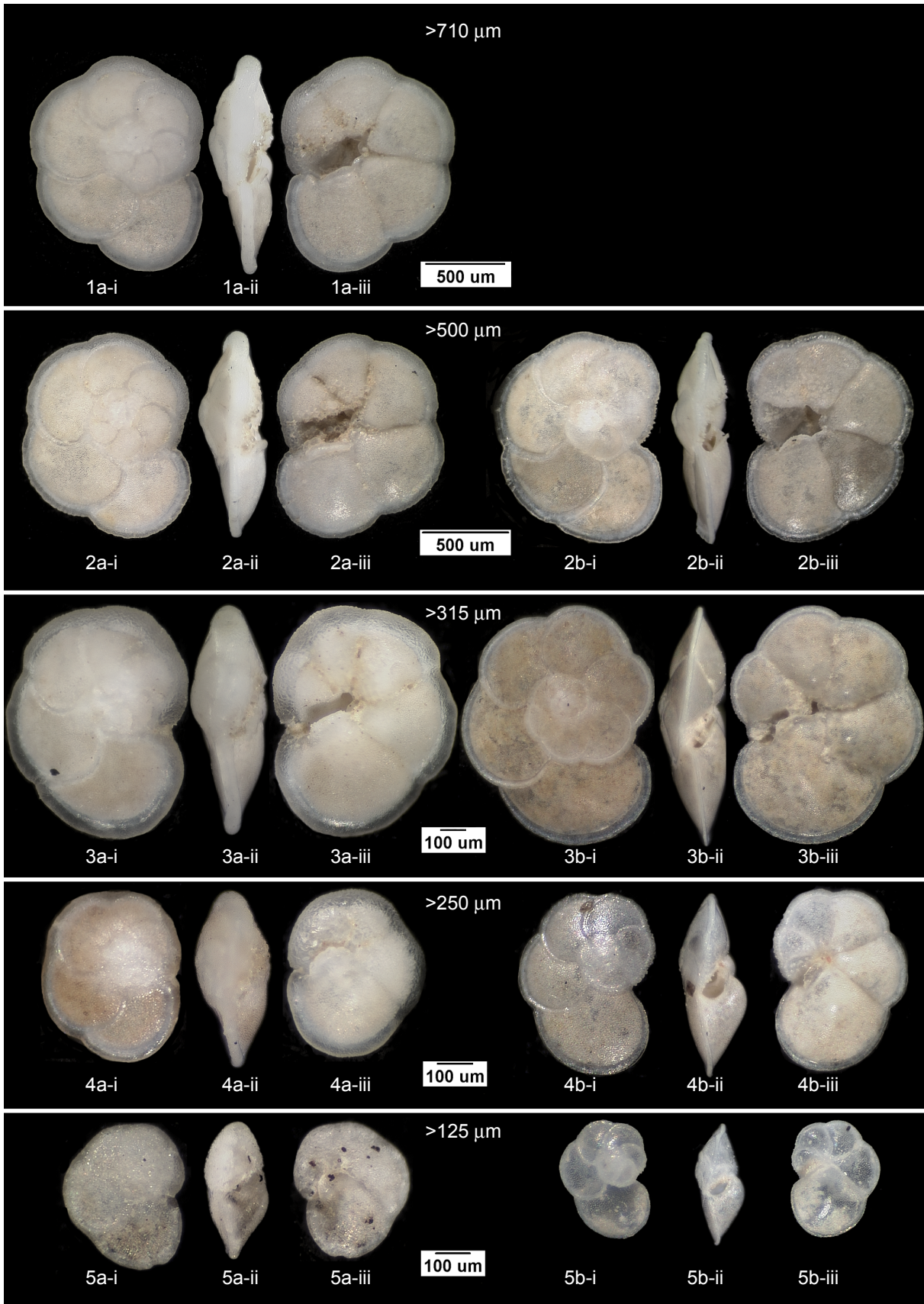
Plate 4-1   Menardiform Globorotalids (Morphocline 1)

Plate 4-2-key   **Tumid-form Globorotalids (morphocline 2).**

Size fraction >500μm
Specimen 1a (1a-i., 1a-ii., and 1a-iii)   *Gr. tumida*
Specimen 1b (1b-i., 1b-ii., and 1b-iii)   *Gr. tumida* (non-crusted) Hyaline appearance of *Gr. ungulata* but lacks diagnostic carinate ridge over aperture of final chamber.

Size fraction >315μm
Specimen 2a (2a-i., 2a-ii., and 2a-iii)   *Gr. ungulata – Gr. tumida* intermediate form, remains of carinate ridge are visible over aperture of final chamber, specimen has an encrusted appearance and more pronounced keel.
Specimen 2b (2b-i., 2b-ii., and 2b-iii)   *Gr. tumida* (non-crusted) form, appearance similar to *Gr. ungulata* but lacks the diagnostic carinate ridge over aperture of last chamber. Also beginning to developed characteristic radial elongation of final chamber seen in *Gr. tumida.*.
Specimen 2c (2c-i., 2c-ii., and 2c-iii)   *Gr. tumida*
Specimen 2c (2d-i., 2d-ii., and 2d-iii)   *Gr. ungulata,* specimen has diagnostic carinate ridge over aperture on last chamber.

Size fraction >250μm
Specimen 3a (3a-i., 3a-ii., and 3a-iii)   *Gr. tumida*
Specimen 3b (3b-i., 3b-ii., and 3b-iii)   *Gr. ungulata*

Size fraction >125μm
Specimen 4a (4a-i., 4a-ii., and 4a-iii)   *Gr. tumida*
Specimen 4b (4b-i., 4b-ii., and 4b-iii)   *Gr. ungulata*

>500 μm

1a-i   1a-ii   1a-iii   1b-i   1b-ii   1b-iii

500 um

>315 μm

2a-i   2a-ii   2a-iii   2b-i   2b-ii   2b-iii

2c-i   2c-ii   2c-iii   500 um   2d-i   2d-ii   2d-iii

>250 μm

3a-i   3a-ii   3a-iii   3b-i   3b-ii   3b-iii

100 um

>125 μm

4a-i   4a-ii   4a-iii   100 um   4b-i   4b-ii   4b-iii

Plate 4-2   Tumid-form Globorotalids (morphocline 2).

4.7　References

Bandy O.R., 1972. Origin and development of *Globorotlia (Turborotalia) pachyderma* (Ehrenberg) Micropaleontology, 18, 3:294-318.

Banner, F.T., and Blow, W.H., 1960. Some primary type of species belonging to the super-family *Globinerinaceae*. Contr. Cushman Found. Foram. Re*s*. Vol. 11:1-41, pls. 1-8.

Bé, A.W.H., 1960. Ecology of Recent Planktonic foraminifera Part 2. Bathymetric and Seasonal distribution in the Sargasso Sea off Bermuda. Micropaleontology.
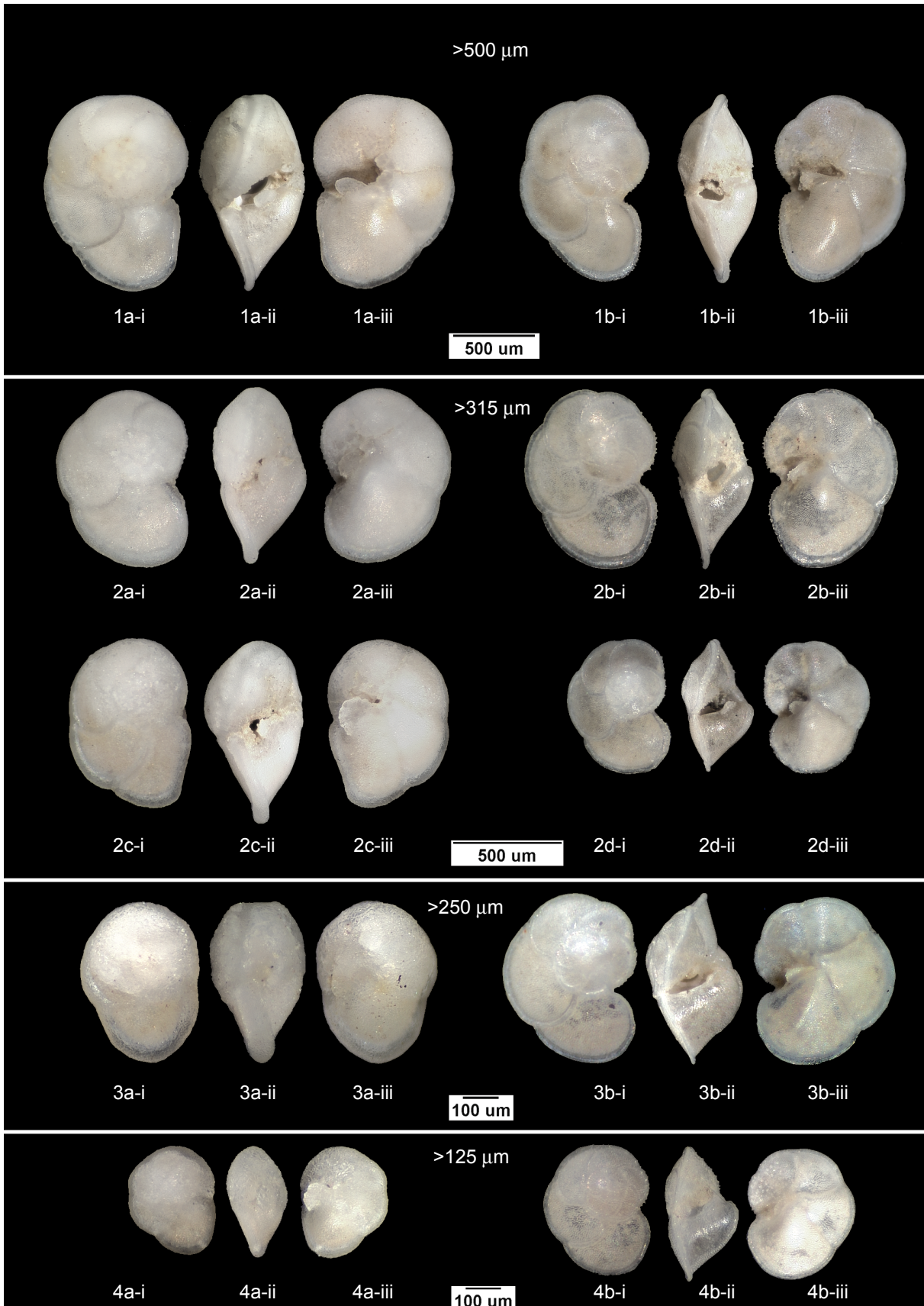
Blow, W.H. 1969. Late Eocene to Recent Planktonic Foraminiferal Biostratigraphy In: *Proceedings of the first international conference on Planktonic microfossils Geneva, 1967* 1:199-422

Blow, W.H. 1979. *The Cainozoic Globigerinida*. E.J. Brill, Leiden (3 vols.), 1413pp

Bolli, H.M. 1970. The foraminifera of Sites 23-31, Leg 4. *Initial Rep. DSDP., 4, 577-643*

Bolli, H.M., and Saunders, J.B., 1985. Oligocene to Holocene low latitude planktic foraminifera. In: Bolli H.M., Saunders J.B. and Perch-Nielsen K., Editors Plankton Stratigraphy Cambridge University Press.

Chaisson W.P., 2003. Vicarious living: Pliocene menardellids between an isthmus and an ice sheet. Geolog,. 31, 12:1085-1088.

Cifelli, R. and Scott, G. 1986. Stratigraphic Record of the Neogene Globorotalid Radiation (Planktonic Foraminifera) Smithsonian contributions to Paleobiology No. 58.

Darling, K.F., Wade, C.M., Stewart, I., Kroon, D., Dingle R., and Leigh Brown A.J., 2000. Molecular evidence for genetic mixing of Arctic and Antarctic subpolar populations of planktonic foraminifers. Nature, 405:43- 47.

Darling, K.F., Kucera, M., Pudsey, C.J., Wade C.M., 2004. Molecular evidence links cryptic diversification in polar plankton to Quaternary climate dynamics Proceedings National Academy of Science 101(20):7657-7662.

Emiliani, C., 1969. A New Paleontology. Micropaleontology, vol. 15, (3). pp. 265-300.

Ericson, D. B., and Wollin, G., 1956. Correlation of six cores from the equatorial Atlantic and Caribbean. Deep-Sea Research., 3, (2), pp. 104-125
Ericson, D. B., Ewing, M., Wollin, G. and Heezen, B.C., 1961. Atlantic deep-sea sediment cores: Geol. Soc. America Bull., 72 : 193-285

Ericson, D. B., and Wollin, G., 1968. Pleistocene climates and chronology in deep-sea sediments. Science, vol. 162, 3859:1227-1234.

Fairbanks, R.G., Wiebe, P.H., and Bé, A.W.H. 1982. Vertical Distribution and Isotopic composition

of Living Planktonic Foraminifera in the Western North Atlantic. Science 20:61-63.

Gasperi, J.T. and Kennett, J.P., 1993. Vertical thermal structure evolution of Miocene surface waters: Western equatorial Pacific DSDP Site 289. Marine Micropaleontology, 22:235-254.

Hemleben, Ch., Spindler, M., and Anderson, O., 1989. Modern Planktonic Foraminifera. Springer Verlag, Berlin, Heidelberg

Kennett, J. P. and Srinivasan, M. S., 1983. Neogene planktonic foraminifera, a phylogenetic atlas. Hutchinson Ross, Stroudburg, Pennsylvania.

Knappertsbusch, M., (2007). Morphological variability of Globorotalia menardii (planktonic foraminiferan) in two DSDP cores from the Caribbean Sea and the Eastern Equatorial Pacific. Carnets de Géologie / Notebooks on Geology, Brest, Article 2007/04 (CG2007_A04)

Lamb, J.L. and Beard, J.H. 1972. Late Neogene Planktonic Foraminifers in the Caribbean, Gulf of Mexico, and Italian Stratotypes. The University of Kansas Paleotological Contributions. Article 57 (Protozoa 8).

Norris, R.D., 1996. Symbiosis as an evolutionary innovation in the radiation of Paleocene planktic foraminifera. Paleobiology, 22(4):461-460

Norris, R.D., 1998. Recognition and Macroevolutionary significance of Photosymbiosis in molluscs, corals, and foraminifera. Isotope Paleobiology and Paleoecology. The Paleontological society papers 4:68-100.

Pearson, P.N., 1995. Planktonic Foraminifer Biostratigraphy and the Development of Pelagic Caps on Guyots in the Marshall Islands Group. In: Haggety, J.A., Premoli Silva, I., Rack, F., and McNutt, M.K. (Eds.), Proceedings of the Ocean Drilling Program, Scientific Results, Vol. 144.

Schmid, K., 1934. Biometrische Untersuchungen an Foraminiferen
Ecologae geol. Helvetiae, 27(1):45–134.

Schweitzer P.N., and Lohmann G.P., 1991. Ontogeny and Habitat of Modern Menardiiform Planktonic Foraminifera Journal of Foraminiferal Research. 21(4):332-346.

Spero, H.J., 1998. Life History and stable isotope geochemistry of Planktonic Foraminifera Isotope Paleobiology and Paleoecology. The Paleontological society papers 4:7-36.

Spötl, C. and Vennemann, T. 2003. Continuous-flow isotope ratio mass spectrometric analysis of carbonate minerals. Rapid Communications in Mass Spectrometry, 17,

Stainforth, R.M., Lamb, J.L., Luterbacher, H., Beard, H.J., and Jeffords, R.M., 1975. Cenozoic Planktonic Foraminiferal zonation and characteristics of index forms. Article 62 The University of Kansas Paleontology Institute.

Todd, R., 1964. Planktonic Foraminifera From Deep-Sea Cores off Eniwetok Atoll – bikini and nearby atolls, Marshall Islands. Age interpretations of samples of Globigerina ooze from an
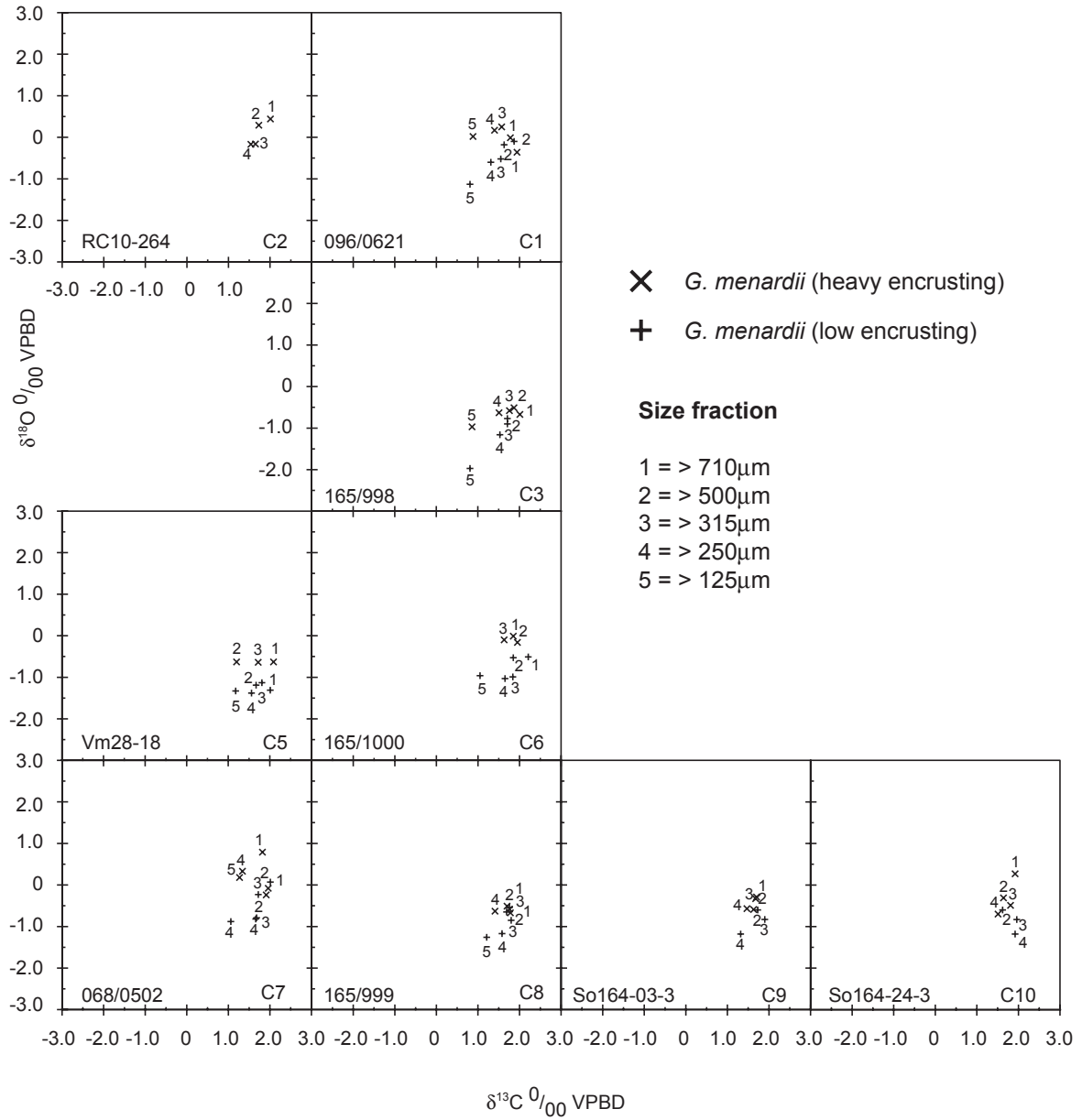
adjoining guyot southwest of Eniwetok Atoll.
Geological survey professional Paper 260-CC.

Thompson, P.R., 1982. Foraminifers of the Middle American Trench. In: *Initial Rep. DSDP.,* 67:351-381.

Appendix 4.1   Sample site data

Map ID No.	Sample	Repository	latitude	longitude	water depth (m)	Core type	Dating
C1	096-0621	ODP / DSDP	26.732	-88.497	2481	Rotary drill	Holocene (Leg 096 initial report) - age depth model
C2	RC 10 / 264	LDEO	22.083	-94.833	3464	Piston core	Pleistocene @ base of core length = 946cm
C3	0165-0998 A	ODP / DSDP	19.8551	-80.9706	3179.9	Rotary drill	*E. huxleyi* acme zone (Leg 165 initial report) age depth model - Holocene
C4	SO164-18-1	Bremen	21.2336	-74.35	1629	multicore	Holocene (So164 - Rasta cruise report)
C5	Vm 28 / 118	LDEO	16.317	-78.8	1348	Piston core	Pleistocene @ base of core length = 1023cm
C6	0165-1000 A	ODP / DSDP	16.6517	-78.1211	915.9	Rotary drill	*E. huxleyi* acme zone (Leg 165 initial report) age depth model - Holocene
C7	068-0505	ODP / DSDP	11.492	-79.378	3051	Rotary drill	Holocne (leg O68 Report) - age depth model.
C8	0165-0999 A	ODP / DSDP	12.9108	-77.1644	2827.9	Rotary drill	*E. huxleyi* acme zone (Leg 165 initial report) age depth model - Holocene
C9	SO164-02-3	Bremen	15.3081	-72.785	2979.6	multicore	Holocene (So164 - Rasta cruise report)
C10	SO164-24-3	Bremen	14.2681	-63.4286	1545	multicore	Holocene (So164 - Rasta cruise report)
C11	0165-1002 C	ODP / DSDP	10.8017	-64.7872	892.6	Rotary drill	Holocene (Leg 165 Initial report)

Appendix 4.2a *G. menardii* $\delta^{18}0$ against $\delta^{13}C$

Appendix 4.2b *G. tumida* δ^{18}0 against δ^{13}C
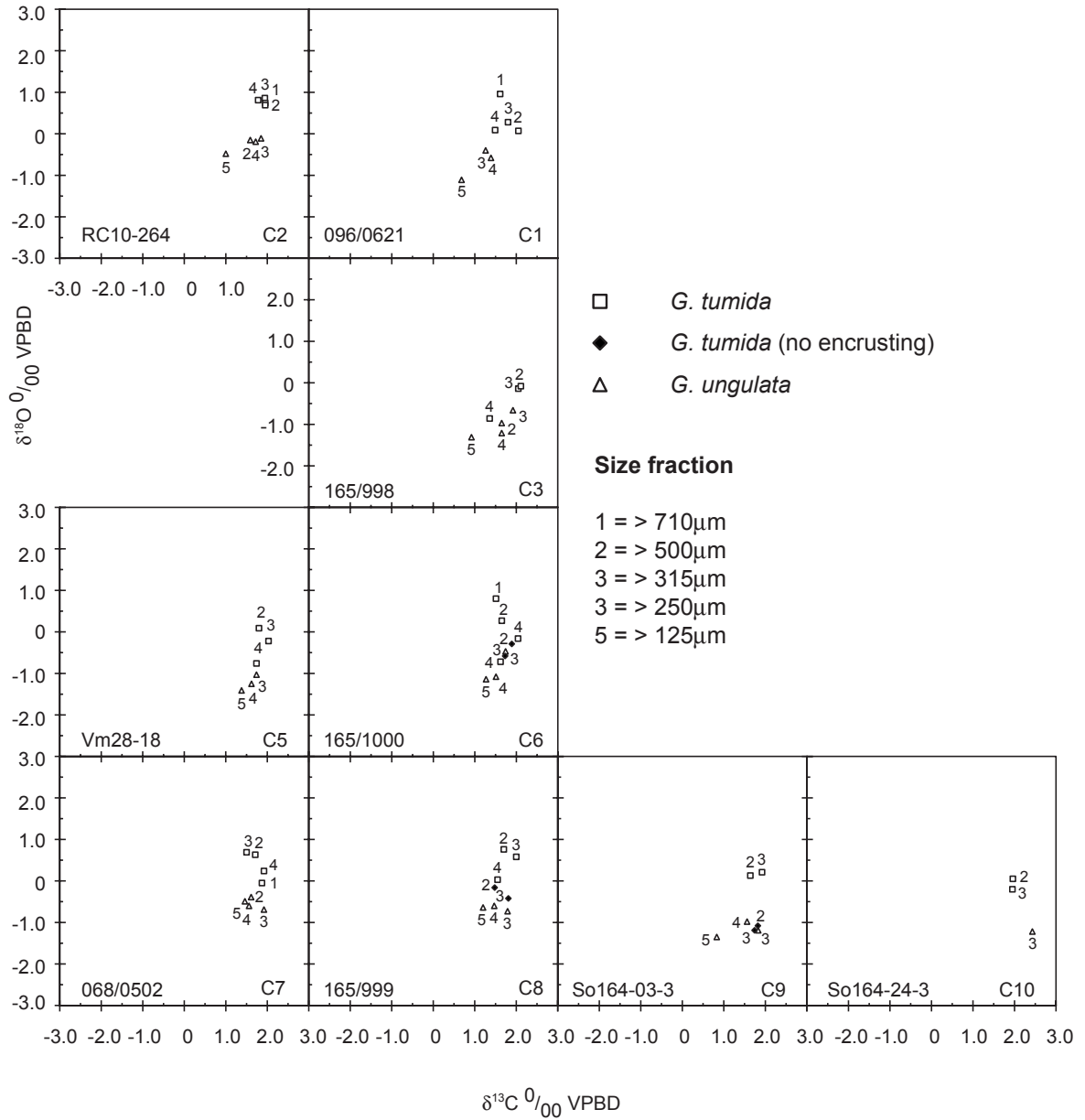
Appendix 4.2c *G. sacculifer* δ^{18}0 against δ^{13}C

Size fraction

1 = > 710µm
2 = > 500µm
3 = > 315µm
4 = > 250µm
5 = > 125µm

δ^{13}C $^0/_{00}$ VPBD
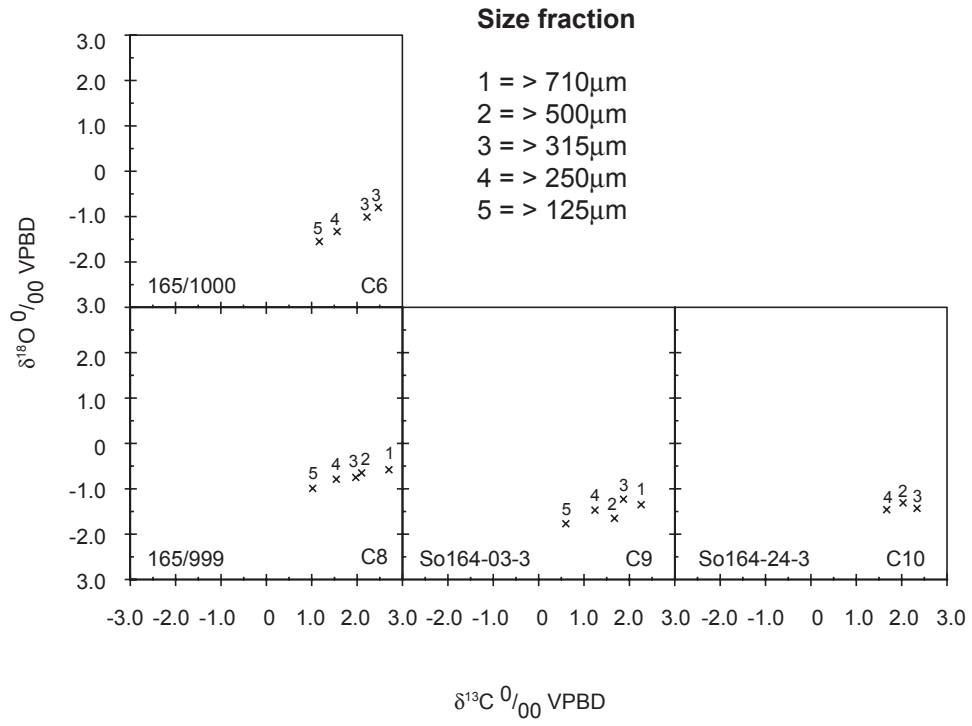
Ontogenetic growth in Recent menardiform globorotalids

Kevin Brown

Natural History Museum Basel

Augustinergasse – 2

Basel

CH 4001

Switzerland

Email: kevin-r.brown@unibas.ch

Tel: +00 41 61 2665 561

Fax   +00 41 61 2665 546

5.1   Introduction

Morphological variation, through time of foraminiferal shells provides the key information to unravel evolutionary and paleoenvironmental changes in these organisms. In foraminifera the shell of individuals is a result of rapid and discrete accretion of chambers leading to step-wise growth, in contrast to the continuous growth pattern seen, for example, in mollusks.

At the beginning of ontogenetic shell growth is the proloculus, which forms right after fusion of the gametes. Environmental conditions influence the further ontogenetic growth, which can lead to variable morphological and ecophenotypic signals seen in the adult form.

On the population level the growth pattern of individuals may therefore bear interesting and important information for the morphometric analysis for fossil assemblages. Is it, for example, possible to discriminate between clearly related species with very similar morphology by the stud of growth rates? Do specific growth rates inform us about (Palaeo)environmental conditions during the life of the individuals? These are the goals of the study:

1.   Determine if any the relationship between morphology and rate of growth within modern Globorotalid foraminifera.

2.   Attempt to identify the stages of growth within the Globorotalid foraminifera.

3.   Determine the pore density and compare intraspecific variation between closely related species and the interspecific variation between morphological variants within a single species.

Growth in foraminifera is achieved by addition of new chambers and deposition of a calcite crust (Hemleben et al 1989, Schweitzer and Lohmann 1991). The volume of a chamber provides a space for the cytoplasm of the organism, and any change in the size of a chamber can be interpreted as a combination of changing metabolic activity or growth rate (Bijma, et al 1990). To successfully investigate this growth we need to look inside foraminifera.

5.1.1 Previous work

Brummer et al. (1987) measured the developmental changes in test diameter to infer stages in development of planktonic foraminifera; the method they chose was contact X-ray imaging. Huber (1994), applied serial dissection of the foraminiferal test as a method, there by, accurate measurements of the cross-sectional area for each successive chamber can be obtained. This information was used to characterizing the rate of chamber growth throughout ontogeny. Serial dissection has a number of advantages over previous contact X-ray techniques: it allows an accurate measurement of the total number of chambers, where in high trochoidal forms, the smaller chambers may be obscured, and pores which may be masked on the surface of the test by secondary calcification or chamber overlap can be seen on the insides of the test. The disadvantages of the dissection technique are obvious: it is very labor intensive; the use of two-dimensional images allows no estimation of the curvature of the test to be made. Special equipment may be required; Huber (1994) used a micromanipulator, which is not readily available. The serial dissections carried out during this research were carried out by hand under a binocular microscope.

5.1.2 Ontogenetic growth stages

The ontogenetic growth stages e.g. Proloculus, juvenile, neanic, adult and terminal stages, were first introduced by Brummer et al (1987)

The proloculus is the first chamber formed after fusion of the gametes. It is circular in cross-section with a flattening on the wall, which it shares with the deuteroconch or second chamber; this is also the position of the aperture, which at this stage is a simple opening. It has already been noted that the proloculus is larger than the deuteroconch (Sverdlove and Bé 1985, Huber 1994). The size of the proloculus is believed to have a strong influence on the development of planktonic foraminifera. Generally, the larger the proloculus, the smaller the number of chambers required to reach a certain size in the final whorl. This means the individual reaches reproductive size quicker (Sverdlove and Bé 1985).

The Juvenile stage starts with the deuteroconch. The juvenile stage lasts for about 1.5 whorls, but is variable with a species-specific number of chambers (Brummer et al 1987). These chambers show a uniform rate of growth.

An abrupt change in the growth rate marks the onset of the neanic stage. Brummer et al. (1987), show that it occurs at test diameters between $65 - 95\mu m$, although there is variation within species. Change in trophic behavior has been suggested as a cause for an increase in the amount of cytoplasm and test size (Brummer et al. 1987).

The term adult stage is used to indicate that the foraminifera have reached sexual maturity. The transition from neanic to adult stages was placed at a test diameter of 180-200μm in modern globigerine species (Brummer et al. 1987). However the species in this study have maximum sizes that range from 700μm to 1200μm, so some adjustment of the onset of the various stages of ontogeny needs to be made.

The terminal stage is used to describe the onset of reproduction (Brummer et al., 1987). It is characterized by addition of aberrant, kummerform chambers or normalform chambers that are related to reproduction rather than normal growth (Hemleben et al., 1989). Gametogenetic calcification occurs during this stage in the form of deposition of a calcitic crust, which may be deposited at some depth below where the organism lived. Reproduction ends the life cycle of the foraminiferal individual. The cytoplasm of the parent foram is transformed into numerous gametes, which are released to begin the cycle a new.

5.2   Method.

5.2.1   Selection of material

To investigate growth within the group of *G. menardii*, large adult specimens were selected from tropical to subtropical Atlantic and Caribbean sample sites. Bulk sample material was dried for 24 hours at 40°C prior to disaggregation with hot water. Disaggregated material was wet sieved through a 63μm sieve, the <63μm fraction was retained. Samples were oven dried over night at 40°C then dry sieved at 125μm. Specimens were selected to investigate the cross section of the observed morphological variation seen within the morphotypes identified by Knappertsbusch (2007). All selected specimens were undamaged, with >700μm maximum diameter, and had no indication of missing chambers. Only specimens that had very little sign of sediment infilling were used, even so some specimens still contained some infilling which masked the pores in the

test wall. The selected specimens were washed in distilled water in an ultrasonic water bath for periods of several seconds in an attempt to remove sediment infilling.

5.2.2 Mounting in Canada balsam

Two methods were employed during this investigation. Initially the specimens were mounted in Canada balsam on a SEM stub, following the method outlined by Huber (1994). This method initially proved successful, allowing the cross-sectional areas of individual chambers to be determined. However, the liquid Canada balsam often passed through the pores of the shell wall and mixed with remnant sediment infilling, which prevented its removal and measurement of the chamber area.

For the second method dried solid Canada balsam was powerderized and dissolved in sufficient xylene to produce a thick viscous solution. A microscope glass slide was cleaned with acetone, and a small amount of the liquid Canada balsam was placed onto its surface. The slide was then gently heated on a hot plate allowing the Canada balsam to flow into a thin film. The slide is removed from the hot plate and allowed to cool slightly, and then small indentations are made in the surface of the Canada balsam to accommodate the spire of the foram shell. Several specimens are positioned in the indentations. A small amount of xylene was then brushed onto the foraminiferal shell with a fine paintbrush; this assists the shell to adhere to the Canada balsam. An excess of xylene will result in the shell being completely embedded within the Canada balsam and will have to be removed and cleaned. Once the specimens are firmly attached to the Canada balsam, the slide is gently heated again. When the Canada balsam has become soft the foram specimens were gently pressed into it surface, the slide is then left to cool. Once the Canada balsam has set the umbilical-side test walls were cut and removed using a phonograph needle that had been ground to a small knife blade the tip of which is approximately 60μm. A fine paintbrush was used to remove particles of broken test and any remaining infilling material. Once the umbilical side chamber walls had been removed a fine paintbrush was used to clean the internal shell walls of the remaining sediment infilling.

Removal of the dissected specimen was achieved by heating the glass slid on the hot plate until the Canada balsam is molten. A drop of xylene is then pipette over the shell. This produces a hydrophobic-like reaction, where the Canada balsam is forced away from the specimen. The specimen was then removed from the slide to a clean slide where traces remaining traces of Canada balsam could be removed by brushing the specimen with acetone. Prepared clean specimens were then mounted on SEM stubs using adhesive carbon pads.

Imaging of prepared specimens was carried out at Zentrum für Mikroskopie at the University of Basel, using a Philips XL30 FEG ESEM. Images were stored in Tiff format. Measurement of chamber and pre areas was carried out using public domain was carried out using the public domain "Image J" software (http://rsb.info.nih.gov/ij/). Direct calibration of pixels to micrometers was carried out for each image using the scale bar on the SEM image.

5.3   Results

5.3.1   Chamber measurements

5.3.1.1 Total numbåer of chambers

The data presented here include measurements form 62 dissected specimens. 40 morphologically identified as *G. menardii* morphotype α, 8 identified as *G. menardii* morphotype β, and 14 G. tumida. Separation of *G. menardii* into two differing morphologies was carried out following criteria from Knappertsbusch 2007. *G. menardii* morphotype α specimens show a range maximum number of chambers from 15 to 21 (mean 18) in three whorls, all chambers show the "C" type arrangement of Cifelli and Scott (1986). *G. menardii* morphotype β specimens have a maximum number of chambers ranging from 18-23 (mean 20.5), and again, chamber arrangement showed the "C" type arrangement in three whorls. *G. tumida* specimens showed a maximum number of chambers from 16-21 (mean 18.5), chambers have the menardii "C" type arrangement, but the chambers in the third (final) whorl become visibly radially elongated in the direction of coiling.
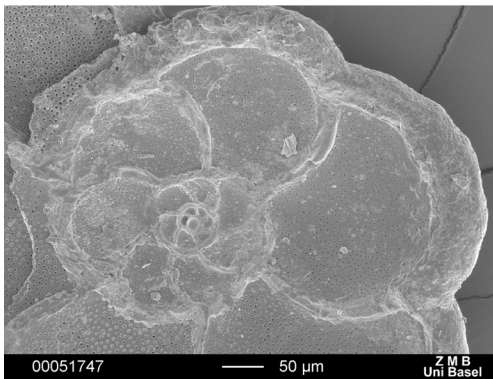
1 - a

1 - b

1 - c

1 - d

1 - e
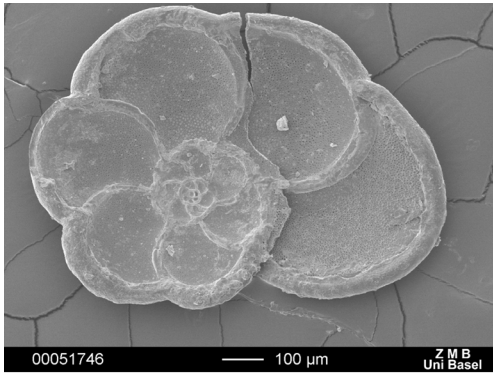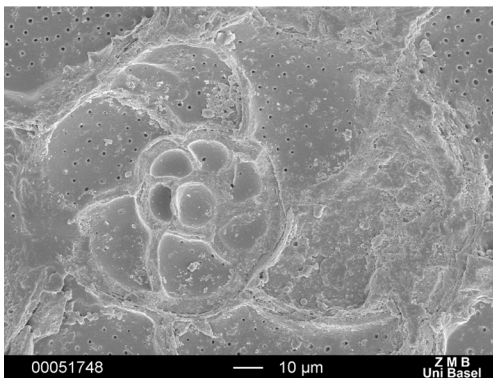
Plate 5-1 Example of a serially dissected specimen

(Specimen No. 69 in Table 5.1)
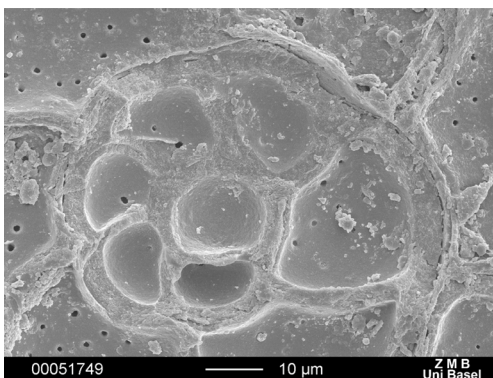
5-1 – a   shows whole specimen (lowest magnigication)
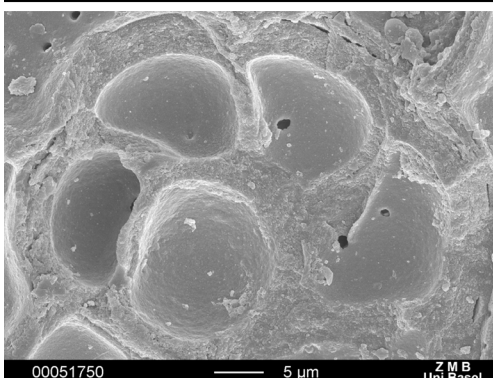5-1 – e   highest magnification, centered on the proloculus

The cracking of the specimen occurred during the sputtering while preparing the specimen for the scanning electron microscope.

5.3.1.2 Chamber area

Measurement of cross-sectional areas of successive chambers provides a means of describing the rate of chamber increase throughout ontogeny. This method allows changes in chamber size and shape to be investigated, whereas the measure of developmental changes in test diameter used by Brummer et al (1987) only recognizes growth increase in the direction of coiling (Huber 1994). Figure 5.1 shows the log10 of the cross-sectional area of each chamber plotted against the chamber number, with the smallest chamber, (proloculus) being chamber one. *G. menardii* (fig. 5.1a) is divided into morphotype α and morphotype β following the designations fromKnappertsbusch (2007).

The mean values (fig 5.1c) calculated by summing the chambers areas for *G. menardii* morphotype α and morphotype β and *G. tumida* separately. All specimens show an initial decrease in chamber area from the proloculus to second chamber, before showing monotonous increase in the successive chambers. Both *G. menardii* and *G. tumida* species show a range of chamber areas for corresponding chambers. Some specimens show aberrant final chambers, which have a significant size reduction from preceding chambers. *G. menardii* morphotype β morphology (fig. 5.1a) is seen typically along the lower limits of chamber number versus area distribution of the *G. menardii* species, although there is overlap with the measurements of *G. menardii* morphotype α to some degree. The plot of the mean values emphasizes the trends within the species, where it is clearly seen that *G. tumida* and *G. menardii* morphotype α show similar mean chamber areas, while *G. menardii* morphotype β has a significantly lower corresponding area at every instar. Chamber growth from the second chamber onwards was found to follow an exponential relationship in all specimens. *G. menardii* morphotype α shows a reduction in the rate of increase around the 16th chamber, while *G. tumida* shows a similar reduction in area increase around the same chamber. *G. menardii* morphotype β initially shows a lower slope in the rate of chamber size increase up to the 7th chamber then area increases parallel to that seen in *G. menardii* morphotype α and *G. tumida*, but at an overall lower level.

5.3.1.3 The percentage increase in area per additional chamber

Figure 5.1d. shows the mean percentage increase in chamber area from the second chamber. The
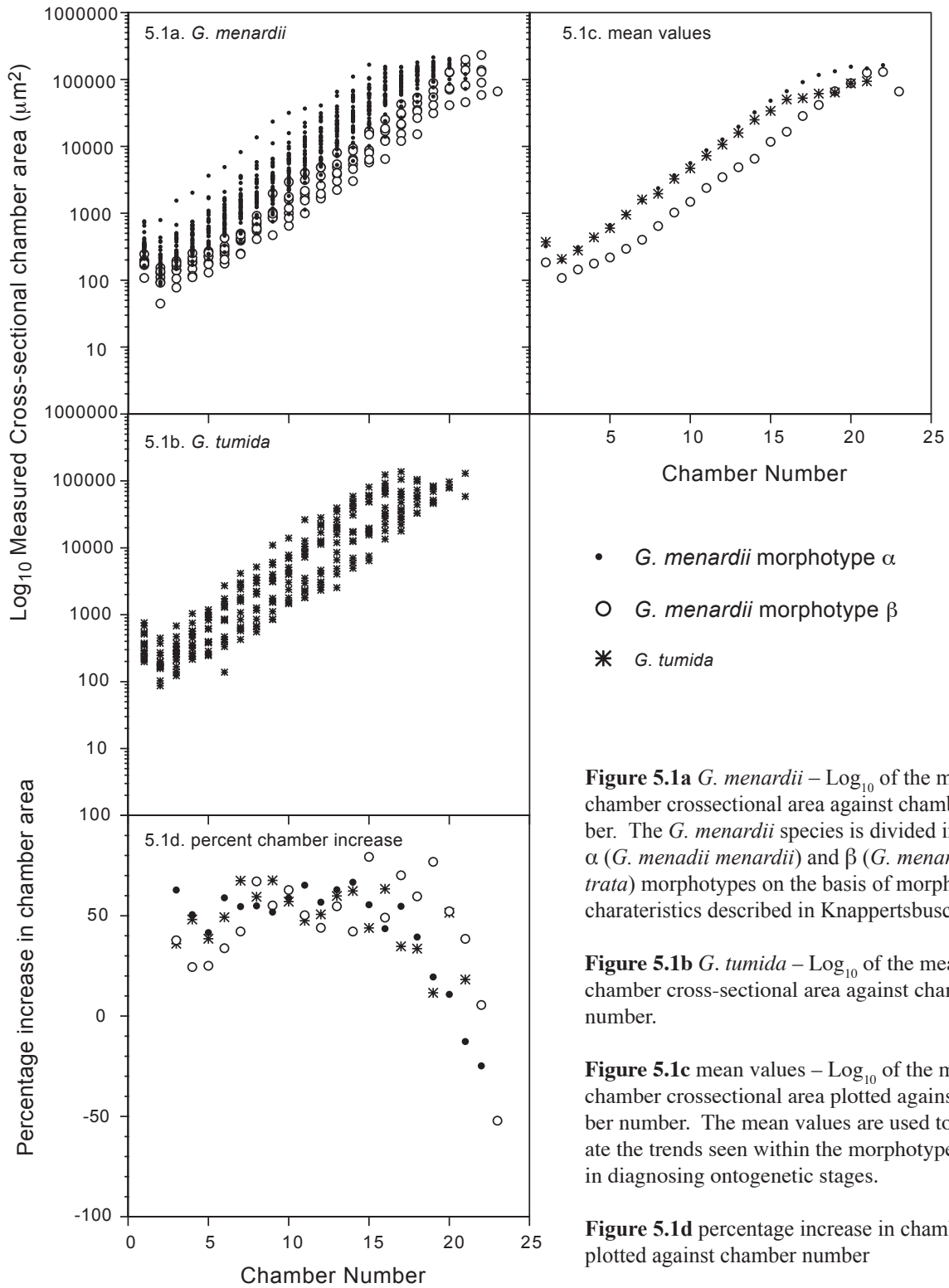
Figure 5.1a *G. menardii* – Log$_{10}$ of the measures chamber crossectional area against chamber number. The *G. menardii* species is divided into the α (*G. menadii menardii*) and β (*G. menardii cultrata*) morphotypes on the basis of morphological charateristics described in Knappertsbusch 2007.

Figure 5.1b *G. tumida* – Log$_{10}$ of the measures chamber cross-sectional area against chamber number.

Figure 5.1c mean values – Log$_{10}$ of the measures chamber crossectional area plotted against chamber number. The mean values are used to exaggerate the trends seen within the morphotypes to aid in diagnosing ontogenetic stages.

Figure 5.1d percentage increase in chamber area plotted against chamber number

Figure 5.1   A composite of all chamber area data.

percentage increase at each instar was determined by the following formula:

Where An is the area of the nth chamber, An+1 is the area of the instar n+1.

The relative chamber increase from one chamber to the next in *G. menardii* morphotype α fluctuates around 60 % but with an overall increasing trend until the 17th chamber. Thereafter the relative increment is seen to be negative. This decrease in the relative chamber increase curve (fig. 5.1d.) is reflected in a plateau in the final chambers of Figures 5.1a-c.

G. menardii morphotype β shows an increasing rate of overall chamber area up to the 7th chamber. After that chamber the values again show a fluctuation around a value of 52%. *G. menardii* morphotype α shows a reduction in area increase starting at the 19th chamber, which is ontogenetically later than observed in *G. menardii* morphotype α. *G. tumida* shows a similar pattern to that observed in *G. menardii* morphotype α, but the fluctuation is around a value of 58%, and the reduction in area increase again starts at the 16th chamber. Fluctuation observed in the increase in chamber area is thought to be caused by errors in the measuring of the cross-section area of the chamber, resulting from the curvature of the test.

5.3.1.4 Prolocular size

The proloculus is the first chamber formed by the individual and represents the starting point for growth. All proloculi measured have a circular outline with a flattening of the wall where the second chamber develops (see plate 5-1e). In Figure 5.1 *G. menardii* morphotype α, *G. menardii* morphotype β and *G. tumida*, show a range of sizes for prolocular area. In those specimens with large prolocular chambers the succeeding chambers are all comparably large throughout ontogeny. Figure 5.2 illustrates histograms of the prolocular cross-sectional areas showing for the two *G. menardii* morphotypes and *G. tumida*. The histogram bin-width has been optimized for all the data using the procedure described in Keating and Scott (1999), allowing direct comparison of the three separate species. The corresponding normal distributions are plotted on each histogram. The histograms clearly show that on average the specimen's *G. menardii* morphotype β have a smaller size than *G. menardii* morphotype α, (but note also the smaller number of specimens). *G. tumida*

shows a wider range of values.

5.3.2   Identification of growth stages

Figure 5.3 is a combined plot of log10 mean values of chamber cross-sectional area and the relative chamber area increase versus the number of instars. The juvenile stage starts at the deuteroconch (second chamber). Its end is identified with a change in the rate of cross-sectional chamber aerial growth. In *G. menardii* morphotype β this change is seen after the seventh chamber. It coincides with a constant relative growth rate of chamber. *G. menardii* morphotype α and *G. tumida* have very similar trends and do not show a change in the relative growth rate of chamber area. Therefore identification, for the step from juvenile to neanic stage is not possible this data. However, looking at the relative rate of chamber increase both *G. menardii* morphotype α and *G. tumida* show an increase until chamber 7, and from then on the rate seems to fluctuate about a constant mean value. The onset of the adult stage is clearly identified in *G. menardii* morphotype α and *G. tumida* as a plateauing in the slope of chamber area (Figure 5.3, upper panel). This step occurs between chamber No. 15 and 16 for G. tumida and between chamber No. 17 and 18 for *G. menardii* morphotype α. Along with the plateauing a sharp decrease in the relative growth rate of chamber cross-sectional area is observed. No plateauing but a peak of the change in chamber area is observed with *G. menardii* morphotype β. In the relative growth rate a decrease is observed after the nineteenth chamber, which marks the onset of the adult stage in *G. menardii* morphotype β.

5.3.3   Pore size and density

Shell porosity has been shown to have positive correlated to temperature in modern Globigerinid foraminifera (Bé 1969, Hemleben et al 1989, Bijma, Faber and Hemleben, 1990). Shell porosity is related to the in and efflux of ions between the ambient environment to the cytoplasm and so mirrors in part the metabolic functions within the cell. Therefore, it is reasonable to assume, that changes in the number and size of pores can be used to recognize changes in the growth rate (Bijma et al 1988). Estimation of the porosity or change of porosity is therefore interesting to learn about metabolism, growth-state, and sexual maturation of the cell.
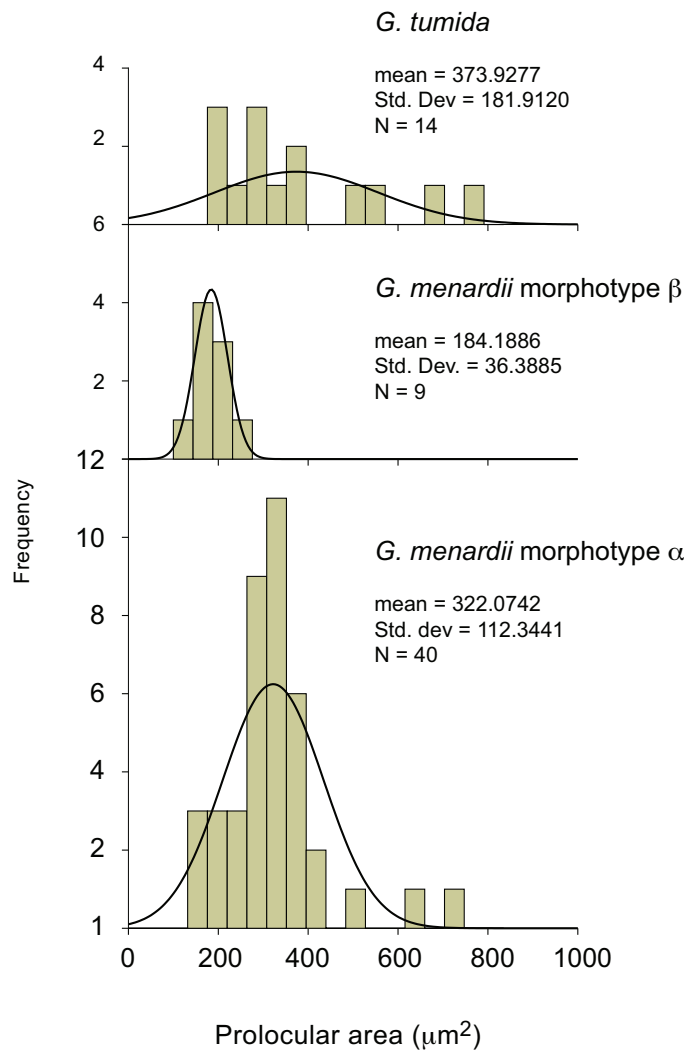
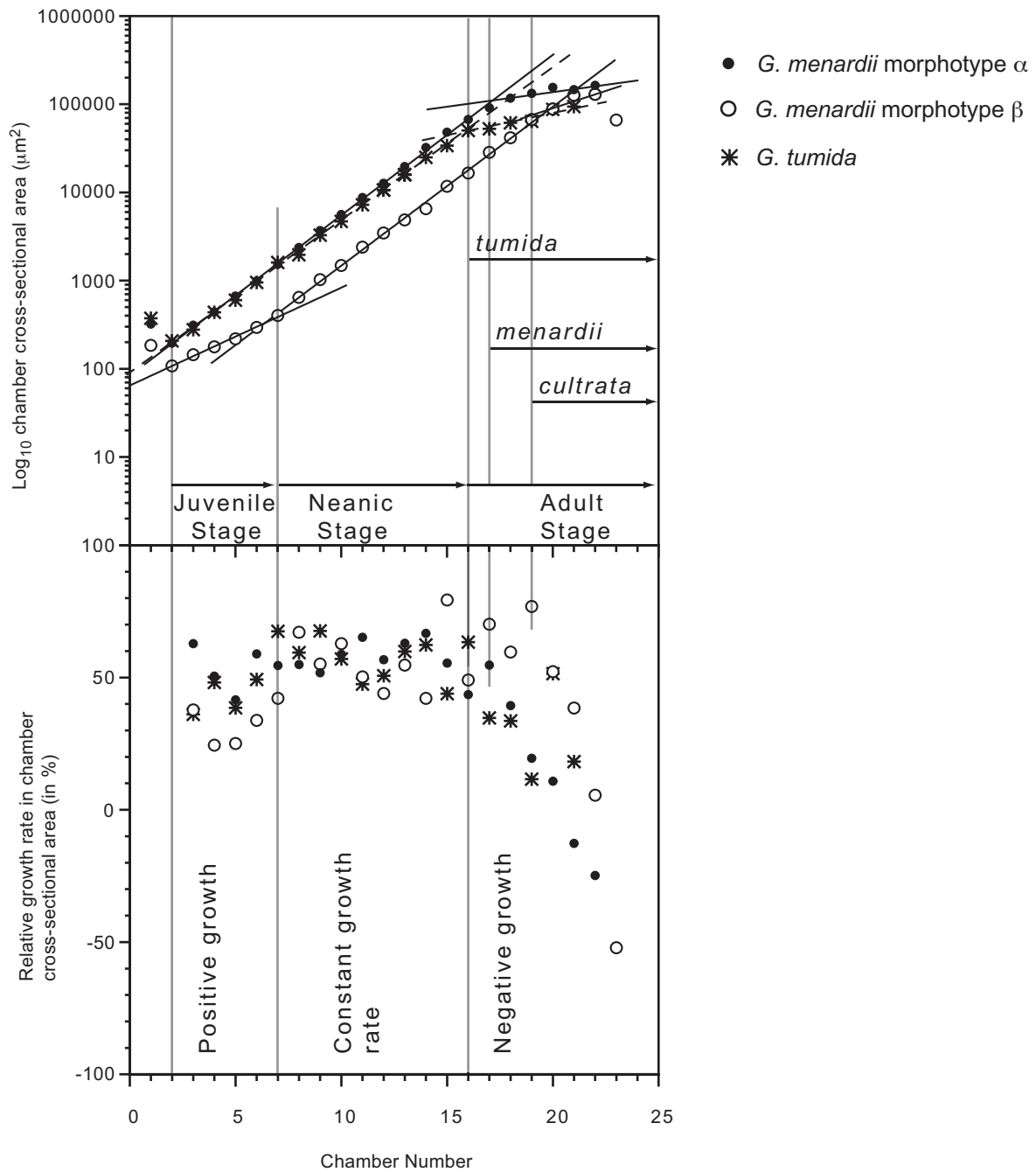**Figure 5.2**   **Histogram of the prolocular size of all specimens**

Figure 5.3   Ontogenetic stages

Combined plot of $\log_{10}$ mean values of chamber cross-sectional area and the Relative growth rate in chamber cross-sectional area (in %) against the chamber number.

(See section 5.3.2 for discussion of how ontogenetic stages are determined.)

Towards this goal six specimens of *G. menardii* showing exceptional preservation were selected allowing pore density and pore size to be measured. No specimens of *G. tumida* were selected as the high curvature of the test wall, made accurate measurements of pore areas difficult. In each specimen of *G. menardii* multiple areas were investigated per chamber for pore areas. For each chamber per specimen a mean pore density and an integrated pore area per chamber was calculated. Plots of the results are shown in figure 3. The correlation to exponential splines for all specimens is listed in table 5.1.

5.3.3.1 Pore density

The pore density in a chamber (fig 5.4c) is estimated by dividing the total number of pores counted in each sub-sample area by that area (in μm^2). In small, juvenile chambers the pore density is high because of the comparably large area of a few pores. As the foram gets older the chambers increase and pore density decreases rapidly. This decrease in pore density when plotted against chamber number was found to follow an exponential function (see table 5.1 for correlation coefficients). Estimation of the total number of pores per chamber was calculated by multiplying the mean pore density by the total chamber area (fig. 5.4a). The increase in the number of pores with instar was found to have an exponential function (Equations and R2 values shown in Table 5.1). No distinct change in pore density, which can be directly attributed to growth stage, was observed during this study. However, the pore density is seen to have an exponential relationship with chamber number and hence with chamber area.

5.3.3.2 Mean pore area

The mean cross-sectional area of individuals pores for each chamber was calculated and plotted against the chamber number (fig. 5.4d). The mean pore size was found to increase exponentially throughout ontogeny with the function:

Where: Ap is the mean pore area, K is a constant, α is a constant and C is the chamber number. The correlation seen for individual specimens is good, e.g. >90% (the exception being specimen 100 which had an R2 value of 79.55 see table 5.1). However there is variation between specimens.

Tabel 5.1   Equations and Correlation values

5.4_a Total number of pores		
	Equation	Correlation (r^2)
69	$y = 7.341\ e^{\,0.1876x}$	85.73
100	$y = 32.848\ e^{\,0.1456x}$	20
101	$y = 1.7031\ e^{\,0.4251x}$	95.62
103	$y = 4.1753\ e^{\,0..3154x}$	87.35
107	$y = 93.949\ e^{\,0.1426x}$	73.03
110	$y = 3.6527\ e^{\,0.3424x}$	97.58

5.4_b Calculated total pore area		
	Equation	Correlation (r^2)
69	$y = 7.5391\ e^{\,0.1872x}$	86.14
100	$y = 34.719\ e^{\,0.1435x}$	20
101	$y = 1.7837\ e^{\,0.4225x}$	95.7
103	$y = 4.4222\ e^{\,0.3129x}$	87.6
107	$y = 94.351\ e^{\,0.1433x}$	73.75
110	$y = 3.9913\ e^{\,0.3377x}$	97.71

5.4_c Pore density		
	Equation	Correlation (r^2)
69	$y = 0.3127\ e^{\,-0.2048x}$	85.05
100	$y = 3.811\ e^{\,-0.2226x}$	51.87
101	$y = 0.0258\ e^{\,-0.0303x}$	16.24
103	$y = 0.586\ e^{\,-0.1034x}$	38.69
107	$y = 0.041\ e^{\,-0.1169x}$	63.39
110	$y = 0.0556\ e^{\,-0.0672x}$	61.32

5.4_d Mean pore area		
	Equation	Correlation (r^2)
69	$y = 0.5036\ e^{\,0..6772x}$	90.71
100	$y = 1.4683\ e^{\,0.0.853x}$	79.55
101	$y = 0.6099\ e^{\,0.1033x}$	95.89
103	$y = 0.9123\ e^{\,0.0782x}$	95.36
107	$y = 0.8776\ e^{\,0.0995x}$	97.55
110	$y = 1.3624\ e^{\,0.0518x}$	95.16

5.4_e Calculated total pore area against chamber area		
	Equation	Correlation (r^2)
69	$y = 1.7395\ x^{\,0.4723}$	85.18
100	$y = 1.2986\ x^{\,0.5271}$	40.78
101	$y = 0.039\ x^{\,0.9216}$	95.7
103	$y = 0.2015\ x^{\,0.7371}$	86.3
107	$y = 1.434\ x^{\,0.5443}$	73.75
110	$y = 0.1391\ x^{\,0.8153}$	98.24

Figure 5.4   A composite of all pore analysis data

5.4a. Total number of pores

5.4b. Calulated total pore area

5.4c. Pore density

5.4d. Mean pore area

Specimen

□	100
◇	101
○	103
△	107
✳	110
+	69

5.4e. Calulated total pore area against chamber area.

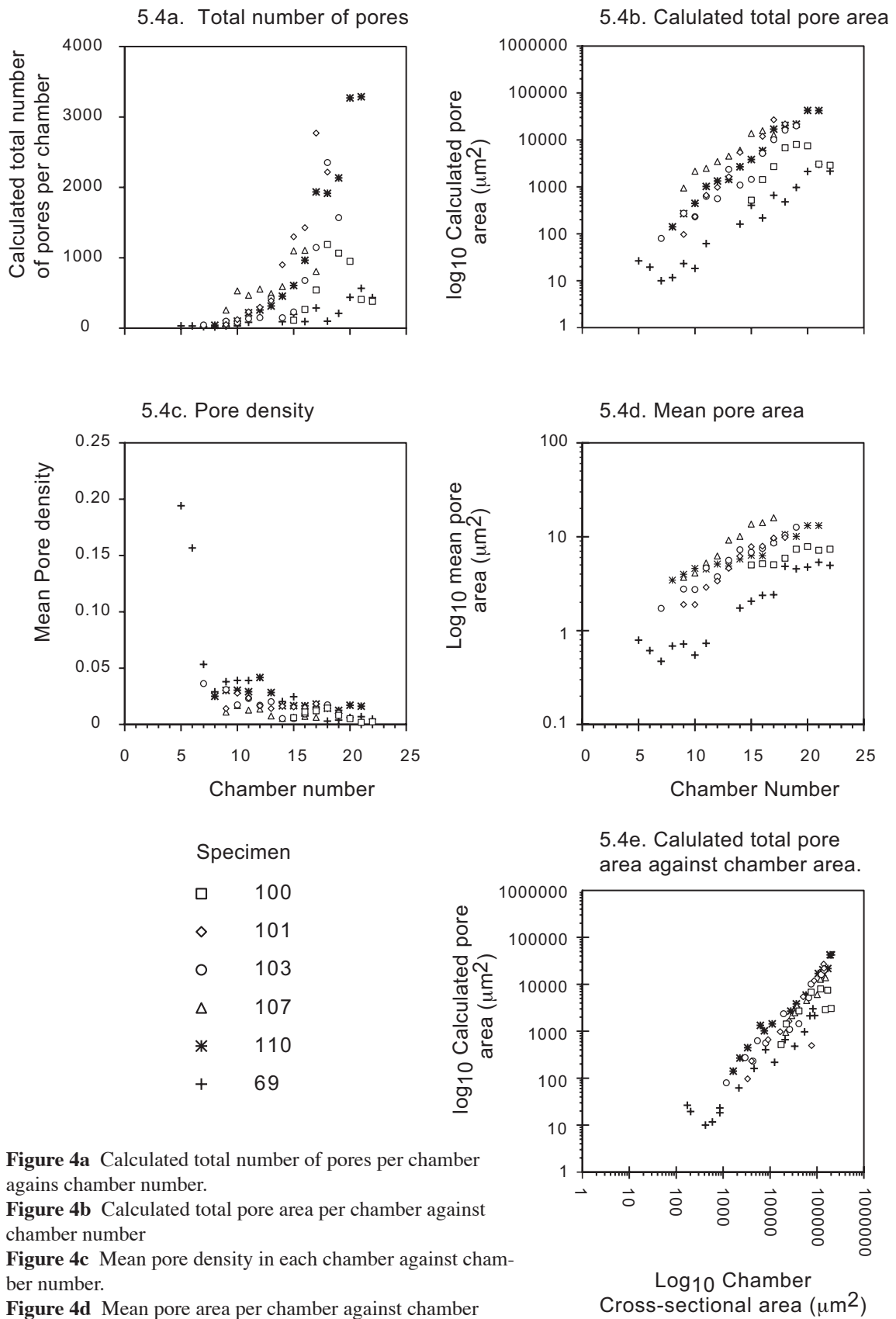**Figure 4a** Calculated total number of pores per chamber agains chamber number.

Figure 4b Calculated total pore area per chamber against chamber number

Figure 4c Mean pore density in each chamber against chamber number.

Figure 4d Mean pore area per chamber against chamber number

Figure 4e Calculated total pore area ($\log_{10}$ μm^2) against chamber cross-sectional area (μm^2).

5.3.3.3 Integrated pore area per chamber

The total pore area per chamber was estimated by multiplying total number of pores per chamber by the mean pore size for that chamber (fig 5.4b). High correlation values were found for all specimens (see table 1), except specimen 100, which showed an R^2 value of 20%.

Specimen No.100 showed poor correlation on all plots, which is due to sediment infilling of the pores and curvature of the shell leading to inaccurate count about the pore density. No abrupt changes in either pore density or mean pore size or estimation of total pore density per chamber was identified; gradual increases in all values are noted in all specimens.

5.4   Discussion

Growth of animals depends on biological and environmental factors (nutrition, trace elements, oxygen, and temperature). In foraminifera growth is seen thought the increased of cytoplasm, which becomes segmented into newly secreted chambers.

Life can be subdivided into 3 functions: a. metabolism, b. growth, c. reproduction.

    a.   Metabolism: input and output of material and according molecular

             transformation - metabolism is the maintenance of life functions.

    b.   Growth: increase in amount of cytoplasm, this is different from metabolism.

    c.   Reproduction:distribution of cell material to new cells.

Changes in the rate of chamber growth indicate multiplication of cytoplasm. Changes in pore density may point to changes in metabolism. Marked changes in pore area and chamber area may point to beginning reproduction.

The results clearly show the cross-sectional area of a chamber increases exponentially. Changes in the slope which define the ontogenetic stages in Brummer et al (1987) are only visible in *G. menardii* morphotype β. However using the change in the rate of chamber increase, similar ontogenetic stages can be identified as well. *G. menardii* morphotype α and *G. tumida* have similar mean prolocular sizes, similar rates of chamber increase through juvenile and neanic development stages

and similar mean maximum number of chambers. This suggests that they have similar metabolic function and growth rates, which suggests similar environmental conditions. A reduction in the rate of chamber increase is seen at the change from neanic to adult stages. The large proloculus and rapid growth may be interpreted, as are adaptive strategies that allow the species to take advantage of more eutrophic conditions that prevail at greater water depths. In contrast *G. menardii* morphotype β specimens have smaller prolocular size and smaller subsequent chambers. The growth rate is lower, but the ontogenetic age is higher, which is experienced in the comparably greater number of chambers between the juvenile and adult stages. The lower growth rate signifies for the cell, a longer life span to reach reproductive maturity. The lower growth rate is interpreted as an adaptation to a more oligotrophic environment at shallower depth than where *G. menardii* morphotype α and *G. tumida*.

Brown (2007) showed that *G. menardii* morphotype α and *G. menardii* morphotype β have distinct depth habitats, and probably different trophic mechanisms, with *G. menardii* morphotype β having a possible photosymbiotic relationship. The present ontogenetic observations support that hypothesis: *G. menardii* morphotype α morphotype being is adapted to a deeper and more eutrophic environment within the upper thermocline and *G. menardii* morphotype β to a shallower, more oligotrophic region within the mixed layer, where it has a possible symbiotic relationship with photosynthesizing algae.

5.5 Conclusions

This study represents a one of the few morphometric investigations into the ontogenetic development of planktonic foraminifera, using the modern menardiform globorotalia as a case study. It was shown that serial dissection of the test provides a promising method to obtain accurate measurements that is complementary to the method of Huber (1994) and that relate test and chamber size to the physiological state of the individual. Because sediment infilling is disturbing the results, plankton tow material or specimens grown in culture are suggested to further support the following preliminary results:

1.   Measurement of chamber area from fossil shells provides a linkage between the

cytoplasmic growth of the organism and its shell.

2.	Investigations into the change in rate of chamber increase can be used to identify differing stages of ontogenetic development. Using this method, ontogenetic stages, which are often masked by the rapid growth through juvenile and neanic stages, can be seen.

3.	Morphological differences observed between the two adult morphotypes of *G. menardii,* shown by Knappertsbusch (2007) can also be identified by their ontogenetic signature: *Globorotalia menardii menardii* (morphotype α) has on average larger mean prolocular sizes and larger mean chamber sizes than *G. menardii cultrata* (morphotype β). This signifies that the specific (or sub-specific) morphological differences between the two morphologies are already differentiated at the first juvenile stages. The lower number of chambers required to reach sexual maturity seen in *G. menardii* (morphotype α) suggests a shorter life span than of the *G. menardii* (morphotype β) morphology. This is interpreted as adaptation to different trophic levels in the water column.

4.	*G. menardii* morphotype α, (with large proloculus and rapid chamber size increase) tends to behave in a more opportunistic and R-selected mode of life. In contrast *G. menardii* morphotype β (smaller mean prolocular diameter, slower rate of chamber increase) tends to have on average longer life span to reach sexual maturity. This behavior resembles an adaptation to more oligotrophic conditions following a K-selected life strategy.

5.	The similar ontogenetic growth signature in *G. menardii* morphotype α and *G. tumida* suggests common life strategies and a similar environmental adaptation.

5.6   Acknowledgement

5.6   References

Bé, A.W.H. 1968. Shell Porosity of Recent Planktonic Foraminifera as a Climatic Index. Science, 161:881-884.

Bijma, J., Faber, W.W., and Hemleben, C., 1990. Temperature and Salinity Limits for Growth ans Survival of Some Planktonic Foraminifers in Laboratory Cultures Journal of Foraminiferal Research, 20:95-116

Brummer G.-J.A., Hemleben C. and Spindler M., 1987. Ontogeny of Extant Spinose Planktonic Foraminifera (Globigerinidae): A Concept Exmplified by Globigerinodies sacculifer (Brady) and G. ruber (d'Orbigny). Marine Micropaleontology, 12:257-381.

Huber, B.T., 1994. Ontogenetic Morphometrics of Some Late Cretaceous Trochospiral Planktonic Foraminifera from the Austral Realm Smithsonian Contributions to Paleobiology number 7

Keating J.P., and Scott D.W.,   1999. Ask Dr. Stats: - A Primer on Density
Estimation for the Great Home Run Race of ,98 - Stats # 25 spring 1999
16-22.

Knappertsbusch, M., 2007. Morphological variability of Globorotalia menardii (planktonic foraminiferan) in two DSDP cores from the Caribbean Sea and the Eastern Equatorial Pacific Carnets de Géologie / Notebooks on Geology, Brest, Article 2007/04 (CG2007_A04)

Rasband, W.S., ImageJ, U. S. National Institutes of Health, Bethesda,
Maryland, USA, http://rsb.info.nih.gov/ij/, 1997-2006.

Sverdlove, M.S. and Bé, A.W.H., 1985. Taxonomic and Ecological Significance of Embryonic and Juvenile Planktonic Foraminifera Journal of Foraminiferal Research 15:235-241.

Synopsis

6.1   Morphological variation in the Globorotalia menardii plexus.

The *Globorotalia menardii* plexus includes at least three intergrading morphotypes, e.g. morphotypes α, β and χ. Attempts to impose quantative limits to these morphotypes may be synthetic but it is believed that the three morphologies represent adaptation to different environments.

6.1.1   Biogeography of major morphotypes of *G. menardii*

The temperature of the world oceans vary in temperature both latitudinally and with depth. The warmer tropical warmer tropical waters in all areas investigated show a dominance of the flatter, thin walled morphotype β which is equated to *Globorotalia menardii cultrata*. Where present in the same samples from the Caribbean region, morphotype α (corresponds to) *G. menardii menardii* shows a consistent enrichment in $\delta^{18}O$ indicating a deeper colder depth habitat than *G. menardii cultrata*. Looking at the ratio of axial diameter / spiral height ($\delta Y/\delta X$) a shift is seen moving from the tropical Atlantic to higher southerly latitudes. Starting in the tropical Atlantic the flatter morphology *G. menardii cultrata* is dominant moving to higher latitudes the ratio shifts through the higher spired and more heavily encrusted *G. menardii menardii* and finishes around 40° south (the southerly extent of sampling) with the highest spired morphology of *G. menardii gibberula* (morphotype η). A similar pattern is identified in the Indian Ocean, but here the signal is not so clear, and it is believed that the differing seasonally imposed oceanographic conditions imposed on the region by the monsoons are the cause. In the warmest parts of the Bay of Bengal and the Arabian Sea, the *G. menardii cultrata* morphology is seen to dominate. Along the north western edge of the Arabian Sea, *G. menardii menardii* was found in large numbers in the surface sediments. It is interpreted that these forms represent the morphology dominant during the June to September monsoon when strong coastal upwelling of cold, nutrient rich waters, occurs in the area. Moving south into higher latitudes, the ratio of $\delta Y/\delta X$ shows a shift to the higher spired forms. *G. menardii gibberula* is found in a band stretching from Australia to Madagascar. In this study *G. menardii gibberula* is only found below the tropical convergence zone in the Indian Ocean and may represent a a single species only found in the southern hemisphere but its total

geographical distribution is still not known. A morphotype endemic to the Northern parts of the Indian Ocean is *G. neoflexuosa* (morphotype χ); it resembles that of *G. menardii cultrata* except for a flexing of the final chamber of between 30-90°. The cause of the flexing is unknown and requires further investigation.

The Pacific Ocean poses problems in obtaining samples as much of the sea floor lies below the lysocline and what material is available is usually of poor carbonate preservation making morphometric analyses difficult. However, the *G. menardii menardii* and *G. menardii cultrata* morphologies are identifiable in both the East and West Pacific. Lack of latitudinal spread of samples in this study prevents investigation into the Pacific distribution of the morphotypes. *G. menardii gibberula* is only found in the Western Pacific below the tropical convergence zone, which supports the hypothesis that its distribution is restricted to the southern hemisphere.

6.1.2 Temperature and ontogenetic signals.

The $\delta^{18}O$ signal for *G. menardii cultrata* places it in correspondingly shallower depth habitats throughout its life cycle than that seen for the corresponding size specimen of *G. menardii menardii*. The $\delta^{13}C$ signal is suggestive that the *G. menardii cultrata* morphotype has a symbiotic relationship, but no evidence for such a relationship is seen for *G. menardii menardii*.

The mean prolocular size of *G. menardii menardii* was found to be larger that that of the mean value of *G. menardii cultrata*. A large proloculus results in subsequently larger chambers and is seen in *G. menardii menardii*. A larger comparative chamber size suggests a higher metabolic rate resulting in more rapid growth, resulting in a shorter number of chambers being required to reach reproductive stage. *G. menardii cultrata* has a greater number of chambers before it reaches reproductive size, suggesting that on average this morphotype lived longer.

The isotopic signal and the mean chamber size suggest that the two morphologies, *G. menardii menardii* and *G. menardii cultrata* have differing depth habitats and differing life strategies.

6.2 Morphological variation in the Globorotalia tumida plexus

Based on several lines of evidence (δX/δY ratios, observations on shell internal, juvenile morphologies presence / absence date of the two forms in the same sample), the *Globorotalia tumida* plexus includes two members, e.g. *G. tumida* (morphotype ε) and *G. ungulata* (morphotype ϕ). Both have a similar tumid morphology, but *G. tumida* shows greater encrusting of the test and heavier keel development with radial elongation of the chambers in the last whorl than *G. ungulata*. *G. ungulata* has a hyaline appearance and a distinctive carinate band over the aperture of the last chamber. In the δX/δY morphospace both species share a similar axis of morphological variation: while the *G. menardii* plexus shows morphological variation in the amount of inflation of the test, the *G. tumida* plexus shows variation along the δY axis, which suggests that the two morphotypes may be ontogenetic variants.

6.2.1 Latitudinal and depth variation.

The geographical distribution of the *G. tumida* plexus is restricted to the warmest tropical waters. It is found in all the tropical samples investigated in this study. The morphological variation of the *G. tumida* plexus is very tightly constrained compared to that of *G. menardii*. The extent of morphological variation was found to be the same in all sample sites investigated. This suggests that either, *G. tumida* represents a global population; with unrestricted gene flow through out the worlds oceans, or that they inhabit a more stable environment at greater depth resulting in a uniform morphology. A decrease in the overall size of *G. tumida* is observed in southerly higher latitude sample sites, and *G. ungulata* is not found. *G. ungulata* is only found in sample sites that contain *G. tumida*, and never on its own. In the Indian Ocean its highest abundance is seen about the subtropical convergence zone, in the Arabian Sea. Only 9 specimens of *G. ungulata* were found in the Indian Ocean, all in the Arabian Sea. *G. ungulata* were only observed in the western Pacific Ocean.

6.2.2 Temperature and ontogenetic signals.

Isotopic studies carried out during this project show that *G. tumida* and *G. ungulata* have different

depth habitats. *Globorotalia tumida* shows the greatest enrichment in $\delta^{18}O$ of all the menardiform morphotypes investigated. *Globorotalia ungulata* shares a similar signal to that seen for *G. menardii cultrata* and the shallow dwelling species *Globigerinodies sacculifer*. However, there is no indication in the $\delta^{13}C$ signal that it has a symbiotic relationship, as was seen for *G. menardii menardii*. Of note is a few specimens that are described as non-crusted *G. tumida*, which show the typical tumid shape of *G. tumida*: They have radially elongated chambers, the test has the hyaline appearance of *G. ungulata* but they lack the diagnostic carinate band on the last chamber. Isotopically, the non-crusted *G. tumida* they show the same signals of *G. ungulata*. Globorotalia tumida has a similar prolocular size as G. menardii menardii, and both show a similar rate of chamber area increase, reaching the reproductive size in a similar number of chambers. Unfortunately, there are no ontogenetic observations possible for G. ungulata because the delicate test made it difficult to carry out serial dissection.

6.3   Conclusions

Globorotalia menardii represents recognizable morphologies which can be separated by the use of quantifiable characters. The three morphologies *G. menardii cultrata, G. menardii menardii* and *G. menardii gibberula*, have distinct biogeographical regions, but there is overlap which confuses the signals.

The isotopic data and the ontogenetic growth studies suggest, that selection for differing environmental conditions is occurring. *Globorotalia menardii cultrata* shows an isotopic signal indicating shallower warmer waters, a slower growth rate and longer life span are possibly adaptations to a more K-selected mode of life in the warm oligotrophic mixed layer of the tropics. The range of $\delta^{13}C$ data suggests the possible presence of symbionts in *G. menardii cultrata*, which still needs confirmation from plankton tow samples. *Globorotalia menardii menardii* has an isotopic signal enriched in $\delta^{18}O$ indicating a deeper and colder water. The comparably larger proloculus and a more rapid growth rate indicate that it reaches sexual maturity earlier, which are adaptations believed favorable to a more R-selected mode of life within the more eutrophic

conditions found in the upper part of the thermocline.

At this moment there is no clear indication, whatsoever, that *G. menardii menardii* and *G. menardii cultrata* represent separate species. Instead, the two morphotypes show divergence to differing environments and selection towards differing modes of life. However if this selection continues long enough then true speciation may occur.

Globorotalia tumida shows a similar environmental signal to that seen in *G. menardii menardii*. It also shares a similar mean prolocular size and subsequent chamber growth rate. This suggests similar habitats and modes of life. *Globorotalia ungulata* shows an isotopic signal similar to that of shallow dwelling *G. menardii cultrata*. Initially, the impression emerged that *G. ungulata*, may just be a shallow dwelling juvenile form of *G. tumida*. On the other hand, *G. ungulata* is only known in sediment cores from the Late Pleistocene / Holocene onwards, while *G. tumida* occurs from the Late Miocene until recent. In this context it is believed that *G. unguata* represents a relatively recent environmental adaptation of *G. tumida* to a shallower environment.

6.4   Suggestions for further work

To further resolve the question of the relationship of the *G. menardii* morphologies and answer new question opened by the current study further investigations are required:

Molecular studies on live material would show the relationship between the three *G. menardii* morphotypes: *G. menardii menardii, G. menardii cultrata,* and *G. menardii gibberula* morphoseries to determine their relationship, (same species, separate species or sub-species). Open questions about *G. tumida* and *G. ungulata* are: are they ecophenotypic variants or do they represent ontogenetic variants?

G. neoflexuosa: is it *G. menardii cultrata* and the observed flexing of the final chamber caused by environmental conditions or are there identifiable genetic differences?

Whether or not *G. menardii menardii* and *G. menardii cultrata* are two separate populations living separately within the water column could be answered by seasonal plankton sampling programs

at different water depths. If ecological forcing of the morphology of one of the morphotypes that has sufficient genetic plasticity to produce the observed morphological variation (ecophenotpy) it could be investigated in well selected plankton-tow transects along known environmental gradients. Such tests could prove or disprove the hypothesis that *G. ungulata* really is an adaptation of *G. tumida* to shallower warmer waters as suggested in this study.

Detailed morphological investigations at selected sites in the Atlantic and Indian Oceans would give greater understanding of the phylogenetic relationship of three *G. menardii* morphotypes, the first occurrence of *G. menardii gibberula* is still not known. Further sampling in the Pacific needs to be carried out to extend the biogeography of the forms.

Sediment traps could be used to study the variation in abundance though out the year. In particular, material the sediment traps are expected to unravel the dynamics of depth-dependent ontogenetic growth of these forms and so could help to better interpret the isotopic signal of *G. menardii* in the underlying sediment.

Culture experiments could be carried out to investigate the effect of temperature and available food upon the development of the test. This would provide greater a greater understanding of the morphological variation of the shells and their isotopic signals of specimens collected from deep sea sediments.

Investigations of *G. menardii* through geological time at selected cores could hightlight the phylogenetic history of the extant forms and their endemic biogeography along with that of extinct descendents of the *G. menardii* stock.

(Kevin Richard) Brown

Address: Leibniz-Institute of Marine Sciences
                IFM-Geomar
                Wischhofstr. 1-3
                D-24148 Kiel   Telephone (work)   0431 600 2652
                Germany   Email: kbrown@ifm-geomar.de
                Date of Birth: 15 October 1965

Personal Profile

- Flexible and enthusiastic micro-palaeontologist with a strong background in statistical analysis
- Motivated self-starter comfortable working in structured environments
- Inquisitive researcher adept at drawing conclusions from rigorously interrogated data sets.
- A fast learner who works to very high standards – but always makes sure the job gets done

Academic interests

- Evolution of Foraminifera, how they evolved, and driving mechanisms of that evolutionary change.
- The application of these data to bio/chrono-stratigraphy and palaeoenvironmental / oceanographic reconstructions.
- Palaeoceanography and the evolution of the ocean basins, and how the opening and closing of the ocean gateways has affected global climatic changes through the Cenozoic
- The application of quantative methods to biostratigraphy to improve temporal resolution.

Education

University of Basel: *January 2003 – June 2007*
PhD Earth Sciences (*Summa cum laude*)   Thesis title: *"Biogeographic and morphological variation in late Pleistocene to Holocene globorotalid foraminifera"*

University College London: *September 2001 – September 2002*
MSc Micropalaeontology (*Pass*)

University of Wales, Bangor: *September 1998 – June 2001*
BSc (Hons.) Geological Oceanography (*2.1*)

Management and Leadership

- Twelve years served in British Royal Navy
- Proven track record of effectively leading specialist naval personnel on board patrolling submarines and in shore based medical centres

- Rose to the rank of Petty Officer – direct responsibility for over 20 naval and civilian personnel
- Courses in Leadership and Management at the Royal Navy School of Leadership and Management

Technical aptitude

- A track record of embracing new technology, and is comfortable using MS Office, Adobe imaging software, and SPSS statistical analysis program.
- Trained to very high standards in a range of technical fields in the Royal Navy – for example, Radiation Safety
- Experience living and working onbaord a ship
- First Aid insturctor

Employment History

September 1998 – September 2001

Various part-time and seasonal employments to fund my way through University

October 1984 – January 1997

Royal Navy

I spent 12 years in the Royal Navy serving with the Royal Marines and on Submarines. It was a tremendously rewarding career that offered me the chance to travel all over the world. I obtained Enrolled Nurse status and worked as an occupational hygienist with specialisation in Radiation Safety Practice.

In the Navy I obtained the following vocational City and Guilds certification:

Emergency Medical Care	December 1988
Radiation Safety Practice (Stage One)	January 1990
Advance Emergency Care	February 1991
Radiation Safety Practice (Stage two)	August 1994

Activities and Interests

I enjoy hill walking and most other outdoor pursuits. I enjoy swimming and have worked as a lifeguard. Although I no longer play rugby I still keenly follow the game, a both an international and national level. I have an interest in vintage guitar amplifiers and building replicas along with other musical orientated electrical equipment. I enjoy cooking and have catered for friend's parties in the past.